공학박사 학위논문

A Supervisory Control Method of Hybrid AC/DC Microgrids Considering Uncertainty in Loads and Renewable Energy Sources

부하와 신재생에너지 불확실성을 고려한 혼합형 AC/DC 마이크로그리드의 감시제어에 관한 연구

2019년 2월

서울대학교 대학원

전기·컴퓨터공학부

이 진 오

A Supervisory Control Method of Hybrid AC/DC Microgrids Considering Uncertainty in Loads and Renewable Energy Sources

지도교수 문 승 일

이 논문을 공학박사 학위논문으로 제출함
2018년 12월

서울대학교 대학원
전기·컴퓨터공학부
이 진 오

이진오의 공학박사 학위논문을 인준함
2018년 12월

위 원 장 _____ (인)

부위원장 _____ (인)

위 원 _____ (인)

위 원 _____ (인)

위 원 _____ (인)

Abstract

A Supervisory Control Method of Hybrid AC/DC Microgrids Considering Uncertainty in Loads and Renewable Energy Sources

Jin-Oh Lee

School of Electrical Engineering and Computer Science

The Graduate School

Seoul National University

As the power system has recently become smaller and more decentralized and the DC technology is developed, the hybrid AC/DC microgrid (HMG) has been constructed. In addition, with interests in environmental issues and efforts to obtain sustainable energy sources, the penetration level of renewable energy sources (RESs) is significantly increasing. However, it inevitably increases the uncertainty in the system. If the microgrid operates in grid-connected mode, the power imbalance caused by the uncertainty leads to the burden of the main grid. It becomes more severe under the high uncertainty and multi-microgrid. In islanded mode, the droop control results in the frequency and voltage deviations, and the output power of resources may be far from the cost-effective operating point.

This dissertation presents the supervisory control method of HMG for grid-connected and islanded mode in order to obtain the reliable and cost-effective operation under the high uncertainty. In grid-connected mode, to operate as a single controllable entity, the internal net load fluctuation within a HMG should be compensated by itself. To this end, bus-dependent participation factor (BDPF)-based generation adjustment method is proposed. The conventional participation factor considers only the generators; however, the location of the variation may also affect the operation performance owing to the line loss. To accurately reflect the cost

change of output variation, the generation-load incremental cost (GLIC) which is the total cost variation that considers both the generator and load position is introduced. Using the GLIC and its derivative, the optimal participation factor can be calculated for each bus. The GLIC can fairly reflect line loss changes; in addition, the second-order loss sensitivity is used to improve the accuracy of the BDPF. The output power can be easily adjusted from the base point, using each load variation and the corresponding BDPF. Subsequently, re-adjustment is performed if constraint violations exist. Since the BDPF that was previously obtained at the base point is used, the amount of generation adjustment can be calculated instantly.

In islanded mode, the operation method is divided into two stage, long-term and short-term, in order to maintain the power balance using only internal resources. Regarding the long-term operation, the on/off decision of DGs and controllable loads is decided. In this process, the machine learning-based forecasting algorithm is used for net load prediction and the HMG is linearized to solve the mixed integer linear programming. In the short-term operation where the final set-point is determined, an MPC-based operation method is proposed. The problem for restoring the frequency, AC and DC voltage and reducing the generation cost is formulated using the sensitivities of the AC and DC grids considering the droop control. In addition, second-order frequency sensitivity, which can accurately account for the influence of the reactive power on the frequency, is selectively utilized. In this case, the performance for frequency restoration and cost reduction can be enhanced with slight modification of only the frequency constraint.

The proposed method was implemented and case studies were conducted in MATLAB. Its effectiveness is verified by comparing with conventional methods for grid-connected and islanded mode, respectively. The proposed method is helpful to increase the penetration level of intermittent RESs and the utilization of the DC technology into the power system. Further, the system operation can be more reliable and economical, particularly in situations, where frequent and rapid variations in the load demand and RES output power occur.

Keywords : Distributed Generation, Hybrid AC/DC Microgrid, Incremental Cost, Model Predictive Control, Renewable Energy Source, Participation Factor
Student Number : 2013-20862

Contents

List of Tables

List of Figures

Chapter 1. Introduction

1.1 Motivations and purposes

Motivation for studying hybrid AC/DC microgrids

With increasing awareness of environmental, social and geographical issues, additional transmission expansion and large-scale power plant construction, such as nuclear and fossil-fuel plants, have become difficult. Because of fast depletion and high cost of fossil fuel, global warming impacts, and accidents and waste of the nuclear plant, the efforts to look for new clean energy source have been made. Accordingly, the penetration of renewable energy sources (RESs) has significantly increase as a solution of providing sustainable energy without the emission of pollutants and generation cost. Two most typical RESs are wind and photovoltaic power. Their energy sources, wind and solar, can be obtained from anywhere, which means they can be installed near the local load demand in contrast to conventional power plants generally constructed near the coast. It also corresponds the fact that the power system has been further subdivided and microgrids have attracted considerable attention to meet the load demand locally via distributed generators (DGs).

In recent years, growing power electronic technology has led to an interest in DC systems [1]. High voltage direct current (HVDC) has been used to connect large-scale grid connection between countries and to incorporate the large wind farm in transmission system. In medium or low voltage system, as increasing in DC loads and inverter-interfaced DGs, DC grid is being constructed by converting AC lines to DC operation. It can cause the power losses and initial building cost of voltage sourced converter (VSC), but can control the line power flow and increase power capability [2]. In addition, integrating RESs, such as wind and photovoltaic power,

into the DC grid can be more efficient [3], [4]. The development of the DC grid has led to the development of hybrid AC/DC microgrids (HMGs), which consist of AC and DC grids interconnected via an interlinking converter (IC). The HMG helps to reduce the energy conversion stage and combine the benefits of AC and DC systems [5].

Meanwhile, uncertainty is inevitable in power systems. Unexpected line faults or outage of generators and other power system devices are included in the uncertainty, but they rarely occur. Rather, variations in the load demand and the output power of RESs, which are the large portion of the uncertainty, should be handled frequently because they are instantaneous and cannot be expected exactly. Especially, the variation of RESs is highly correlated among RESs in similar geographical areas due to the similarity of weather conditions in such areas. This situation causes high uncertainty of RESs. Moreover, the load demand has a wide range of variation especially in subdivided areas due to the reduced number of loads (limit averaging effect) [6]. In other words, the actual load demand and RES output are more likely to differ from the forecasted value over a short time period in microgrids. These uncertainties may disrupt the optimal operations.

The high development of sensing, communicating, and computing technology makes the power system operation better. Especially the system operator can obtain more measured data via communication infrastructure and can compute various applications more often. Among the applications, the optimal allocation of generation has long been an important topic in power system operations. The optimization objectives can vary depending on the system operator, but the most typical objective is the minimization of the total generation cost, which is also called the economic dispatch (ED) problem [7]. Optimal power flow (OPF), first introduced in the 1960s [8], is a powerful tool for solving the ED problem using various optimization techniques that both maintain the power balance between the total generation and the forecasted load demand and satisfy other constraints. The OPF has been recently studied not only in traditional bulk systems but also in small-scale

systems such as microgrids with other objectives as well as cost minimization. The OPF is generally based on the forecasted values of load demand and RES output, so the operation scheme that respond to the uncertainty in a short period is needed.

Based on the recent issues in power system, the research of the HMG operation under high uncertainty is consistent with current technical and practical trends.

Specific topics of this dissertation

Among the many technical issues of HMG such as inverter controller design, protection scheme, market operation, and analysis of small signal stability, this dissertation focuses on the operation method of central controller to cope with high uncertainty that refers to the instantaneous change of load demand and output of RES.

For the operation of grid-connected mode, there are many optimization methods whose major objective is to reduce the operation cost. However, high uncertainties are likely to disrupt the optimal operation due to the difference between predicted value and real value. In addition, as the number of microgrids increases, the burden of the main grid to cover the fluctuation also increases in grid-connected mode (even worse under high uncertainty). It is difficult to resolve it locally due to the topology dependency and the lack of information. To prevent the impact on the main grid and to obtain cost-effective operation continuously, the generation should be properly adjusted in centralized manner, which is one of the main topic of this dissertation.

The other topic of this dissertation is an operation method in islanded mode. The droop control is generally used in islanded mode, but it necessarily results in the frequency and voltage deviation. There are many combination of the generation allocation to restore the frequency and voltage, so economic operation as well as reliability can be obtained if the problem is formulated and solved properly. In addition, due to the lack of the main grid which acts as a slack generator, the sufficiency and deficiency of generation should be handled. Like grid-connected mode, high uncertainties make the problem worse. Thus, operation method for reliable and cost-effective operation in islanded mode is needed.

1.2 Highlights and contributions

Generation adjustment based on bus-dependent participation factor

Base point and participation factor method is typically used for generation allocation in power systems. The base point would be calculated through the optimal power flow (OPF) method, and between two consecutive base points, the generation is adjusted using the participation factor. The conventional participation factor consider the generation cost function and additionally the network line loss. However, only one set of the participation factor does not reflect the line loss accurately, so the power balance and optimal operation may not be obtained with high accuracy. Thus, new incremental cost is introduced and second-order derivative of line loss is calculated in order to reflect the impact of the line loss precisely. Then, the optimal participation factors can be obtained for each bus, which is called bus-dependent participation factor (BDPF). Using BDPF, generation cost can be reduced with simple implementation while maintaining power balance in a microgrid. The method can be utilized as a feeder flow control because the energy received from the main grid can be kept almost constant by the internal power balance in real time. Indeed, the proposed generation adjustment method is a general way to maintain the power balance considering the line loss variation. Therefore, the method can be applied to a pure AC and DC microgrid as well as a hybrid AC/DC microgrid.

Developing formulation of model predictive control for droop-based microgrid

The DGs usually adopt the droop control for power sharing in an islanded microgrid, and it inevitably results in frequency and voltage deviation. To restore the deviations and obtain cost-effective operation, the optimization problem formulation for model predictive control (MPC), which is quite suitable to cope with rapid disturbance variation during short time interval, is developed. The sensitivity of frequency and voltage magnitude with respect to the injected power can be obtained from the Jacobian matrix containing droop-controlled DG. Using the sensitivity, the

variation in frequency and voltage is linearized, and the formulation can be converted to a form suitable for MPC. In addition, the second-order frequency sensitivity is calculated and used in order to reflect the reactive power on the frequency properly. Because the method considers the AC and DC grid separately and connects them to the IC, it can be extended to a pure AC or DC islanded microgrid.

Increasing utilization of DC technology and penetration level of RES

One issue of the recent power system is to accommodate the DC technology. Unlike the AC grid, DC network has no global variable (frequency) and the active power is shared through the local voltage. Active power directly affects the generation cost that should be reduced for better economic operation, and the voltage should be kept within safe range for reliable operation; thus both of them should be investigated in detail. The other issue is the introduction of a large scale RES over the world. The RES is prevailing at distribution level more and more, but the intermittency makes the system operation difficult. The proposed operation method analyzes the network containing the DC grid and presents a novel operation scheme to cope with the output fluctuation of RES. Consequently, using the proposed method, the utilization of DC technology at the system level and the high penetration level of RES are anticipated in the future power system.

1.3 Dissertation organization

Chapter 1 consists of the motivations and purposes of this dissertation and then the highlights and contributions of this dissertation are followed. The last part of this chapter describes the organization of this dissertation.

Chapter 2 explains the concept of a hybrid AC/DC microgrid and presents the mathematical model of its components. The technical issues on hybrid AC/DC microgrid for grid-connected mode and islanded mode are explained in this chapter.

Chapter 3 describes the operation methodology for grid-connected mode proposed in this dissertation. The new concept of the incremental cost is introduced, and the optimal bus-dependent participation factor for power balance and economic operation is calculated. Using the bus-dependent participation factor, the method for generation adjustment is proposed.

Chapter 4 describes the operation methodology for islanded mode proposed in this dissertation. The proposed operation scheme is divided into two stage. The long-term on/off decision of DGs and loads is decided, and model predictive control-based short-term operation is conducted using droop-based sensitivity and new optimization problem formulation.

Chapter 5 presents the simulation results for various case studies. The effectiveness of the proposed methods for both grid-connected mode and islanded mode is verified.

Chapter 6 concludes this dissertation and discusses future extensions.

In addition, the calculation of the second-order derivatives of power flow equations is shown in Appendix A. The verification of the singularity to obtain the bus-dependent participation factor is shown in Appendix B.

Chapter 2. Hybrid AC/DC Microgrid

2.1 Concept of hybrid AC/DC microgrid

Typical hybrid AC/DC microgrid

A microgrid refers to a small-scale distribution network designed to actively supply and manage the power and energy locally, which is essentially an active distribution system [9]. HMG is the same concept as a conventional pure AC microgrid, and additionally has a DC grid. A typical HMG structure is shown in Fig. 2.1. The static switch is placed at the point of common coupling (PCC), and there are various energy resources and some controllable loads in a HMG. Not necessarily but typically, AC loads are connected to the AC grid and DC loads are connected to the DC grid to improve the energy efficiency. The energy resources are also placed in similar way. The DC grid is connected to the AC grid via an interlinking converter (IC). The ICs can be connected to the same AC and DC bus in parallel, and even connected to other buses.

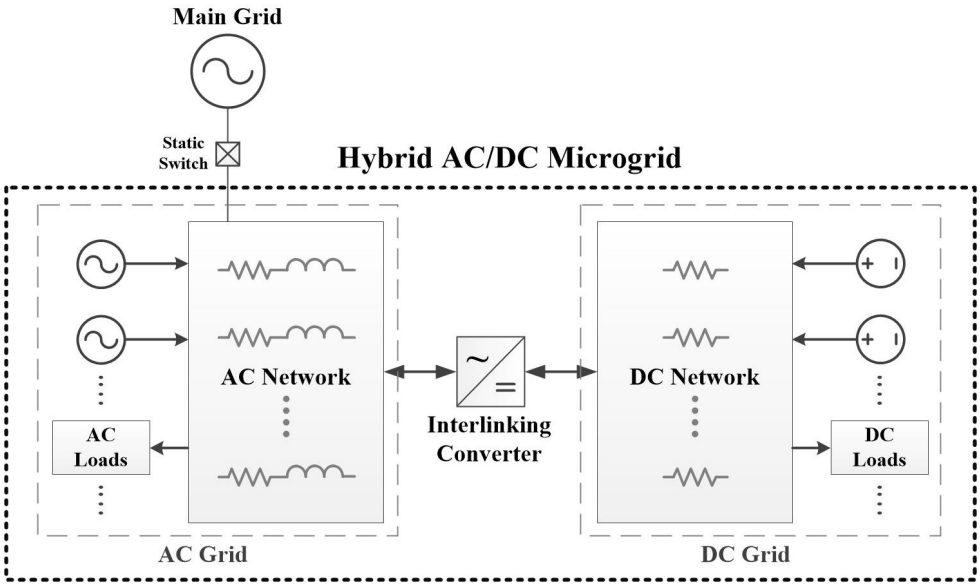

Fig. 2.1 Typical hybrid AC/DC microgrid structure.

Unlike the typical structure, where the main grid is connected to the AC grid, another HMG structure where the DC grid is connected to the main grid through the converter and static switch is possible as shown in Fig. 2.2 [10]. In this structure, the frequency of the AC grid can be different from the main grid (e.g. the nominal frequency of the main grid and the AC grid are 60 Hz and 50 Hz, respectively) because of two voltage conversion (between the DC grid and the main grid, and the DC grid and the AC grid). This structure is more typical in the medium or high voltage level to inter-connect to other regions. However, it can be extended to the microgrid level depending on the physical limitation. The operation scheme, control strategy, and the major devices are equivalent to the typical structure. Figs. 2.1 and 2.2 are the electrical structure, and the control structure will be discussed in the later subsection.

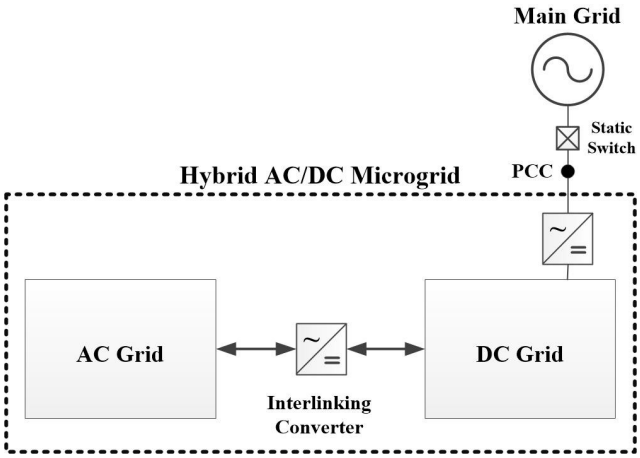

Fig. 2.2 HMG structure with DC grid and main grid connected.

Hierarchical control structure

Microgrids are typically operated with a hierarchical control structure [11]. There are several researches only consider primary control of local controller (i.e. autonomous control). It can offer 'plug and play', which means that a DG can be placed at any point without re-formulation of other control scheme, and can be robust against the communication failure. However, the coordination of local controller (LC)

and central controller can conduct more functions such as optimal schedule of resources and handling line faults while retaining the aforementioned characteristics of the autonomous control. The hierarchical structure divides the control level into several sections by functions and the time frame in which they operate. As shown in Fig. 2.3, the hierarchy is generally three steps, primary, secondary and tertiary control. The hierarchical control can also be applied to HMGs.

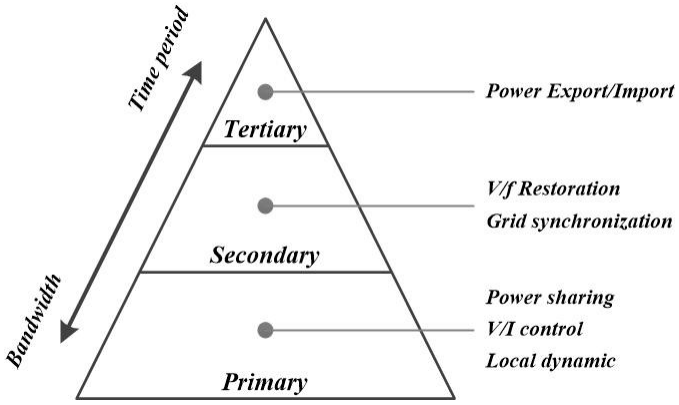

Fig. 2.3 General hierarchical control scheme [12].

The main function of the primary control is to control the output power, voltage, and current of its own generator. The basic control is to follow the set-points given by the central controller or its own calculation. It is implemented in local controller of energy resources. One of the most representative method is the droop control, which is suitable for power sharing in real-time. It measures the local quantities such as frequency, voltage, and output power and reacts in pre-defined ways depending on the generator or inverter control types. It does not require the communication infra, so it can be repeatedly performed in a very short cycle. In other words, the primary control responds to instantaneous variation of disturbance such as load demand and output of RES. This control method avoids the complexity and high cost, and is necessary to reliable operation.

The secondary control method can be divided into the centralized, decentralized, and distributed control according to the strategy. In this dissertation, the centralized

secondary control is focused, which utilizes the microgrid central controller (MGCC) to monitor and supervise the whole system while gathering the necessary information. The main task is to reduce the operation cost by re-allocating the amount of the generation. In addition, the frequency and voltage magnitude deviated by the droop control can be restored. Grid synchronization is also conducted to re-connect to the main grid in this control level. Depending on the controller and system operator, the operation cycle can be from several seconds to tens of minutes. This is the highest control level in the islanded mode [6], because the tertiary control manages the power flow between the microgrid and the main grid.

Tertiary control is the highest control level in grid-connected mode. This control level is responsible for the power exchange between a microgrid and the main grid. Using the price of intake power or the amount of the power contract from the main grid, this control level sets long-term optimal set-points for economic purpose. Thus, many of them uses sophisticated optimization techniques with consideration of the system conditions. In addition, it can support the voltage and frequency regulation of the main grid when it is needed. In some cases, tertiary control can be considered as a part of the main grid, not microgrid itself [6].

Local controller

The LC basically performs the primary control, according to the hierarchical control scheme. Power sharing is a major purpose, but the LC also enhances the dynamic performance and protects its own devices. Not only the DG with primary control but the RES and the controllable load are able to have their LC. The LC of RES controls in maximum power point tracking (MPPT) mode and conducts power curtailment when it is needed. The LC of the controllable load determines the on/off decision and shifts its load demand to other time. The LC is able to control energy resources without any communications. However, in the hierarchical control structure, the LC communicates with MGCC every pre-defined cycles in order to update the set-points of the droop control and change the mode to grid-connected or

islanded. Especially in islanded mode, the LC has more important role because the instantaneous power variation of load should be compensated by measuring the frequency and voltage in very short cycles.

Central controller

The MGCC performs the essential role of microgrid operation. It performs various functions which is known as an energy management system (EMS) applications, including the aforementioned secondary and tertiary control. Fig. 2.4. shows the data flow of a MGCC [6]. It collects the weather information and historical data to predict the load demand and the RES output. Subsequently, the optimal operation of energy resources is calculated with consideration of the network model and operation constraints, and the optimal solutions are transmitted to the LCs. The MGCC receives the feedback signal from the LCs and the price of the intake power or emergency state from the transmission system operator (TSO). It also receives the current frequency, bus voltage, and net load demand of the system. Note that the purpose of the MGCC is reliable and economic operation.

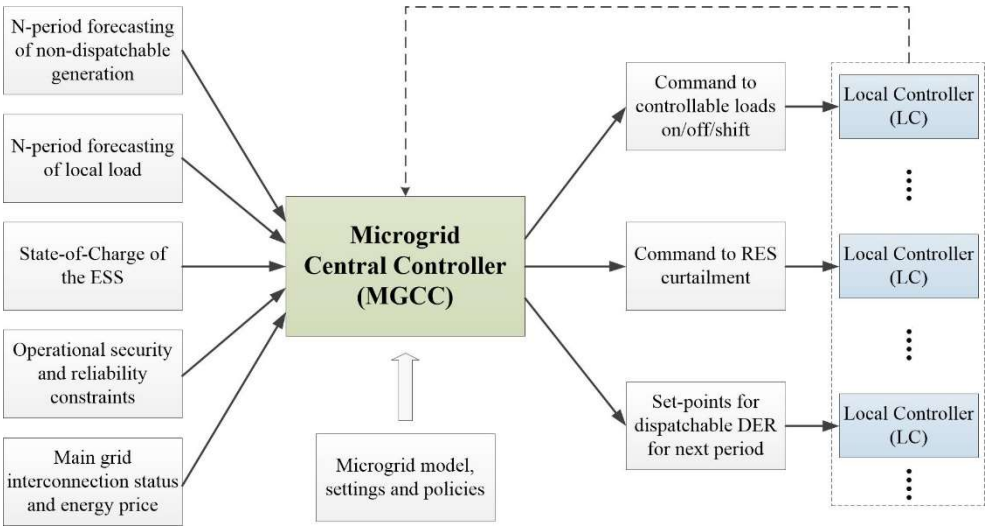

Fig. 2.4 Data flow of a microgrid central controller [6].

Operation mode

The most important feature of a microgrid is that it can be operated either grid-connected mode or islanded mode. In grid-connected mode, the main grid acts as a large slack generator with constant frequency and constant voltage magnitude. It can also consume active and reactive powers from the viewpoint of the microgrid when there is sufficient generation in the microgrid or an emergency of the main grid. As long as the grid-connected microgrid is controlled well, it gives an advantage that the microgrid can be seen as a controllable load in the perspective of the main grid. This means that the microgrid can operate reliably in relation to the main grid. In this mode, the frequency is considered to be a variable determined by the main grid [13], [14], and operation objectives can include the reduction of cost, the voltage regulation of end-user, and the reduction of line loss.

When faults caused by natural disaster or unexpected accident occur in the main grid, the static switch is off and a microgrid operates in islanded mode. In addition to the islanded mode by static switch off, there is natural remote areas such as mountainous territories or islands, which cannot be connected by the transmission line. They should operate on their own continuously and they are called “standalone microgrid”. In this dissertation, the terminology “islanded” includes the standalone microgrid since the characteristic that they both are not connected to the main grid is mainly utilized. The characteristic of the islanded microgrid is dependent on their energy resource types, the synchronous machine and the inverter. The synchronous machine-based microgrid has rotational mass similar to the conventional bulk grid, but it has low inertia and is vulnerable to the fluctuation of active power [15]. Recently, with developing the power electronic technology, the inverter-based microgrid is evolving. If all DGs are inverter-interfaced, it has no inertia and called zero inertia system. The frequency and voltage of this system can be directly generated by the inverter while immediately compensating for the constantly changing load in the form of electric energy. However, because of the lack of the main grid, an elaborate operation methodology should be developed.

2.2 Mathematical model of hybrid AC/DC microgrid

The components of the HMG have their own steady-state and dynamic characteristics, and they can be expressed as mathematical models. The focus of this dissertation is the supervisory control which is performed at the MGCC to find the steady-state values for better operation. Thus, the mathematical model of the steady-state is investigated in the later subsections.

2.2.1 Control of distributed generators

A microgrid consists of various type of energy resources, and we categorize the energy resources as controllable DG, battery energy storage system (BESS), and RES. In general, the terminology, DG, contains all the resources such as micro turbine, fuel cell, gas turbine, energy storage system, and renewable sources. However, for convenience sake, the terminology DG, is used as a controllable distributed generators other than BESS and RES to distinguish their control logic in this dissertation. In the following expressions, superscript 0 denotes the set-point value, subscripts i and j denote the bus indices, and B_{ac} and B_{dc} are the sets of the AC and DC buses, respectively.

Controllable DGs

There are various types of controllable DGs such as internal combustion engine, microturbine, fuel cell, and so on [16]. The detail characteristics of each DG are different with the types, but it takes advantage of the facts that their output power is adjustable and the droop control is adopted. The output active and reactive powers of DGs with the droop control in the AC grid can be expressed as

$$P_{g,i} = P_{g,i}^{0} + k_{p,i}\left(\omega^{0} - \omega\right), \qquad i \in B_{ac} \tag{2.1}$$

$$Q_{g,i} = Q_{g,i}^{0} + k_{q,i}\left(V_{i}^{0} - V_{i}\right), \qquad i \in B_{ac} \tag{2.2}$$

where ω is the frequency, V is the voltage magnitude, and k_p and k_q are the droop slopes of the active power–frequency (P–ω) and reactive power–voltage magnitude (Q–V), respectively. Note that the relationship between active power and voltage magnitude (P–V) and reactive power and frequency (Q–ω) are relatively large owing to the high R/X ratio in the low voltage network. However, not the operation for a low voltage system such as a building or factory but for the network of the distribution system scale are focused in this dissertation, so the typical droop control (2.1) and (2.2) of the AC grid are used.

The same principle can be applied to the DC grid. The output power of the DGs in the DC grid can be expressed as

$$P_{g,i} = P_{g,i}^{0} + k_{p,i}\left(V_i^{0} - V_i\right), \qquad i \in B_{dc} \tag{2.3}$$

In contrast to (2.1), the active power of the DGs in the DC grid is regulated via local voltage measurement. The set-points of (2.1)–(2.3) can be adjusted using the MGCC in a short cycle. Note that unlike frequency droop control, because the voltage magnitude is different from bus to bus due to the line impedance, the reactive power and output of DGs in the DC grid cannot be shared accurately. Equations (2.1)–(2.3) are expressed with respect to the output power. In other words, the equations are formulated from the perspective of a grid feeding inverter, which measure its local voltage and frequency, and then calculate the reference of active and reactive power, as shown in Fig. 2.5.

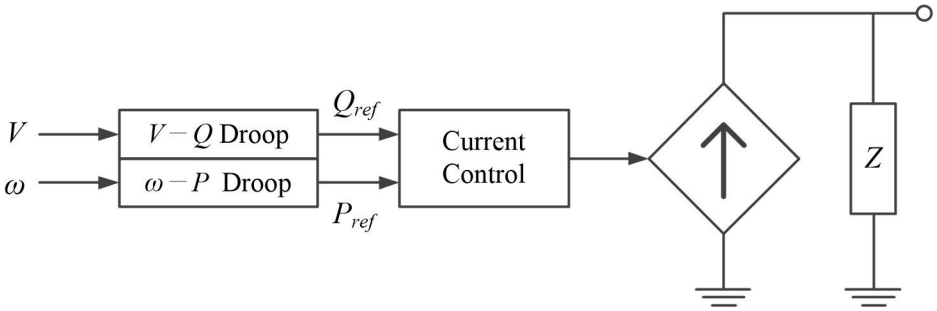

Fig. 2.5 Grid feeding inverter control type [17].

The grid feeding inverter acts as a current source based on the grid frequency and voltage generated by other sources. Meanwhile, inverters can also be controlled by the grid forming type. This type of inverter measures its active and reactive output power and then calculates the reference frequency and voltage magnitude, as shown in Fig. 2.6. It acts as a voltage source since the reference voltage is generated. In particular, at least one grid forming inverter should exist to generate the system voltage in islanded mode. The reference frequency and voltage magnitude of a grid forming inverter can be expressed as follows:

$$\omega_i = \omega^0 + \frac{1}{k_{p,i}}\left(P_{g,i}^0 - P_{g,i}\right), \qquad i \in B_{ac} \tag{2.4}$$

$$V_i = V_i^0 + \frac{1}{k_{q,i}}\left(Q_{g,i}^0 - Q_{g,i}\right), \qquad i \in B_{ac} \tag{2.5}$$

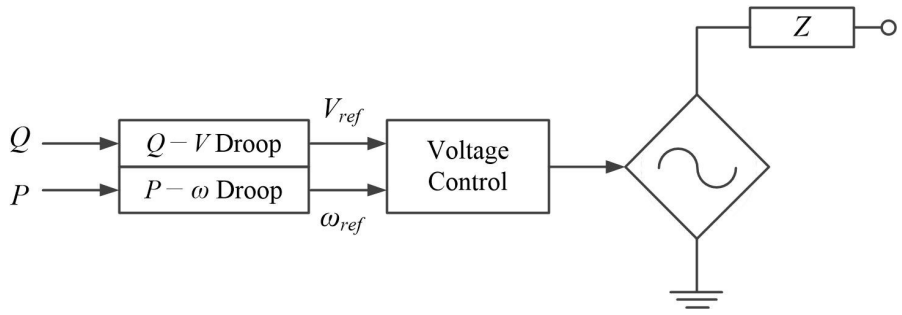

Fig. 2.6 Grid forming inverter control type [17].

The output frequency of DG i and j (ω_i and ω_j) can be different at short time range, but they converged to the same steady-state value by adjusting their output power. For the steady-state, the only difference between grid feeding and grid forming inverter is the reciprocal droop slope, and two inverter types operate well in parallel under the well-defined droop slope. Similar to the AC grid, the reference voltage of the grid-forming inverter DG in the DC grid can be expressed as

$$V_i = V_i^0 + \frac{1}{k_{p,i}}\left(P_{g,i}^0 - P_{g,i}\right), \qquad i \in B_{dc} \tag{2.6}$$

Thus, loss of generality, the relationship of the frequency–active power and voltage–reactive power in the AC grid and the voltage–active power in the DC grid can be expressed as (2.1)–(2.3).

The response time of DGs should be short enough to update the set-point in a short cycle. For conventional synchronous generators, the time constants of the valve actuator and diesel engine are generally in order of 0.05 seconds and 0.5 seconds, respectively [15]. To reach 98% of the output reference value, it takes four times of the largest time constant [18], and the synchronous generator takes about 2 seconds. On the other hands, the inverter-interfaced generator takes much less time. For the grid-side inverter, the switching frequency is about 10–20 kHz, and the bandwidths of the current controller, voltage controller, and low pass filter for measurement are reduced by 10% in order (it can be slightly different depends on the controller design). Thus, it takes several hundreds of milliseconds for the output to reach the reference value, which is suitable for adjusting the output power in a short cycle.

Battery energy storage system

The BESS is one of the key facilities to help construct and operate a microgrid. There are many different types of the energy storage system, such as super-capacitor, flywheel, compressed air system, Li-ion battery and NaS battery. Among them, Li-ion battery-based storage system is suitable for a microgrid, since it has high energy efficiency and density and it is eco-friendly and easy to commercialize. Typically, the functions of the BESS can be a frequency regulation, peak load shaving, RES smoothing, voltage support, uninterruptible power source, energy arbitrage, and so on. In a microgrid, the operation of the BESS is dependent on whether a microgrid is grid-connected or islanded mode, proximity to the RES, and current energy self-sufficiency. One of the most important feature of the BESS is bidirectional power flow. Thus, the output of BESS can be divided into discharge and charge powers and is expressed as

$$P_{b,i} = P_{b,i}^{dch} - P_{b,i}^{ch} \tag{2.7}$$

The superscripts *dch* and *ch* denote the discharge and charge powers, respectively. The positive output refers to the discharge like a generator, and the negative output refers to the charge like a load. By separating the discharge and charge variables, we can consider the discharge and charge efficiencies separately, and also consider the battery usage cost. The state of charge (SOC) variation of the BESS can be expressed as

$$\Delta SOC_{b,i} = -\frac{1}{E_{b,i}}\left(\frac{1}{\eta_{b,i}^{dch}}P_{b,i}^{dch} - \eta_{b,i}^{ch}P_{b,i}^{ch}\right)\Delta t_s \tag{2.8}$$

where η_b and E_b denote the energy efficiency and total capacity of the BESS, respectively, and Δt_s is the time interval at which output variation occurs. It is assumed that the output power keeps constant value for the short time Δt_s. The SOC significantly impacts the battery lifetime. It should be kept in a safe range (e.g. 20% to 90%), in addition, the amount of the BESS discharge and the SOC interval at which discharge occurs at one time are important factors of the BESS lifetime. Therefore, the SOC should be carefully managed for cost-saving operation.

Regarding the reactive power control, the droop control can be adopted or the set-point obtained from the scheduling algorithm can be kept for the scheduling time, whose objective is the voltage support. However, the reactive power is accompanied by the internal power loss due to the reactive current flow. In addition, it may result in the loss of the opportunity to increase the output active power since the operation range is limited with an apparent power rating. This phenomenon can also be applied to the preceding DGs. There are several researches considering the cost of the reactive power [19], [20]. They convert the adverse effect about the active power into the cost function. However, this effect is usually small and can be ignored [19].

Renewable energy source (RES)

The hosting capacity of the RES has been increasing with awareness of environmental issues, and the RES has become an important factor that must be considered for system operation. The two most typical RES is wind and photovoltaic

(PV) power. Their LC determines the output power from the ambient weather condition, but they can communicate with the MGCC to send their status and receive a reference output.

A variety of wind power configurations can be classified into four types depending on the speed control method and the usage of the power electronic devices. Among them, permanent magnetic synchronous generator-based wind power, with variable speed by full use of power electronics, is used recently because of their high efficiency, gearless construction, and light weight quality. In this case, the output of the wind turbine is given as [21]:

$$P_{wind} = \frac{1}{2}\rho\pi r^2 C_p v_w^3 \tag{2.9}$$

where ρ is the air density, r is the radius of the rotor blade, C_p is the power coefficient, and v_w is the wind speed. Fig. 2.7 shows the output power of the wind turbine against the wind speed. The output is zero when the wind speed is lower than cut-in speed v_{cl} and higher than cut-out speed v_{co} ($v_w<v_{cl}$ or $v_w>v_{co}$). If the wind speed is larger than v_{cl}, the output is determined by (2.9) which is shown as MPPT region. In (2.9), C_p is a function of the pitch angle and tip speed ratio, and they can be controlled for C_p to be set its maximum value. It means the output is maximum available power for given wind speed and it is called MPPT control. When the wind speed exceeds the rated value v_{rated}, the output is regulated to its rated value P_{rated}.

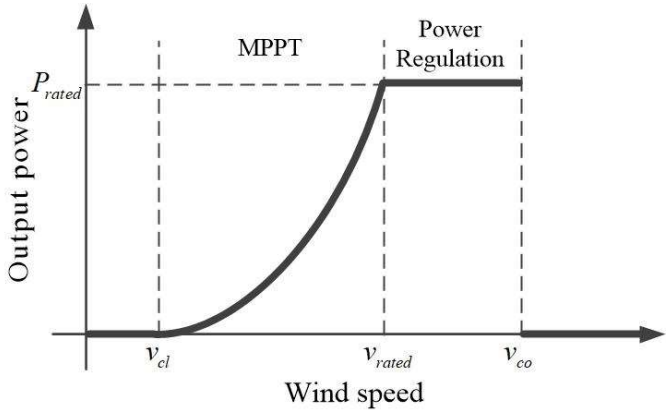

Fig. 2.7 Power curve for wind power [21].

The PV power is generated from a solar irradiance. This energy source is heavily time-dependent, but it is sustainable source and is readily available in most areas. In addition, there is little operation noise compared to wind power. Thus, the PV is rapidly spreading over the world recently, especially in small scale. In other words, it has a large portion of energy source of a microgrid. The solar irradiance makes the current in the PV system. The output current I_A of a PV array with N_P modules in parallel can be expressed as [22]:

$$I_A = N_P I_{SC,ref}\left[\left(\frac{S}{1000}\right)+\frac{J}{100}\left(T-T_{ref}\right)\right] \tag{2.10}$$

where $I_{SC,ref}$ is a short circuit current at reference irradiance and cell temperature, S is the irradiance, J is a temperature coefficient at short circuit current, T is a cell temperature, and T_{ref} is a reference cell temperature. The power of the DC system is the product of the voltage V_A and current I_A, and by substituting (2.10) to I_A and neglecting the temperature variation (second term on the right-hand side of (2.10)), the PV output can be given as follows:

$$P_{pv} = V_A I_A = V_A N_P I_{SC,ref}\frac{S}{1000} \tag{2.11}$$

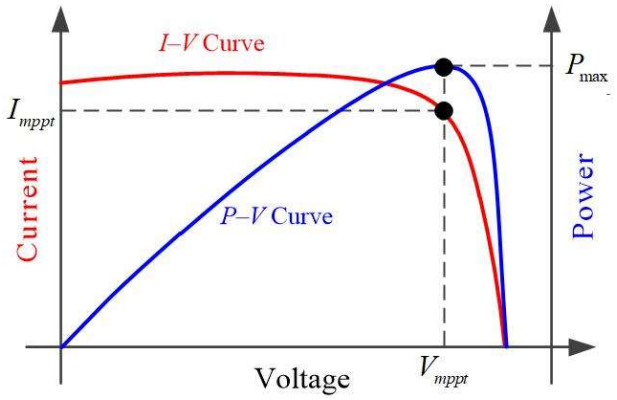

Fig. 2.8 Current and power of PV power against voltage [23].

Fig. 2.8 shows the principle of MPPT control of PV power. The PV operates on one point of *I–V* curve, and corresponding power is generated. If the voltage and

current of PV system is set V_{mppt} and I_{mppt}, respectively, the output power is maximized as $P_{\max}$, which is MPPT control of PV system. The current level is affected vertically by the solar irradiance. As the solar irradiance increases, more current can flow and it results in more output power.

Equations (2.9) and (2.11) are maximum available output power of wind and PV power, respectively. From the viewpoint of the system operator, they can be regarded as disturbances like the variation of load demand due to their intermittency, and they should be curtailed for the system security when it is necessary. Accordingly, the final output of the RES, including both wind and PV power, can be expressed by subtracting the curtailed output from the maximum available output as follows:

$$P_{r,i} = P_{r,i}^{MPPT} - P_{r,i}^{cur} \tag{2.12}$$

where the superscripts *MPPT* and *cur* represent the MPPT and curtailed outputs of the RES, respectively. Since the wind and PV power can perform MPPT control and reduce their output power in real-time when it is needed, the terminology, "RES", and (2.12) are used in later chapters regardless of whether it is wind or photovoltaic power.

2.2.2 Control of interlinking converter

The AC and DC grids are connected to each grid via the IC, which is the key component of the hybrid system. In grid-connected mode, the IC usually generates the DC voltage similar to the grid-forming inverter and keeps the voltage depending on the active power flow of IC and droop slope [24], [25]. The reactive power can be controlled to support only the AC grid. The active and reactive powers injected into the AC grid from the IC, which is connected to the AC bus *i* and DC bus *j*, can be expressed as

$$P_{IC,i} = P_{IC,i}^{0} + k_{pIC,i}\left(V_j^{0} - V_j\right) \tag{2.13}$$

$$Q_{IC,i} = Q_{IC,i}^{0} + k_{qIC,i}\left(V_i^{0} - V_i\right) \tag{2.14}$$

where k_{pIC} and k_{qIC} are the droop slopes of the IC for the active and reactive power, respectively.

In islanded mode, the IC functions as an energy transferring entity to alleviate the burden on a single grid due to sudden load changes. For this purpose, the normalized error–active power (*e–P*) droop control can be used to share the active power, such that [26]

$$P_{IC,i} = P_{IC,i}^{0} + k_{pIC,i}\left(e_j^0 - e_j\right) \tag{2.15}$$

where e_j is the error between the normalized frequency and DC voltage *j*. The normalized error, frequency and DC voltage *j* are expressed as follows [26]:

$$e_j = \hat{\omega} - \hat{V}_{dc,j} \tag{2.16}$$

where

$$\hat{\omega} = \frac{\omega - 0.5\left(\omega^{\max} + \omega^{\min}\right)}{0.5\left(\omega^{\max} - \omega^{\min}\right)} \tag{2.17}$$

$$\hat{V}_{dc,j} = \frac{V_{dc,j} - 0.5\left(V_{dc}^{\max} + V_{dc}^{\min}\right)}{0.5\left(V_{dc}^{\max} - V_{dc}^{\min}\right)} \tag{2.18}$$

The superscripts max and min denote the upper and lower limits, respectively. When the frequency in the AC grid decreases, the error e_j is negative and $P_{IC,i}$ is positive, implying that the DC grid helps the AC grid to balance the active power, and vice versa. This is illustrated in Fig. 2.9. The error bound e_B is calculated based on the maximum and minimum allowable value of the frequency and the DC voltage. For the same normalized error, more power flows through IC 2 since the rated power of IC 2 is larger than that of IC 1. The fundamental principle is equivalent to the droop control of DGs, which implies that ICs are also able to operate in parallel and their set-point can be adjusted.

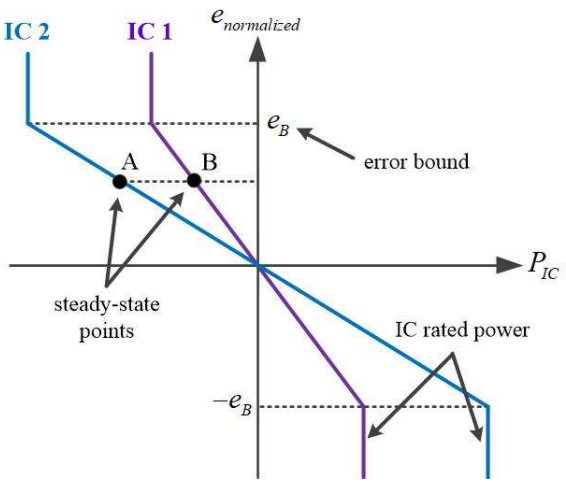

Fig. 2.9 *e–P* droop control of interlinking converter [26].

It is assumed that the active power exchanges by the same amount between the AC and DC grids given the high efficiency (the internal loss of the IC can be neglected.). Thus, the active power injected into the DC grid from the IC can be expressed as

$$P_{IC,j} = -P_{IC,i} \tag{2.19}$$

The reactive power is only concerned with the AC grid. Thus, like the grid connected mode, the control of the reactive power is same as (2.14) in islanded mode.

2.2.3 Static model of composite loads

Similar to the energy resources, there are various kinds of loads different characteristics in the system. The operator cannot consider each load characteristic, but their composite characteristics can be mathematically defined and then utilized for optimal operation. The AC loads can be represented in terms of the voltage dependency. The ZIP model, which is a typical static model, is employed in this dissertation. The letters Z, I, and P denote the constant impedance, constant current, and constant power loads, respectively. The active and reactive AC load demands can be expressed using the basic formulation of the ZIP model as follows:

$$P_{L,i} = P_{L,i}^{n}\left[z_{p,i}\left(\frac{V_i}{V_i^n}\right)^2 + i_{p,i}\left(\frac{V_i}{V_i^n}\right) + p_{p,i} \right], \quad i \in B_{ac} \tag{2.20}$$

$$Q_{L,i} = Q_{L,i}^{n}\left[z_{q,i}\left(\frac{V_i}{V_i^n}\right)^2 + i_{q,i}\left(\frac{V_i}{V_i^n}\right) + p_{q,i} \right], \quad i \in B_{ac} \tag{2.21}$$

where the superscript n represents the nominal value, and z_p, i_p, and p_p and z_q, i_q, and p_q are the ZIP coefficients of the active and reactive load demands, respectively. The sum of the ZIP coefficients in (2.20) and (2.21) must be equal to one, respectively. Note that the coefficients do not indicate the exact ratio of each load type (Z, I, and P). The coefficients are determined by fitting the characteristic of voltage magnitude and composite load demand near the voltage magnitude 1.0 p.u., so the coefficients may have negative values. Typically, the dependency of the reactive power is higher than active power due to the magnetic saturation of the motors [27]. The load bus or feeder of a microgrid can be classified into three types, residential, commercial, and industrial loads, and the coefficients representing each type can be experimentally obtained [28].

This static model can be utilized for the conservative voltage reduction, which is a technology for reducing energy consumption by decreasing the voltage magnitude while maintaining a safe voltage range and ensuring the normal operation of the loads. Since the coefficients are based on the combination of the number of the loads with different characteristics, they depend on the time of season and/or temperature. In addition, the load demands are influenced by the frequency. However, in grid connected mode, the entire transmission system determines the frequency that has a nearly nominal value under normal condition. In islanded mode, the frequency deviates but it can be restored quickly if the secondary control works well. Therefore, only the voltage dependency is considered in (2.20) and (2.21).

Similar to the AC load, the DC load can also be modeled with constant power, constant current, and constant resistance. Constant resistance loads can be directly incorporated into the system conductance matrix, so the DC load can be expressed

using the constant power and constant current load, such that

$$P_{L,i} = P_{L,i}^{n} + V_i I_{L,i}^{n}, \qquad i \in B_{dc} \tag{2.22}$$

where $I_{L,i}^{n}$ is the nominal current of the constant current load. Like the AC load, the DC load can be expressed using the ZIP model formulation, which means that the constant resistance load term is included in the load equation. However, the majority of the DC load is inverter-interfaced, and they usually require constant power or constant current, so (2.22) is used.

2.3 Technical issues on hybrid AC/DC microgrid

One major issue of the recent power system is the introduction of DC technology to the system. Initially, DC devices were connected to the AC grid via inverters, but as the number of DC devices increases and the awareness of the energy efficiency arises, the DC grid in which the energy is transmitted through the DC line has been being constructed recently. In the DC grid, there is no system frequency and reactive power flow. Frequency acts as a global variable, and it can be used to recognize the generation and load mismatch in the AC grid. However, in the DC grid, the DC voltage is used in a similar way, but it may not give accurate information because voltage magnitude is different in buses due to the line resistance. In addition, the voltage should be regulated by the active power. Since a HMG has characteristic of the AC and DC grids, the operation method should consider each grid properly.

A microgrid can be managed as one independent power system if they have their own operator. For the reliable and economic operation, the operator should analyze the system state such as frequency, voltage magnitude, and current, and should allocate the optimal output power to its energy resource. To this end, power flow methods and OPF methods of HMG for grid-connected and islanded mode have been developed using Newton-Raphson (NR) method like the conventional power system operation or other heuristic algorithms [29]–[33]. Regarding the power flow methods, modeling the VSC in a solvable formulation was performed considering various configurations. Especially in islanded mode, there is no slack bus and the power balance equation should be satisfied including the P–ω and Q–V droop control bus. The IC control mode should also be included in the power balance equation. It may result in the convergence problem depending on the droop coefficients and base quantities. To solve the aforementioned problem, some researches have proposed new power flow methods for islanded HMG using NR algorithm method, which can be extended to other applications using the linearization relationship.

High penetration level of RES raises a new issue for the OPF method due to the

high uncertainty. Because the size of the conventional power system is large and the penetration level of RES was not sufficiently high previously, the operation would have been performed well in a long cycle (e.g., 5 min or longer cycle). However, recently, the penetration level of RES has considerably increased, and a microgrid operator will operate a relatively small-sized system in which the uncertainty of the load demand is not likely to be offset [6]. In this situation, it would be more practical and effective to operate the system in a short cycle.

Fig. 2.10 shows an actual PV output power for one day in summer with different time step (1, 15, and 60 min). The PV outputs are generated at day time (around 06:00 to 19:00). The data of each time step are calculated as the time average of generated power over each time step. Therefore, the data of 60 min time step shows a little fluctuation over the time owing to the averaging effect. In 15 min data, the amount of fluctuation increases, and the data of 1 min time step shows severe fluctuation of the output power. The result for data fluctuation depends on the change of the weather condition over the time. If the weather condition such as precipitation and cloud data is rarely changed over the day time, the output power curves are almost same regardless of the time step. However, the weather conditions are in essence likely to fluctuate and even cannot be perfectly predicted. The real RES output data implies that if the optimal set-point of resources is calculated in a long cycle, the actual optimal values can differ between two consecutive points due to the high fluctuation of RES output power.

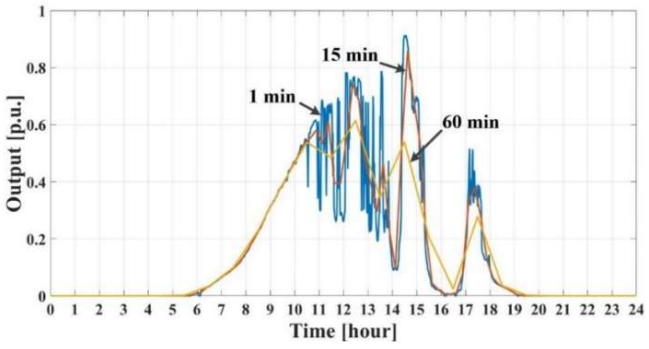

Fig. 2.10 PV output with 1, 15, and 60 min time step.

The aforementioned issues due to the high uncertainty of load and RES can cause different problems in grid-connected mode and islanded mode, respectively.

2.3.1 Feeder flow control for grid-connected mode

Except the microgrid planned as a standalone system, most microgrids are usually operated in grid-connected mode, and it is also applied to HMG. Recently, as the distributed energy resources reach a certain level of penetration, they have an impact on the overall steady-state and dynamic performance of the main grid. It reduces the system inertia and eventually the system becomes vulnerable to frequency [34]. If the microgrid is able to control the amount of the power flow from the main grid, it is considered as a controllable load from the viewpoint of the main grid and the impact on the main grid can be relieved. This is called feeder flow control (FFC). Since the load and RES output constantly change from the predicted value, the FFC should be conducted locally or MGCC sends the reference signal in a short cycle. Recently, instead of having the resources for frequency regulation, the TSO can maintain the frequency through the contract with the distributed system operator (DSO), which is called the power exchange for frequency control (PXFC). In this concept, the TSO and DSO contract the interface flow reference value and the allowable fluctuation band. Details of the contract method and process are currently being designed [35]. If the DSO participate in the PXFC, the contracted interface flow should be maintained within the band, otherwise a penalty will be imposed. Under the multi-microgrid in which each microgrid has its own operator like the DSO and they participate in the PXFC, the contract violation can affect the economic damage and the stability of the entire system. In this respect, a control method to tightly keep the feeder flow such as the FFC is needed.

Fig. 2.11 shows the basic FFC logic of a DG. The DG in front of the feeder measures the line flow P_{Line} locally. The line flow difference between the reference value $P_{Line,ref}$ and current value P_{Line} is injected to the PI controller which is

commonly used in industrial application for reference tracking. The PI controller makes the input zero if the measured value keeps constant and the controller gains are set properly. The output of the PI controller is added to P_{ref}. The power reference P_{ref} and Q_{ref} are determined from other control logic, which can be implemented in the MGCC. The line flow reference $P_{Line,ref}$ can be determined by the scheduling process based on the price of the main grid or the contract between the upper system operator and the microgrid operator.

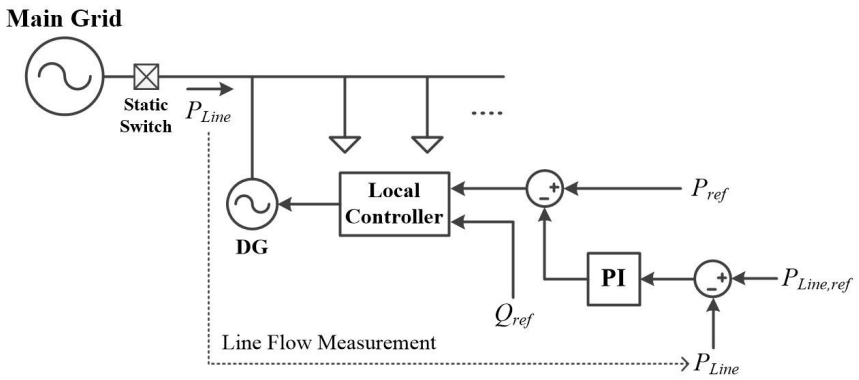

Fig. 2.11 Feeder flow control logic.

Using the simple control logic like Fig. 2.11, P_{Line} can be kept constant locally [36]. However, this control scheme is valid as long as the location of DG is in front of the feeder. Further, the total amount of injected line flow between the main grid and the microgrid should be measured. Depending on the microgrid configuration, the local FFC logic may not be performed well.

Fig. 2.12 shows the total of three microgrid configuration with different location of DGs. In Fig. 2.12(a), DGs are located at the front of each feeder. In this case, each DG can conduct FFC well because they can directly measure the total injected line flow of each feeder locally. However, DGs may be placed in the middle or end of feeder, as shown in Fig. 2.12(b). In this case, the load variation in front of the DGs cannot be compensated if the DGs conduct the FFC using local measurement. Thus, the load variations should be compensated in other ways using communication

system. Fig. 2.12(c) is similar to the case of Fig. 2.12(a), but other DGs are located in the end point of the feeder. If the front DGs conduct the FFC, only they have to compensate the entire variation in the microgrid and the DGs at the end cannot respond to the net load variation. This may cause severe burden of the DGs at the front. In addition, the microgrid can be a meshed or ring configuration as well as a radial configuration. In this case, controlling the amount of the line flow may not be effective because the power can be provided through other distribution lines. Therefore, power sharing method of upper controller such as MGCC is needed.

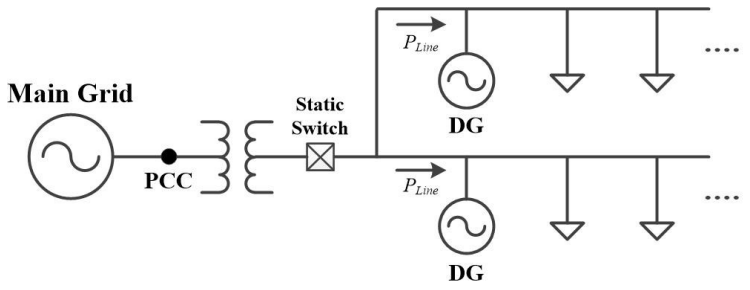

(a)

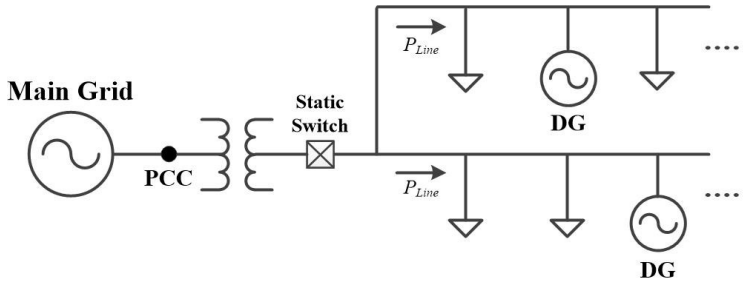

(b)

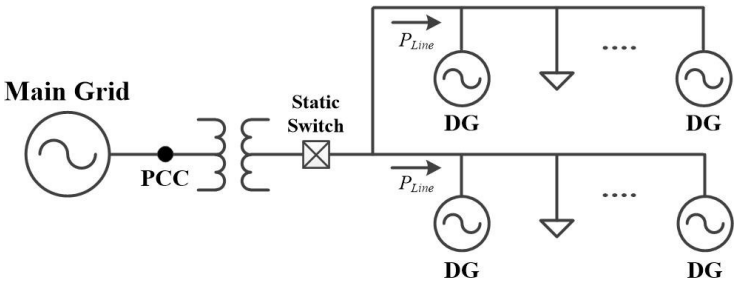

(c)

Fig. 2.12 Location of DGs for feeder flow control.

There have been several studies regarding the FFC. In [37], a simple one bus system was used to conduct the FFC. The radial system was divided into several areas, and the zone control architecture was applied in [36], [38]. However, the feeder flow sharing can be achieved only if the DGs are operated in parallel at the same bus, and it is also dependent on the location where the load fluctuation occurs. Moreover, in the case of HMG, the local control method of a DG in the DC grid is not simple due to the IC, unlike the control of a DG in the AC grid. Hence, the MGCC should allocate the output power at short time intervals. The ED was conducted to update the set-points of the DGs periodically, but real-time variation was compensated by the LC [36]. In [39], the total amount of the generation adjustment was distributed by the upper controller based on the participation factor of resources in real-time, but it only considered the availability of the resources. In the case of a multi-bus system and central operation, the loss variation as well as the net load variation should be considered and allocated to the DGs. In general, the variation of the network loss is modeled as a linear function in order to allocate the amount of generation or calculate locational marginal price. However, the network loss is naturally quadratic [40], [41]. To handle the internal variation accurately (which means the high performance of the FFC), the quadratic properties of the network losses should be considered.

2.3.2 Droop-based control for islanded mode

The inverter-interfaced DGs have been widespread in microgrids in virtue of the development of the power electronic technology. The conventional power system is operated based on the synchronous machine regardless of the system size, in which the continuous power mismatch is compensated by rotational energy of mechanical inertia of rotors, and then, electric output power changes in order to match the total load by sensing the frequency. The frequency response depends on mechanical inertia, but the steady-state frequency is determined by the droop control. Unlike

synchronous generators, inverters have no mechanical inertia. A microgrid composed only the inverter-interfaced DGs is called zero inertia system, in which the frequency can be set specific value because the inverters can change their output voltage angle instantaneously. In this system, in order for the DGs to perceive the power mismatch and share load demand, they mimic the droop control (2.1)–(2.3) thereby the frequency deviation is compulsorily made after the power mismatch occurred. From the viewpoint of steady-state, it is equivalent to the droop control of conventional synchronous machine-based system.

As the HMG has attracted considerable attention, there are many researches dealing with the control method of LCs in islanded mode [26], [42]–[44]. These researches have focused on the improvement of dynamics, accurate power sharing, seamless operation, and so on. The majority of these researches are based on the droop control, but the fundamental issues of the droop control is still remained. According to (2.1) and (2.2), the deviation of the frequency and voltage magnitude in the AC grid is proportional to the power deviation and reciprocal of the droop slopes as follow:

$$\Delta P_{g,i} = k_{p,i}\Delta\omega \tag{2.23}$$

$$\Delta Q_{g,i} = k_{q,i}\Delta V_i \tag{2.24}$$

Fig. 2.13 shows the description of the active power–frequency deviations. It is assumed that the initial operating point of a DG is A, P_A and ω_A. If the droop slope DS 1 is adopted, the operating point moves to B after the load demand increases by ΔP and the deviation in frequency becomes $\Delta\omega_B$. If the droop slope is DS 2, the operating point moves to C and it results in frequency deviation $\Delta\omega_C$. In other words, depending on the droop slope, the amount of the frequency deviation can be different although the same amount of the active power is required. The amount of the frequency deviation decreases as the droop slope becomes smoother (high k_p). However, a higher droop slope ensures better power sharing [45]. In addition, the droop slope affects the dynamic characteristic as well as the steady-state operating

point, and the small-signal stability is susceptible to droop slopes [46]. Therefore, the droop slope should be appropriately selected and it inevitably causes the frequency and voltage deviation. The Q–V droop in the AC grid and P–V droop in the DC grid have same trends.

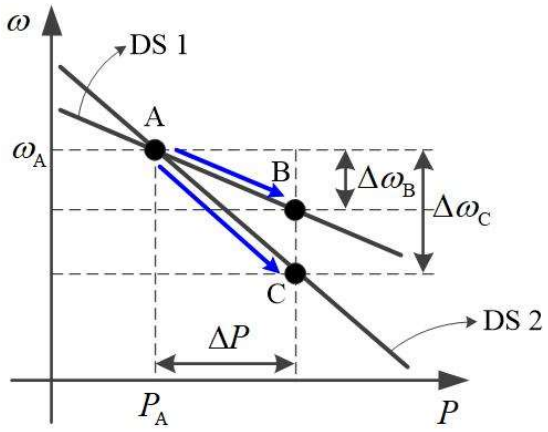

Fig. 2.13 Droop curve with different slope.

The deviations are restored to nominal values at the secondary control level. The frequency should be restored to avoid the high magnetizing currents in induction motors and transformers. In addition, extensive use of electric clocks and the use of frequency for other timing purposes require accurate maintenance of synchronous time [27]. From IEEE Standard 1547, the frequency is desired to be within the range planned for the island system. In addition, as long as the frequency is within the frequency range 59.3–60.5 Hz, DGs can be connected to the network and the reconnection to the main grid can take place [47]. Regarding the voltage magnitude, the load side voltage as well as the DG side voltage should be maintained for normal operation of voltage sensitive loads. By the decentralized or distributed manner, DGs use information of local or other adjacent DGs for restoration, but it may arise the voltage instability at the end of the feeder.

In addition to the frequency and voltage deviation, the output power also may be far from the optimal point that is obtained to reduce the generation cost. In

particular, a well-planned islanded microgrid (standalone microgrid) has sufficient energy resources to provide the energy to remote loads [48]. Since it has to supply the energy continuously while disconnected from the main grid, not only enhancing reliability but also reducing operation cost should be carefully considered. Hence, to this end, it is necessary to construct the operation methodology of MGCC.

The high penetration of RES makes the droop control action more frequent and significant due to high uncertainty. In [49], the frequency deviation was recovered via the LC and the power sharing at the specified ratio was performed by the MGCC using the low bandwidth communication. The method for alleviating the frequency and voltage deviation was proposed in [15], but the power sharing was not achieved in real-time. As uncertainties are inevitable in power systems, a fast and accurate supervisory control should be performed for a reliable and economic operation at short time intervals. The interaction between power dispatch and droop control in terms of the optimization time step and time horizon was analyzed for an isolated system [50]. For the HMG operation, the quasi real-time optimization problem was solved considering operation scenarios based on the advanced metering infrastructure data [32]. In [33], the droop-based small HMG was controlled with hierarchical structure, and the set-point of the IC was determined for economic operation with less computation and communication burden. However, they partially considered the frequency and voltage regulation and generation cost reduction; thus, a comprehensive control method under high uncertainty in islanded HMGs is needed.

So far, mathematical expressions of components in a HMG that can be used in MGCC have been provided, and the technical issues about operation of a HMG have been discussed. On the basis of these formulas and issues, the details of the proposed methods will be described in Chapters 3 and 4.

Chapter 3. Operation Methodology for Grid-Connected Mode

In grid-connected mode, since the main grid acts as an ideal voltage source, it helps to maintain the frequency and voltage magnitude within allowable range. Thus, the microgrid operator usually focuses on the economic operation. In addition to the economic operation, a microgrid should act as a controllable system to lessen the burden of the main grid and to carry out the contract. To obtain the economic operation and maintain the internal power balance, the base point and participation factor method can be a good operation methodology. The method is typically adopted for the conventional bulk power system because the practical implementation and control strategy of this method are quite simple. It is currently being researched for microgrids in both grid-connected and islanded mode [51]–[53]. The OPF whose objective function is to minimize the operation cost gives the base point of DGs and time scheduling of BESS. Between two consecutive base points, a participation factor method implements to adjust the generation. In grid-connected mode, because the frequency is determined by the main grid, the power sharing using the droop control may not be achieved properly. Further, it is difficult for DGs located on other buses to distribute their output power with the local FFC control. In other words, the internal power fluctuation should be handled using the MGCC. Therefore, a new generation adjustment method based on the participation factor is proposed in this chapter.

3.1 Modified Jacobian matrix for hybrid AC/DC microgrid

The steady-state characteristics of the generators, loads, and networks can be analyzed from their static model and power flow equation. The sensitivity matrix, which can be calculated from the Jacobian matrix in the NR power flow method, is mainly used in this dissertation. The conventional power flow method uses the bus models as slack, PV, and PQ bus. However, the sensitivity obtained from this method is valid under the condition that the active power variation is compensated on only the slack bus generator, and the reactive power variation is compensated on the slack and PV bus generators while keeping their voltage magnitude constant. In other words, the conventional method cannot reflect the power sharing and voltage magnitude adjustment, which are made possible using the droop control, and the frequency sensitivity cannot be calculated. In grid-connected mode, the droop coefficients are manipulated to mathematically represent the bus model. Thus, without loss of generality, we use the modified Jacobian matrix including the droop control bus, which can be expressed as

$$\begin{bmatrix} \Delta \boldsymbol{P}_{mis}^{ac} \\ \Delta \boldsymbol{Q}_{mis}^{ac} \\ \Delta \boldsymbol{P}_{mis}^{dc} \end{bmatrix} = \underbrace{\begin{bmatrix} \frac{\partial \boldsymbol{P}_{mis}^{ac}}{\partial \boldsymbol{V}^{ac}} & \frac{\partial \boldsymbol{P}_{mis}^{ac}}{\partial \omega} & \frac{\partial \boldsymbol{P}_{mis}^{ac}}{\partial \boldsymbol{\theta}} & \frac{\partial \boldsymbol{P}_{mis}^{ac}}{\partial \boldsymbol{V}^{dc}} \\ \frac{\partial \boldsymbol{Q}_{mis}^{ac}}{\partial \boldsymbol{V}^{ac}} & \frac{\partial \boldsymbol{Q}_{mis}^{ac}}{\partial \omega} & \frac{\partial \boldsymbol{Q}_{mis}^{ac}}{\partial \boldsymbol{\theta}} & \frac{\partial \boldsymbol{Q}_{mis}^{ac}}{\partial \boldsymbol{V}^{dc}} \\ \frac{\partial \boldsymbol{P}_{mis}^{dc}}{\partial \boldsymbol{V}^{ac}} & \frac{\partial \boldsymbol{P}_{mis}^{dc}}{\partial \omega} & \frac{\partial \boldsymbol{P}_{mis}^{dc}}{\partial \boldsymbol{\theta}} & \frac{\partial \boldsymbol{P}_{mis}^{dc}}{\partial \boldsymbol{V}^{dc}} \end{bmatrix}}_{J_{new}} \begin{bmatrix} \Delta \boldsymbol{V}^{ac} \\ \Delta \omega \\ \Delta \boldsymbol{\theta} \\ \Delta \boldsymbol{V}^{dc} \end{bmatrix} \tag{3.1}$$

where $\boldsymbol{\theta}$ is the voltage angle vector, excluding the angle reference bus, and J_{new} is the modified Jacobian matrix for a HMG. To avoid confusion, the superscript *ac* and *dc* are used to represent the AC and DC quantities in (3.1), respectively. Note that the linkage between the AC and DC grids is affected by the control logic of the IC. The mismatch vector of active and reactive power is as follows:

$$\boldsymbol{P}_{mis} = \boldsymbol{P}_{gen} + \boldsymbol{P}_{IC} - \boldsymbol{P}_{L} - \boldsymbol{P} \tag{3.2}$$

$$\boldsymbol{Q}_{mis} = \boldsymbol{Q}_{gen} + \boldsymbol{Q}_{IC} - \boldsymbol{Q}_{L} - \boldsymbol{Q} \tag{3.3}$$

where bold expression refers to the vector expression, and $\boldsymbol{P}$ and $\boldsymbol{Q}$ are the injected active and reactive power vector, respectively. The subscript *gen* includes the DG, BESS, and RES. Equation (3.2) can be applied to both the AC and DC grids. For the purpose of generalization, buses that are not connected to the generator, IC, and loads have the corresponding term as zero. The mathematical equation of DG, BESS, RES, IC, and loads are provided in Chapter 2, and the injected active and reactive power flow equation of bus *i* in the AC grid can be expressed as [54]

$$P_i = \sum_j V_i V_j \left[G_{ij} \cos\theta_{ij} + B_{ij} \sin\theta_{ij} \right] \tag{3.4}$$

$$Q_i = \sum_j V_i V_j \left[G_{ij} \sin\theta_{ij} - B_{ij} \cos\theta_{ij} \right] \tag{3.5}$$

where G_{ij} and B_{ij} are real and imaginary part of the (i,j) entry of the AC admittance matrix.

Similar to the AC grid, the power flow equation of bus *i* in the DC grid can be expressed as

$$P_i = \sum_j G_{ij} V_i V_j \tag{3.6}$$

where G_{ij} is the (i,j) entry of the DC conductance matrix.

By adjusting the droop slope, the conventional bus model (slack, PV, and PQ) can be mathematically represented. Fig. 3.1 shows the active power–frequency and reactive power–voltage magnitude with different droop slope. If the droop slope is zero (Line A and D), it represents the constant output power regardless of the frequency or voltage magnitude, which implies that the bus can be regarded as a PQ bus if both k_p and k_q are zero. If the droop slope is infinite (Line B and E), the output is determined to be set the frequency and voltage magnitude to their set-point. In other words, if k_p is zero and k_q is infinite, the bus can be regarded as a PV bus. For the slack bus, both k_p and k_q are infinite. Based on the modified Jacobian matrix and droop slope adjustment, the steady-state characteristics of the frequency, voltage,

and active and reactive output power can be identified. A similar method is applied to the DC grid.

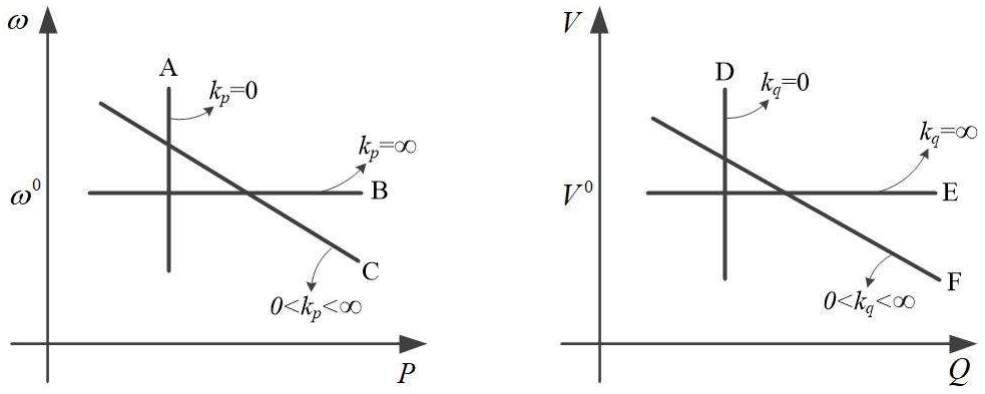

Fig. 3.1 *P–ω* and *Q–V* droop curve by slope.

3.2 Generation-load incremental cost

In grid-connected mode, the system operator usually focuses on the economic operation. For this purpose, the incremental cost which can be defined based on the cost function is a criterion for allocating the output power of DGs. Meanwhile, since the BESS is capable of discharging energy only to the amount of energy previously charged and SOC level should be within a safe range, the operation of BESS is generally scheduled. The scheduling method of BESS for grid-connected microgrid has been studied in [55]–[57]. The BESS initially made with the purpose of frequency regulation or RES output smoothing is allowed to change its output power constantly; however, for general, the frequent output change leads to the reduction of BESS lifetime. It may be better to operate as scheduled despite of the disturbance. Therefore, the output adjustment corresponding to the real-time load fluctuation is applied to DGs except BESSs.

The increase and decrease in the RES output power are equivalent to the decrease and increase of the load demand from the viewpoint of the bus-injected power, respectively. In other words, RESs can be regarded as negative loads [58]. Therefore, here, the load variation contains both the load consumption and output of RES variation.

3.2.1 Concept of GLIC

Our objective is to minimize the total generation cost while maintaining the internal power balance. If the total number of the DGs is m, the total generation cost can be expressed as

$$C = \sum_{i=1}^{m} C_i(P_{g,i}) \tag{3.7}$$

where c_2, c_1, and c_0 are the coefficients of the quadratic cost function, C_i is a generation cost function for the ith DG, which is a function of its own output power,

$P_{g,i}$, and is commonly modeled as a quadratic function:

$$C_i = c_{2,i}P_{g,i}^2 + c_{1,i}P_{g,i} + c_{0,i} \tag{3.8}$$

To determine the output of the generators for minimizing the total generation cost, incremental cost can be used [7]. The conventional incremental cost of the *i*th DG including line loss can be expressed as

$$\lambda_i = pf_i \frac{\partial C_i}{\partial P_{g,i}} \tag{3.9}$$

where

$$pf_i = \left(1 - \frac{\partial P_{loss}}{\partial P_{g,i}}\right)^{-1} \tag{3.10}$$

and P_{loss} is the line loss.

In (3.9), incremental cost includes pf_i, which is the penalty factor. This factor represents the effect of the generator on line loss. If an increase in the generation results in a negative effect on line loss, the incremental cost is higher than the cost arrived at considering only the cost change, and the generator is deemed more expensive. If line loss is neglected, the penalty factor is one, and only the cost function is considered.

Line loss can be expressed as a function of bus-injected power or generator output power [59], [60], and loss sensitivity, $\partial P_{loss}/\partial P_{g,i}$, can be directly calculated by differentiating the line loss. However, to change the output power of a generator, a variation of other power changes should exist in order to maintain the power balance. Even if the output of the *i*th generator is changed by the same amount, the amount of line loss change could differ depending on the buses where the injected power changes because line loss is determined by line current, which depends on the bus-injected power. In addition, the methods to calculate the loss sensitivity in [59] and [60] need the network impedance matrix. However, it can be obtained only if the network includes shunt elements [61]. Moreover, the loss sensitivity in (3.10) is considered as a constant, but its value also varies with bus-injected power. Therefore,

the conventional participation factor derived by the incremental cost (3.9) may result in an operating point that is not close to the optimal point.

Fig. 3.2 shows the conceptual diagram of the power flow change for load variation. DG 1 is assumed to compensate all load changes in order to figure out the effect of its output change. In Fig. 3.2(a), the load at bus 3 changes by ΔP_L, and the line loss change may be small since the DG 1 and bus 3 is close. On the other hand, in Fig. 3.2(b), the load at bus 5 which is relatively far from DG 1 changes by the same amount, and it may result in the high line loss change. In other words, although DG 1 compensates the same amount of the load change, the output power change of DG 1 may differ depending on the load location. The conventional loss sensitivity considers only the generator, but from the situations in Fig. 3.2, it cannot be expressed only one value and cannot accurately reflect the output and corresponding cost change.

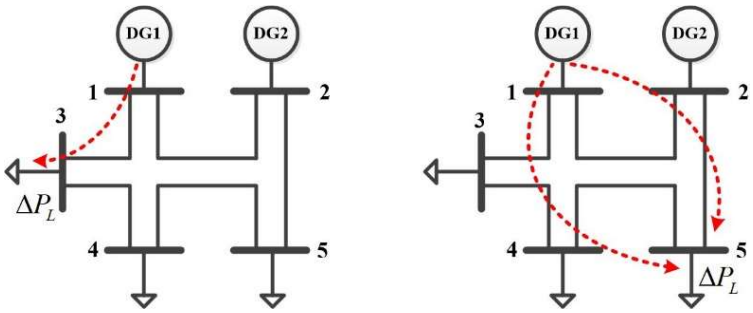

(a) (b)

Fig. 3.2 Concept of power flow by load location.

Hence, more economical operations could be achieved if incremental cost and the following participation factor more accurately reflect the line loss. For this reason, the GLIC is introduced as a derivative of the total cost with respect to the load demand. For an accurate calculation of the cost variation, the specific generator that compensates for the load change and the consequent loss change should be selected. Thus, the GLIC is the cost variation for a generator and a load pair. From section 3.1,

the specific generator that compensates the load fluctuation can be mathematically expressed by adjusting the droop slope. Thus, the generator like the slack bus for calculating GLIC is called “responsible generator”.

3.2.2 Calculation of GLIC and its derivative

Calculation of GLIC

If the load and generation of the *j*th bus change and the *i*th generator is selected as the responsible generator, the output power change of the *i*th generator considering the line loss change can be expressed as follows [62]:

$$\Delta P_{g,i} = \psi_j^i \times \Delta P_{L,j} \tag{3.11}$$

$$\Delta P_{g,i} = -\psi_j^i \times \Delta P_{g,j} \tag{3.12}$$

where

$$\psi_j^i = 1 - \frac{\partial P_{loss}{}^i}{\partial P_j} \tag{3.13}$$

and $\partial P_{loss}{}^i/\partial P_j$ is the loss sensitivity with respect to the *j*th bus-injected power when the *i*th generator is selected as the responsible generator. This generator can be artificially selected in order to know the effect of each generator on the load variation. The meaning of ψ_j^i is the effective power variation gain of the *j*th bus-injected power from the point of the *i*th bus. Calculation of the loss sensitivity with a conventional single slack model based on the chain rule was introduced in [63]. The method can be extended to the HMG with modifications, and the loss sensitivity can be expressed as follows:

$$\frac{\partial P_{loss}}{\partial P_{mis,i}} = \sum_j \frac{\partial P_{loss}}{\partial X_j} \frac{\partial X_j}{\partial P_{mis,i}} \tag{3.14}$$

where

$$\boldsymbol{X} = \left[\boldsymbol{V}^{ac}, \omega, \boldsymbol{\theta}, \boldsymbol{V}^{dc} \right] \tag{3.15}$$

$$P_{loss} = \sum_{i \in B_{ac}} P_i + \sum_{i \in B_{dc}} P_i \tag{3.16}$$

X_j is the jth entry of $\boldsymbol{X}$ and $P_{mis,i}$ is the ith entry of $\boldsymbol{P}_{mis}$.

Using the new Jacobian matrix J_{new}, (3.14) can be re-formulated as follows:

$$\begin{bmatrix} \frac{\partial P_{loss}}{\partial \boldsymbol{P}_{mis}^{ac}} \\ \frac{\partial P_{loss}}{\partial \boldsymbol{Q}_{mis}^{ac}} \\ \frac{\partial P_{loss}}{\partial \boldsymbol{P}_{mis}^{dc}} \end{bmatrix} = \left[\left(J_{new} \right)^T \right]^{-1} \begin{bmatrix} \frac{\partial P_{loss}}{\partial \boldsymbol{V}^{ac}} \\ \frac{\partial P_{loss}}{\partial \omega} \\ \frac{\partial P_{loss}}{\partial \boldsymbol{\theta}} \\ \frac{\partial P_{loss}}{\partial \boldsymbol{V}^{dc}} \end{bmatrix} \tag{3.17}$$

The loss sensitivity obtained from (3.17) represents the loss change after the power balance is maintained according to the DGs' control logic. For the conventional method using the loss sensitivity, the main grid is modeled as the slack bus. This gives the loss sensitivity for each situations. However, our objective is to identify the effect of the responsible generator. This can be achieved by designating one DG to compensate for the load variation. By doing so, J_{new} is changed since it is composed of the DGs control logic, and thereafter, the loss sensitivity is also changed. To indicate the effect of the ith DG, the superscript i is added to the loss sensitivity (i.e. $\partial P_{loss}{}^i / \partial P_j$).

To determine the amount of generation adjustment, the total generation cost is differentiated with the load demand on the condition that the responsible generator is selected. The total generation cost, (3.7), is only a function of the generator output power. However, using (3.11), which represents the relationship between load demand and generation, the total cost can be differentiated by the load demand. The GLIC of the ith generator for the jth load is expressed as follows:

$$\lambda_j^i = \frac{\partial C}{\partial P_{L,j}} = \psi_j^i \frac{\partial C_i}{\partial P_{g,i}} \tag{3.18}$$

Because both the generation and load are considered in (3.18), more economic generators for each load can be known at a specific operating point.

Calculation of GLIC derivative

The GLIC is used as the criterion for determining the amount of generation adjustment. The GLIC represents the effect of the generator on the total cost, and its value varies with network conditions such as the level of the load demand and generation. Therefore, a GLIC derivative is used to predict the variation of this criterion and achieve the desired value.

If the load changes, not only the responsible generator but also the other generators can adjust their output power. The output power of the responsible generator is adjusted to maintain the power balance by responding to the other bus-injected power changes; this adjustment is already reflected in (3.11) and (3.12). Therefore, we should calculate the derivative of the GLIC with respect to all the loads and generators. The derivatives of the GLIC with respect to the *k*th load and generation are as follows, respectively:

$$\frac{\partial \lambda_j^i}{\partial P_{L,k}} = \frac{\partial^2 C_i}{\partial P_{g,i}^{\ 2}} \psi_j^i \psi_k^i + \frac{\partial C_i}{\partial P_{g,i}} \frac{\partial^2 P_{loss}}{\partial P_j \partial P_k}^{\ i} \tag{3.19}$$

$$\frac{\partial \lambda_j^i}{\partial P_{g,k}} = -\frac{\partial^2 C_i}{\partial P_{g,i}^{\ 2}} \psi_j^i \psi_k^i - \frac{\partial C_i}{\partial P_{g,i}} \frac{\partial^2 P_{loss}}{\partial P_j \partial P_k}^{\ i} \tag{3.20}$$

The derivative of GLIC with respect to load demand, (3.19), is directly obtained by differentiating (3.18), and that with respect to the generation, (3.20), has the same formula as (3.19) with the opposite sign because (3.11) and (3.12) differ only in sign. Moreover, loss sensitivity is changed with the operating point. Hence, both (3.19) and (3.20) contain the second-order loss sensitivity. Similar to (3.14), the second-order loss sensitivity can be calculated based on the chain rule for the second-order derivative with multiple variables (faá di Bruno's formula) [64], such that

$$\frac{\partial^2 P_{loss}}{\partial \boldsymbol{X}^2} = \boldsymbol{A} + J_{new}^T \frac{\partial^2 P_{loss}}{\partial \boldsymbol{Y}^2} J_{new} \tag{3.21}$$

where

$$\boldsymbol{Y} = \left[\boldsymbol{P}^{ac}, \boldsymbol{Q}^{ac}, \boldsymbol{P}^{dc} \right] \tag{3.22}$$

$$\boldsymbol{A}(i,j)=\left(\frac{\partial P_{loss}}{\partial \boldsymbol{P}^{ac}}^{T}\quad\frac{\partial P_{loss}}{\partial \boldsymbol{Q}^{ac}}^{T}\quad\frac{\partial P_{loss}}{\partial \boldsymbol{P}^{dc}}^{T}\right)\frac{\partial}{\partial X_i}J_{new,j} \tag{3.23}$$

Here, $J_{new,j}$ denotes the jth column vector of J_{new}. To calculate $\partial^2 P_{loss}/\partial \boldsymbol{X}^2$ and $\partial J_{new,j}/\partial X_i$, the second-order derivatives of power flow equation should be calculated. It can be easily obtained by differentiating the power flow equation twice, and the details are provided in Appendix A. The first column of right-hand side of (3.23) (first-order loss sensitivity) is obtained from (3.17), so $\partial^2 P_{loss}/\partial \boldsymbol{Y}^2$ can be calculated by simply rearranging (3.21).

In general, the IC controls the DC side voltage as a constant (nominal value) in grid-connected mode. In this case, although the DG in the DC grid acts as the responsible generator, the active power of the DGs in the AC grid may fluctuate in order to keep the IC's DC side voltage constant. To prevent this phenomenon and to accurately calculate the GLIC, the droop control equation, (2.3), is slightly modified to virtually represent the constant DC side voltage of IC and responsible generator for only DG in the DC grid. When the IC is connected to the jth bus of the DC grid, the output of the ith DG in the DC grid as the responsible generator can be expressed as follows:

$$P_{g,i}=P_{g,i}^{0}+k_{p,i}\left(V_j^{0}-V_j\right),\qquad i\in B_{dc} \tag{3.24}$$

Note that (3.24) is not the actual output equation of DG i, but it is temporarily modified equation to obtain the GLIC and its related values. Fig. 3.3 shows the calculation process for all values associated with GLIC. The total number of DGs is m. By designating all the DGs one by one as the responsible generator, all the effective power variation gains, GLICs, and derivatives of GLIC can be obtained. In this process, the obtained values in Fig. 3.3 are dependent on the reactive power control mode. In grid-connected mode, the reactive power is generally controlled as a constant output power or a constant bus voltage [13], [31]. If the reactive power of a DG is constant, k_q is zero, and if the bus voltage magnitude of a DG is constant, k_q is infinite. All the obtained values are calculated based on the Jacobian matrix whose

values are dependent on the droop coefficients k_q. Thus, the reactive power control mode should be identified. In addition, the base point should also be calculated considering the reactive power control mode. If k_q is infinite, the voltage constraints referring to the constant voltage magnitude should be included, and if k_q is zero, there is no constraint to keep the voltage magnitude constant, when base point is calculated.

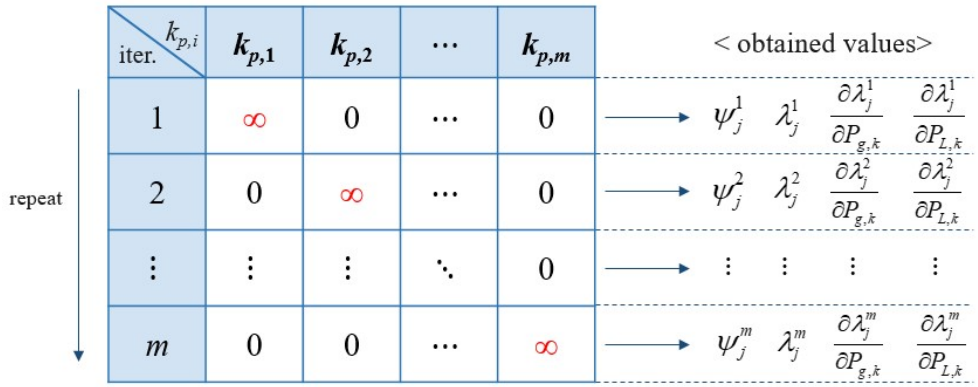

Fig. 3.3 Calculation process for all values associated with GLIC.

3.3 Participation factor-based generation adjustment

3.3.1 Bus-dependent participation factor

Our objective is to adjust the DGs' output power from the base point which can be determined by the generation optimization process whose objective function is generation cost minimization. At the base point, the incremental costs of all generators not operating at their output limits are equal (i.e. equal incremental cost). This property can be applied to the GLIC because the GLIC also indicates the amount of cost variation on the condition that both a generator bus and a load bus are selected. In other words, the GLIC with respect to the same load bus is the same regardless of the DG selection at the optimal base point.

When the load demand of bus r changes, the DGs share the amount of the change and adjust their output power to maintain the power balance. The additional output power of the ith DG can be expressed as follows:

$$\Delta P_{g,i} = \alpha_{i,r} \times \psi_r^i \times \Delta P_{L,r} \tag{3.25}$$

where $\alpha_{i,r}$ denotes the bus-dependent participation factor (BDPF) of the ith DG with respect to bus r. To precisely account for the effective load variation from the ith DG position, ψ^i_r is considered in (3.25). The BDPF is a type of participation factor whose value depends on the load location because the effect of load change on generation cost could differ. The BDPF satisfies the following equation:

$$\sum_{i=1}^{m} \alpha_{i,r} = 1 \tag{3.26}$$

Using the equal incremental cost property with GLIC, the BDPF can be obtained. After the DGs respond to the load change, the variation of the GLIC of the ith DG for the rth load can be calculated using (3.19) and (3.20), such that

$$\Delta \lambda_r^i = \frac{\partial \lambda_r^i}{\partial P_{L,r}} \times \Delta P_{L,r} + \sum_{k=1}^{m} \frac{\partial \lambda_r^i}{\partial P_{g,k}} \times \Delta P_{g,k} \tag{3.27}$$

In addition to the effect of the load change (first term on the right-hand side of (3.27)), the effects of the other DGs (second term on the right-hand side of (3.27)) should be considered. Substituting (3.25) into (3.27) yields

$$\Delta\lambda_r^i = \Delta P_{L,r}\left(\frac{\partial\lambda_r^i}{\partial P_{L,r}} + \sum_{k=1}^{m}\frac{\partial\lambda_r^i}{\partial P_{g,k}} \times \alpha_{k,r} \times \psi_r^k\right) \tag{3.28}$$

After the DGs share the load change and reach a new operating point, all GLIC for bus r should be set to the same value for optimality, which is analogous to the equal incremental cost method; this can be achieved by satisfying the following equation:

$$\Delta\lambda_r^1 = \Delta\lambda_r^2 = \cdots = \Delta\lambda_r^{m-1} = \Delta\lambda_r^m \tag{3.29}$$

By substituting (3.28) into (3.29), $\Delta P_{L,r}$ can be removed since they exist in all terms. Therefore, the only unknown variables are $\alpha_{k,r}$. From (3.29), it is possible to choose m–1 independent equations, and we choose these equations using the following sequence:

$$\Delta\lambda_r^1 = \Delta\lambda_r^i, \qquad i=2,\cdots,m \tag{3.30}$$

An additional equation relating the $\alpha_{k,r}$ variables from (3.26) is added, and a total of m equations, (3.26) and (3.30), are rewritten in matrix form as shown in (3.31). The BDPF with respect to bus r can be calculated by taking the inverse transform of the matrix in (3.31). Since bus r is arbitrarily selected, we can calculate the BDPF at all buses by replacing r with other buses. To take the inverse transform of the square matrix in (3.31), the matrix should be nonsingular. If the cost function is quadratic and the quadratic coefficient is nonzero, the square matrix is usually nonsingular. In other words, the generator cost function as linear or piecewise linear model may not give the BDPF. However, the quadratic cost function is most commonly used [7], and the conventional participation factor method also requires nonzero quadratic coefficients; thus, the quadratic model is adopted in this dissertation. The proof is provided in Appendix B.

$$\begin{pmatrix} \psi_r^1\left(\frac{\partial\lambda_r^2}{\partial P_{g,1}}-\frac{\partial\lambda_r^1}{\partial P_{g,1}}\right) & \cdots & \psi_r^m\left(\frac{\partial\lambda_r^2}{\partial P_{g,m}}-\frac{\partial\lambda_r^1}{\partial P_{g,m}}\right) \\ \vdots & \ddots & \vdots \\ \psi_r^1\left(\frac{\partial\lambda_r^m}{\partial P_{g,1}}-\frac{\partial\lambda_r^1}{\partial P_{g,1}}\right) & \cdots & \psi_r^m\left(\frac{\partial\lambda_r^m}{\partial P_{g,m}}-\frac{\partial\lambda_r^1}{\partial P_{g,m}}\right) \\ \hline 1 & \cdots & 1 \end{pmatrix} \begin{pmatrix} \alpha_{1,r} \\ \vdots \\ \alpha_{m,r} \end{pmatrix} = \begin{pmatrix} \frac{\partial\lambda_r^1}{\partial P_{L,r}}-\frac{\partial\lambda_r^2}{\partial P_{L,r}} \\ \vdots \\ \frac{\partial\lambda_r^1}{\partial P_{L,r}}-\frac{\partial\lambda_r^m}{\partial P_{L,r}} \\ \hline 1 \end{pmatrix} \tag{3.31}$$

So far, a method for finding the BDPF to minimize the total generation cost is introduced. In practice, load variation usually occurs at several buses simultaneously. Therefore, it is necessary to add the individual values of additional output power from each load variation. The generation adjustment value of the *i*th DG can be expressed as follows:

$$\Delta P_{g,i} = \sum_{j \in B_{ac} \cup B_{dc}} \alpha_{i,j} \times \psi_j^i \times \Delta P_{L,j} \tag{3.32}$$

3.3.2 Handling operation constraints

After determining the amount of generation adjustment from (3.32), it should be checked whether the operation constraints are satisfied. There are some major constraints that should be considered in power system operation. Among them, generation output constraint is handled in this dissertation. Regarding voltage constraints, the main grid can be considered as an ideal voltage source with constant voltage magnitude, which helps to maintain the voltage magnitude. In addition, the major uncertainty is active power fluctuation due to the RES output, but the voltage is regulated via reactive power control in medium voltage level system. In the DC grid, the active power is directly related to the voltage, but the IC controls the DC side voltage as nominal value and the voltage violation is not likely to happen; thus, the voltage constraints are not considered. For line flow violation, it rarely occurs under normal condition if the system is well-designed [65]. The violation usually happens when generator or line faults occur, and it can be handled when the base

point is calculated. In addition, DGs can technically relieve the distribution congestion [66]. Thus, it is not considered in this dissertation. Since the proposed method is the active power adjustment, only the method for handling the violation of the generation output limits is considered.

Generation output constraints

The DGs participating generation adjustment should have sufficient output margin for both upper and lower in grid-connected mode. However, under the high uncertainty, they may reach their output limits due to the sudden change of weather condition or load demand. To operate the DGs within their output limits, the amount of generation adjustment should satisfy following inequality condition:

$$P_{g,i}^{\min} - P_{g,i}^{base} \le \Delta P_{g,i} \le P_{g,i}^{\max} - P_{g,i}^{base} \tag{3.33}$$

The superscripts *base* represents the base point values.

If the adjusted output power of some DGs violates constraint (3.33), the amount of violation should be re-distributed to other compliant DGs. From the viewpoint of the compliant DGs, this violation is equivalent to load variation of the buses where the non-compliant DGs are connected. In other words, the violation can be regarded as an increase or decrease of the loads by the amount of violation. Therefore, the re-distribution process can be similar to the previous method. If *i* and *j* are bus indices of the compliant DG and the non-compliant DG, respectively, the new adjusted output power of the *i*th DG can be expressed by

$$\Delta P_{g,i}^{new} = \Delta P_{g,i}^{old} + \sum_{j} \beta_{i,j} \times \psi_{j}^{i} \times P_{g,j}^{excess} \tag{3.34}$$

where

$$\Delta P_{g,j}^{excess} = \begin{cases} \Delta P_{g,j}^{old} + P_{g,j}^{base} - P_{G,j}^{\max}, & j \in G_{\max} \\ \Delta P_{g,j}^{old} + P_{g,j}^{base} - P_{G,j}^{\min}, & j \in G_{\min} \end{cases} \tag{3.35}$$

The superscript *old* represents the last values causing violation, $\beta_{i,j}$ is a new BDPF of DG *i* with respect to bus *j*, and $G_{\max}$ and $G_{\min}$ are the sets of the DGs that exceed their upper and lower output limits, respectively. The new BDPF is calculated by

excluding non-compliant DGs and conducting the previous procedure. The amount of violation is re-distributed on basis of the new BDPF and added to the previous generation adjustment value. The new adjusted output power of non-compliant DG j is set to its limit value:

$$\Delta P_{g,j}^{new} = \begin{cases} P_{g,j}^{\max} - P_{g,j}^{base}, & j \in G_{\max} \\ P_{g,j}^{base} - P_{g,j}^{\min}, & j \in G_{\min} \end{cases} \tag{3.36}$$

If the adjusted output power of DG i violates the output limits, the DG should be included in $G_{\max}$ or $G_{\min}$, and the new amount of violation should be re-distributed to the remaining compliant DGs. By repeating this process until all DGs operate within the output limits, we obtain a feasible solution for the adjusted DG output power.

Note that the principle of equal incremental cost holds only if the value with the constraint does not reach its boundary; this principle is also applicable to the GLIC. With respect to the output constraints, the GLIC for the same load is still equal for DGs that are not operating at their upper or lower limits and this feature is utilized.

Although the generation is adjusted considering the line loss variation using the loss sensitivity, a minor power imbalance may be still remain owing to the usage of the derivatives. The minor imbalance would be compensated by the main grid. However, the amount of the imbalance is small enough to have little effect on the main grid because more accurate first and second-order loss sensitivity are used. Thus, it is unnecessary to find an exact feasible solution in which the DGs perfectly compensate for the internal net load variations in this process. Likewise, if the imbalance is compensated by DGs using other control method such as FFC, the results are almost similar.

Fig. 3.4 shows the flow chart of the proposed method for grid-connected mode. The proposed method is based on the base point and participation factor method. Thus, initially the base point should be calculated by the OPF for cost minimization. At the base point, using all values associated with GLIC, the BDPF of all buses is calculated by (3.31). Then, the net load variation of buses is measured and generation

is adjusted using (3.32). If the generation output violates its output limits, the re-distribution process is conducted and the MGCC sends the amount of the updated generation to the DGs. The measurement and generation adjustment are repeated using the BDPF that is calculated once at the base point. When the base point is updated, the BDPF can also be updated.

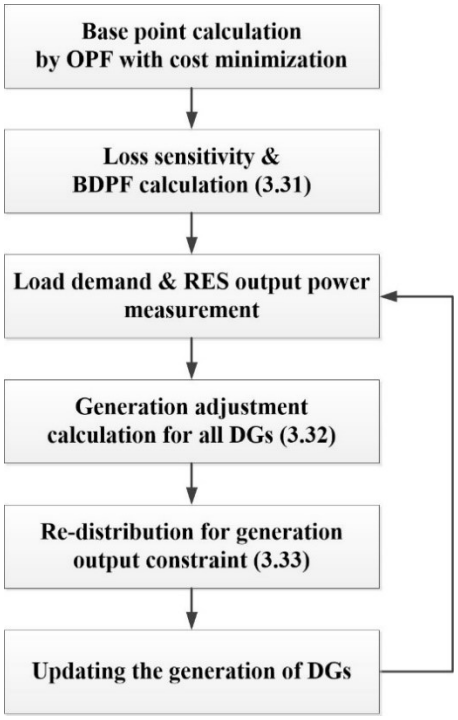

Fig. 3.4 Flow chart for using BDPF.

Chapter 4. Operation Methodology for Islanded Mode

In islanded mode, since there is no import and export power from the main grid, energy self-sufficiency should be realized continuously or for several hours to improve the load reliability. Under the high penetration of the RES, the amount of generation can be either sufficient or deficient depending on the weather condition and the load demand. Because the PCC can no longer act as an ideal source in both islanded microgrid with static switch off and standalone microgrid as well, the operation method should consider both the sufficient and deficient power. In addition to the amount of the generation, the absence of the ideal voltage source leads to more fluctuation of frequency and voltage magnitude. Even the system is composed of only inverter-interfaced resources, the fluctuation exists owing to the droop control. Further, the IC no longer makes the DC side voltage constant, and it tries to share the power between the AC and DC grid (2.15) which results in the DC side voltage deviation. In addition to the reliable operation, the reduction of the generation cost is always one of the most important operation objective for system operator. Therefore, in islanded mode, the operation method ensuring stable operation while reducing operation cost is needed.

Since the secondary control is the highest level in islanded mode, the aforementioned issues caused by the LC are handled in this level by the MGCC. Both LC and MGCC can conduct the secondary control. The LC has a fast response but the limitation of the acquired data, so the role of the MGCC is becoming more important, which is mainly focused in this dissertation.

4.1 Two stage supervisory control scheme

To operate the islanded HMG properly, the key feature of the situation where there are sufficient and deficient generation should be identified. Since the output of the RES results in the sufficient and deficient amount of generation, they are equivalent to the low and high net load demand, respectively. When the net load demand is high (generation is deficient), more DGs should turn on and the controllable loads should be time-shifted or turn off. They may not be able to happen immediately because of the turn on/off time of DGs and reliability of loads, and their operation over the time should be scheduled at some time range based on the predicted values. On the other hands, when the net load demand is low or even negative (generation is sufficient), the output of DGs should decrease and the RESs should curtail their output power. Note that all DGs may turn on at all times to obtain the reserve power and stable operation in islanded mode. It can be conducted in real-time by sending the command to DGs and RESs with well-constructed communication infrastructure. In other words, the time frame of two situations are different; thus, the operation method for islanded microgrid is divided into two stage, long-term and short-term operation.

Fig. 4.1 shows the time horizon and time step of long-term and short-term operation. The execution cycle of the long-term should be larger than that of short-term ($T_L > T_S$), because the short-term operation is based on the long-term result. Between two consecutive long-term time step, the short-term operation is repeated at each short-term time step (at time k, $k+T_s$, $k+2T_s$,…). The long-term operation determines the schedule of resources including controllable loads in order to achieve the reliable and economic operation. The short-term operation determines the set-points considering the results of the droop control, because the active and reactive power is controlled by the droop control of LC at every time, unlike the grid-connected mode.

Because the actual output power of the resources is calculated and it is repeated

in short cycles, the short-term operation is more concentrated in this dissertation. The details about the long-term and short-term operation method will be discussed in the later subsections.

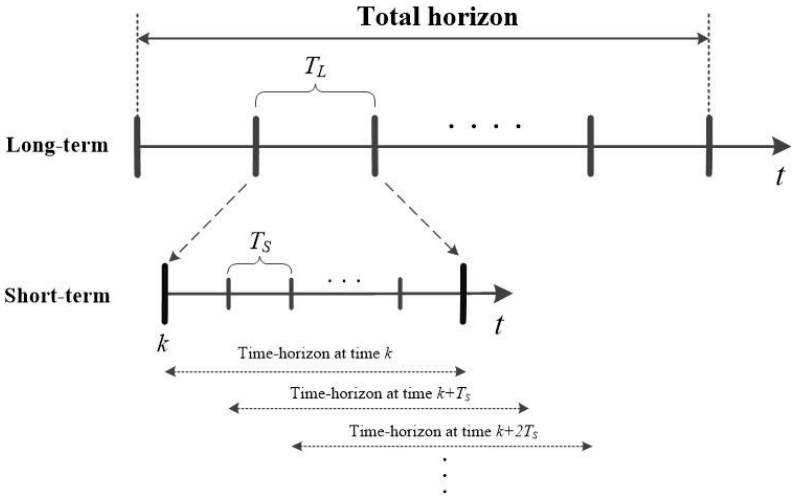

Fig. 4.1 Operation time step for islanded mode.

4.2 Long-term scheduler for on/off decision

4.2.1 Net load forecasting

To decide whether DGs and controllable loads are operating or not (on/off decision), the time series predicted amount of load demand and the output of RES are required. From the viewpoint of the operator, the output of RES can be regarded as a negative load and it can be added to the load demand. Thus, the time series net load, subtracting the RES output from the load demand, is needed. Among the many forecasting algorithms, learning-based algorithm has gained considerable attention with the development of the data storage and parallel computing, recently.

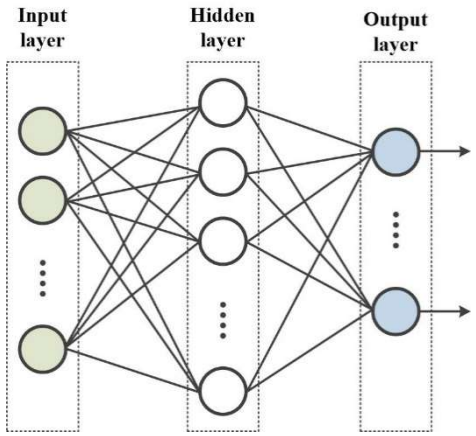

Fig. 4.2 Neural network structure with one hidden layer.

The learning-based algorithm mimics the human neural network mechanism. Fig. 4.2 shows the basic neural network structure for machine learning with one hidden layer. The circle of each layer represents the neuron which has information, and the information can be transmitted to next layer neuron based on the optimal learning algorithm. Many input data and corresponding output data are required to learn their relationship. After the algorithm is learned based on the training data, the validation set is used to estimate the training accuracy and to prevent overfitting.

More neurons and hidden layers enable to learn a complex mechanism having many inputs and outputs, and the performance can be improved. However, too many neurons and hidden layers increase learning computation time and even may slightly deteriorate the performance because the training data set cannot represent the entire mechanism perfectly.

Among the many machine learning structures, nonlinear autoregressive network with exogenous input (NARX) is adopted, which is suitable for predicting the time-series data because they consider the previous input and output data. As shown in Fig. 4.3, NARX architecture is divided into two types according to the loop type. During the learning, the open loop structure like Fig. 4.3(a) is used since we already know the input and true output as training set. Then, the close loop structure like Fig. 4.3(b) is used for actual prediction because the true output cannot be known at the time of prediction. In Fig. 4.3, tapped delay line (TDL) keeps the previous input and output data and sends them to the feedforward network. The number of delay time can be determined by the operator.

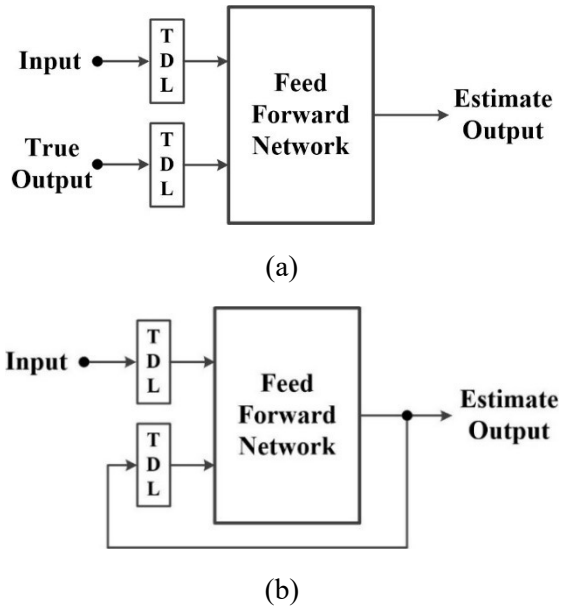

Fig. 4.3 NARX architecture. (a) Open loop. (b) Close loop [67].

To predict the output power of PV by using the NARX, the historical output data with weather condition of the PV location is required and the predicted weather condition should be provided by a weather management center (e.g. Korea Meteorological Administration (KMA) in South Korea). In addition, factors that affect the PV output should be selected to define the input layer. Temperature, precipitation, humidity, and cloud data, which can be obtained from KMA, are selected as input data.

The load demand and wind power can be also forecasted in a similar way if there are many historical data and predicted input data can be obtained. However, the load demand and output of wind power are assumed to be predicted as a general time-series pattern and real data from a specific region due to the lack of the data for forecasting. This assumption is not a critical issue since this dissertation mainly focuses on the operation method given forecasted data.

4.2.2. Linearized problem formulation

Based on the net load forecasting, the optimization problem containing integer variables as decision variables (on/off decision) should be solved. The power system in essence has the nonlinearity with its devices and the network. Solving optimization problem with integer variable and nonlinear objective function or constraints arises unnecessary complexity. The solution may depend on the solving algorithm, and even differ depending on the initial point despite of the same algorithm. The algorithm may not converge and may require a high computation time even if converged. If the nonlinearity can be resolved through linearization, the problem is a form of mixed integer linear programming (MILP), whose solution algorithms have been studied for many decades to improve the convergence and reduce the computation time and are currently being provided by many commercial software.

Although all DGs may always be turn on in islanded mode, the problem of

determining on/off of the DGs is formulated to prepare for situations with a lot of DGs. The first objective is to reduce the generation cost considering DG's on/off decision. The generation cost function considering on/off decision can be expressed as follow:

$$C_g\left(P_g\right)=c_2P_g^2+c_1P_g+c_0X_g \tag{4.1}$$

where X_g is a binary value representing on/off of DG g (X_g=1 is on, and X_g=0 is off). The difference between (3.8) and (4.1) is that on/off variable X_g is multiplied to c_0 in (4.1). The quadratic cost function (4.1) can be converted to piecewise linear function by dividing the range of P_g and approximating linearly the divided small interval [68].

The second objective is to turn off the load in order to prevent the lack of generation. This objective function is as follows:

$$C_L\left(P_L\right)=w_LP_LX_L \tag{4.2}$$

where X_L is a binary value representing on/off and w_L is a weight factor of load L according to the importance of the load. It is assumed that turning off or shifting the load can be converted into a monetary value by using w_L. Thus, with adding the superscript t representing time index, the final objective function can be expressed as the summation of (4.1) and (4.2), such that

$$\sum_t C_g\left(P_g^t\right)+C_L\left(P_L^t\right) \tag{4.3}$$

The equality constraints are power flow balance equations of the AC and DC grid. The active and reactive power flow equations are as follows:

$$P_{gen,i}+P_{IC,i}-P_{L,i}=\sum_j P_{ij} \tag{4.4}$$

$$Q_{gen,i}+Q_{IC,i}-Q_{L,i}=\sum_j Q_{ij} \tag{4.5}$$

Equation (4.4) is applied to both AC and DC grid. The active and reactive power flow between bus i and j in the AC grid can be linearized in the vicinity of nominal voltage magnitude and zero voltage angle [69], [70], such that

$$P_{ij} = g_{ij}\left(V_i^2 - V_i V_j \cos\theta_{ij}\right) - b_{ij} V_i V_j \sin\theta_{ij} \simeq g_{ij}\left(V_i - V_j\right) - b_{ij}\theta_{ij} \tag{4.6}$$

$$Q_{ij} = -b_{ij}\left(V_i^2 - V_i V_j \cos\theta_{ij}\right) - g_{ij} V_i V_j \sin\theta_{ij} \simeq -b_{ij}\left(V_i - V_j\right) - g_{ij}\theta_{ij} \tag{4.7}$$

where g_{ij} and b_{ij} are the conductance and susceptance of line between bus i and j, respectively, and θ_{ij} is the angle difference between bus i and j. Similar to the AC line flow, the DC line flow between bus i and j can be linearized in the vicinity of nominal voltage magnitude, such that

$$P_{ij} = g_{ij}\left(V_i^2 - V_i V_j\right) \simeq g_{ij}\left(V_i - V_j\right) \tag{4.8}$$

The approximated equations of (4.6)–(4.8) represent the linear relationship of the line power flow and voltage; it makes the equality constraints linear equations.

The inequality constraints are as follow:

$$P_{g,i}^2 + Q_{g,i}^2 \le X_{g,i} S_{g,i}^{\max^2}, \qquad i \in B_{ac} \tag{4.9}$$

$$X_{g,i} P_{g,i}^{\min} \le P_{g,i} \le X_{g,i} P_{g,i}^{\max}, \qquad i \in B_{dc} \tag{4.10}$$

$$P_{ij}^2 + Q_{ij}^2 \le S_{ij}^{\max^2}, \qquad i, j \in B_{ac} \tag{4.11}$$

$$P_{ij} \le P_{ij}^{\max}, \qquad i, j \in B_{dc} \tag{4.12}$$

$$V^{\min} \le V_i \le V^{\max}, \qquad i \in B_{ac} \bigcup B_{dc} \tag{4.13}$$

Constraints (4.9) and (4.10) represent the output limits of DGs for the AC and DC grid, respectively. Unlike (4.10), (4.9) is the inverter apparent power limit; thus, it is not a linear constraint. Constraints (4.11) and (4.12) represent the line flow limits for the AC and DC grid, respectively. Similarly, (4.11) is apparent power limits (not linear constraints). Note that the squared value is not applied in (4.12) because both P_{ij} and P_{ji} are applied for one line (bi-directional power flow). Voltage constraints of the AC and DC grid are represented by (4.13). Constraints (4.9) and (4.11) should be converted into linear functions to make the problem a MILP formulation.

Fig. 4.4 shows the linearization method of circular constraints (4.9) and (4.11). Using N-regular polygon inscribed in original limit circle, one constraint for apparent

power can be converted into N linear constraints. The converted inequality of $P^2+Q^2 \le S^{max2}$ into N linear constraints can be expressed as follows:

$$P\cos\left(i\frac{2\pi}{N}\right)+Q\sin\left(i\frac{2\pi}{N}\right) \le S^{max}\cos\left(\frac{\pi}{N}\right) \tag{4.14}$$

where i=1,…,N. For all i, (4.14) should be satisfied simultaneously. The right-hand side of (4.14) is the length of the perpendicular line from the origin to the sides of the polygon, and the left-hand side is the length from the origin to the orthogonal projection of the current point to the perpendicular line. (e.g., for point A, the left-hand side is the summation of P_A and Q_A). Point B satisfies the constraints because B1 to B4 which are the orthogonal projection to the perpendicular lines are within the polygon. There is always a space between the circle and the polygon, and it results approximation error. If N increases, the error space decreases but it causes more computation time. In addition, the solution with high N may not considerably improve the operation performance. Thus, N should be selected in consideration of trade-off between error and computation time.

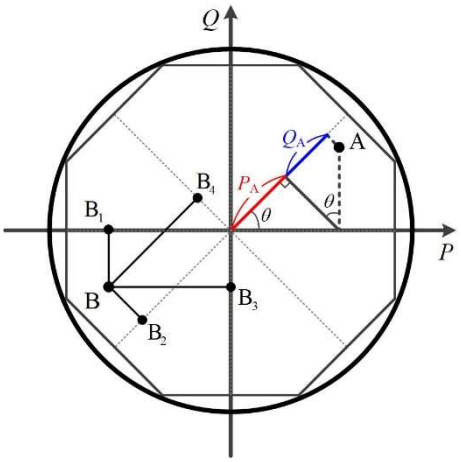

Fig. 4.4 Piecewise linear approximation of apparent power limits.

Based on the above approximation method, the objective function and all constraints can be expressed as linear functions. Thus, the optimization problem can

be solved using MILP. Note that approximation of (4.6)–(4.8) cannot consider the line loss because the line loss is expressed as a quadratic function of voltage. There are some recent studies regarding linearization to consider the line loss [71], [72]. However, in the long-term operation, the major objective is to decide the time schedule of on/off decision, and the determining the amount of the output power taking considering the line loss is conducted in the short-term operation.

The circular constraint can be simply approximated into the rectangular constraints. Fig. 4.5 shows the rectangular power capability region of the inverter [73]. This constraint cannot fully exploit the inverter capability, but the number of output constraints reduces significantly and the inverter operates conservatively. In the short-term operation, which will be discussed in the next subsection, the rectangular constraints can be suitable because the output set-point is adjusted from the previous operating point by a relatively small amount. The system operator can select the operating region based on the current operating point.

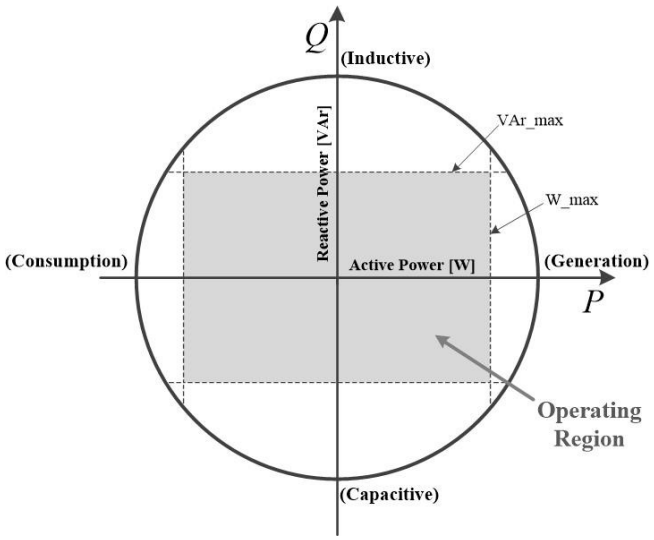

Fig. 4.5 Rectangular power capability region.

4.3 Short-term sensitivity-based model predictive control

4.3.1 Model predictive control

After the long-term on/off of resources and controllable loads is decided, the short-term control is conducted to cope with the high uncertainty of loads and RESs. The model predictive control (MPC), which is an online receding horizon optimal control method and is quite appealing to cope with high uncertainties [6], is used to update the set-points of resources in a short period. The MPC-based approach which is employed in this dissertation is shown in Fig. 4.6.

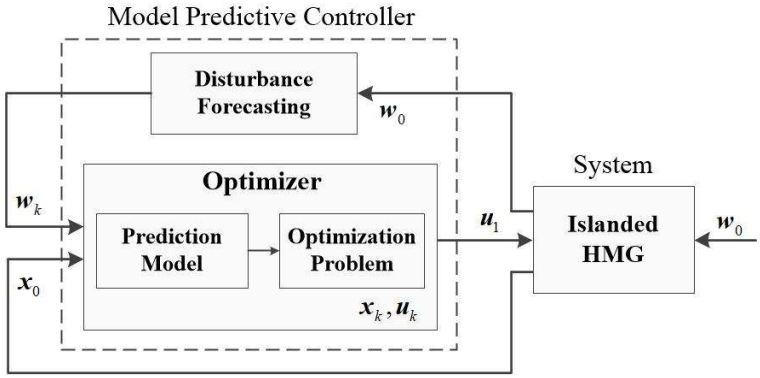

Fig. 4.6 Model predictive control for islanded HMG.

For the supervisory control, the MGCC obtains the generation, load, and network data with communication links. For the subscript k representing the time step, x_k refers to the variables we need to handle to solve the problem, u_k represents the control variables, and w_k represents the disturbance forecasted values. Using the current disturbance w_0 and historical data, w_k can be obtained by the disturbance forecasting algorithm. Based on w_k and the current system measurement x_0, the optimizer can be run. The system prediction model is incorporated into the optimization problem, and the problem is solved for the prediction time horizon. Although solutions for the prediction time horizon can be obtained, only the first set

of solutions u_1 is sent to the resources according to the receding horizon principle. The same process is repeated at every step.

The disturbance forecasting block creates predicted time-series load and RES values. The disturbance forecasting algorithm can be any prediction algorithm, such as autoregressive integrated moving average (ARIMA) or artificial neural network (ANN), if the weather condition or other data required to predict the disturbance can be used. However, it is difficult for MGCC to gather this kind of information in short time interval. Further, although ARIMA, ANN or other prediction algorithm is adopted, the accuracy of the prediction may not be significantly improved owing to the high uncertainty. In contrast, a persistence model in which the predicted values are set to the current measured values does not require any data except for the current measured value. Thus, a persistence model is appropriate for prediction at short time intervals with easy implementation [74], so it is used in the disturbance forecasting algorithm in this dissertation. In the persistence model, after load and RES output are measured at time k=0, the predicted amount of the active load variation $\Delta P_{L,i,k}$, reactive load variation $\Delta Q_{L,i,k}$, and RES output variation $\Delta \boldsymbol{P}_{r,i,k}^{MPPT}$ from the current value, for k=1,…,T_h, can be expressed as

$$\Delta \boldsymbol{P}_{L,i} = \boldsymbol{0}_{T_h \times 1} \tag{4.15}$$

$$\Delta \boldsymbol{Q}_{L,i} = \boldsymbol{0}_{T_h \times 1} \tag{4.16}$$

$$\Delta \boldsymbol{P}_{r,i}^{MPPT} = \boldsymbol{0}_{T_h \times 1} \tag{4.17}$$

where $\Delta \boldsymbol{P}_{L,i}=[\Delta P_{L,i,1},\ldots,\Delta P_{L,i,T_h}]^T$, $\Delta \boldsymbol{Q}_{L,i}=[\Delta Q_{L,i,1},\ldots,\Delta Q_{L,i,T_h}]^T$, and $\Delta \boldsymbol{P}_{r,i}^{MPPT}=[\Delta P_{r,i,1}^{MPPT},\ldots,\Delta P_{r,i,T_h}^{MPPT}]^T$.

4.3.2. Problem formulation

Objective Function

The objective of the short-term control is to restore the frequency and voltage close to the nominal values while reducing the generation cost. For B_g, B_b, and B_r, which represent the sets of both AC and DC buses to which the DG, BESS, and RES

are connected, the generator cost function for time k can be expressed as

$$f_{c,k} = \left[\sum_{i \in B_g} \left(c_{2,i} P_{g,i,k}^2 + c_{1,i} P_{g,i,k} + c_{0,i} \right) + \sum_{i \in B_b} c_{b,i} P_{b,i,k}^{dch} + \sum_{i \in B_r} c_{r,i} P_{r,i,k}^{cur} \right] \Delta t_s \tag{4.18}$$

where c_b is the coefficient of the battery usage cost, and c_r is the RES curtailment cost coefficient. The first term on the right-hand side of (4.18) is the cost function of DGs. The second term refers to the battery usage cost, which represents the life reduction. The coefficient c_b should not be multiplied by P_b but by the discharge power, because c_b refers to the capital cost divided by the maximum depth of discharge and lifetime cycle [75]. The last term refers to the penalty factor of the RES curtailment. To ensure that the RES is curtailed in situations when the BESS is no longer able to charge or constraints are violated, c_r should be selected appropriately. The BESS may not charge if c_r is too small, and the RES tries not to be curtailed while hindering other purpose if c_r is too large.

One of our objectives is to restore the voltage of the entire bus close to its nominal value. However, it may be impossible to keep the entire voltage at a nominal value, because the voltage magnitude can be different for each bus because of the line impedance. Therefore, the second objective function is voltage restoration, which is a squared norm of the difference between the voltage magnitude at time k and nominal value, such that

$$f_{v,k} = \left\| \boldsymbol{V}_k - \boldsymbol{V}^n \right\|_2^2 \tag{4.19}$$

Both the AC and DC voltage magnitude should be included in (4.19). The total objective function is a combination of $f_{c,k}$, and $f_{v,k}$ for prediction time horizon T_h, which is a multi-objective formulation, such that

$$f = \sum_{k=1}^{T_h} \left[w_c f_{c,k} + w_v f_{v,k} \right] \tag{4.20}$$

where w_c and w_v are the weight factors of the cost function and voltage restoration function, respectively. An appropriate weight factor combination depends on the unit of cost and the total number of buses. It is assumed that appropriate weight factors

can be determined empirically by the system operator.

Constraints

The optimization problem should keep security constraints and mathematical limitations regarding the resources and system. There are one equality constraint and some other inequality constraints as follows:

$$\omega_k = \omega^n \tag{4.21}$$

$$P_{g,i}^{\min} \le P_{g,i,k} \le P_{g,i}^{\max}, \qquad i \in B_g \tag{4.22}$$

$$Q_{g,i}^{\min} \le Q_{g,i,k} \le Q_{g,i}^{\max}, \qquad i \in B_g \tag{4.23}$$

$$P_{b,i}^{\min} \le P_{b,i,k} \le P_{b,i}^{\max}, \qquad i \in B_b \tag{4.24}$$

$$Q_{b,i}^{\min} \le Q_{b,i,k} \le Q_{b,i}^{\max}, \qquad i \in B_b \tag{4.25}$$

$$0 \le P_{b,i,k}^{dch}, \qquad i \in B_b \tag{4.26}$$

$$0 \le P_{b,i,k}^{ch}, \qquad i \in B_b \tag{4.27}$$

$$SOC_{b,i}^{\min} \le SOC_{b,i,k} \le SOC_{b,i}^{\max}, \qquad i \in B_b \tag{4.28}$$

$$0 \le P_{r,i,k}^{cur} \le P_{r,i,k}^{MPPT}, \qquad i \in B_r \tag{4.29}$$

$$P_{IC,i}^{\min} \le P_{IC,i,k} \le P_{IC,i}^{\max}, \qquad i \in B_{IC} \tag{4.30}$$

$$Q_{IC,i}^{\min} \le Q_{IC,i,k} \le Q_{IC,i}^{\max}, \qquad i \in B_{IC} \tag{4.31}$$

$$V_i^{\min} \le V_{i,k} \le V_i^{\max}, \qquad i \in B_{ac} \bigcup B_{dc} \tag{4.32}$$

After the frequency reaches a steady-state value, it can be restored to the nominal value by adjusting the droop set-point; therefore, an equality constraint (4.21) is defined. Note that the restoration of voltage magnitude is obtained from the objective function. Constraints (4.22)–(4.25) define the upper and lower limits of the DGs and BESSs. Constraints (4.26) and (4.27) are defined to completely separate the discharge and charge powers, and (4.28) defines the SOC range of the BESS for a

safe operation. Constraint (4.29) refers to the limits of the RES curtailment. Constraints (4.30) and (4.31) refer to the active and reactive power limits of the IC due to the converter capacity; B_{IC} is the set of buses to which the IC is connected. The voltage magnitude limits of both AC and DC buses are defined in (4.32). Note that constraints (4.23), (4.25) and (4.31) should be applied to the AC grid. For the short-term operation, because the amount of the output change is small, the output limits of DGs, BESSs, IC of the AC grid are applied to the rectangular power capability, like Fig. 4.5.

Fig. 4.7 shows the operation of a DG. The initial operating point is A and later moves to B on the droop curve by the primary control after disturbance. Based on the measurement, a supervisory control is then implemented to adjust the set-point of the DG, and the operating point reaches the new point C (droop curve is shifted). As the operating point moves from B to C, the output can be changed; in this case, the output of the other DGs should be adjusted for power balance. The frequency set-point holds the nominal value; however, as shown in Fig. 4.7(b), the voltage set-point may differ from the previous one because the voltage profile to keep the entire voltage close to the nominal value can differ depending on the load demand changes. The droop-based operation for the DGs in the DC grid is similar to the Q–V droop-based operation in the AC grid.

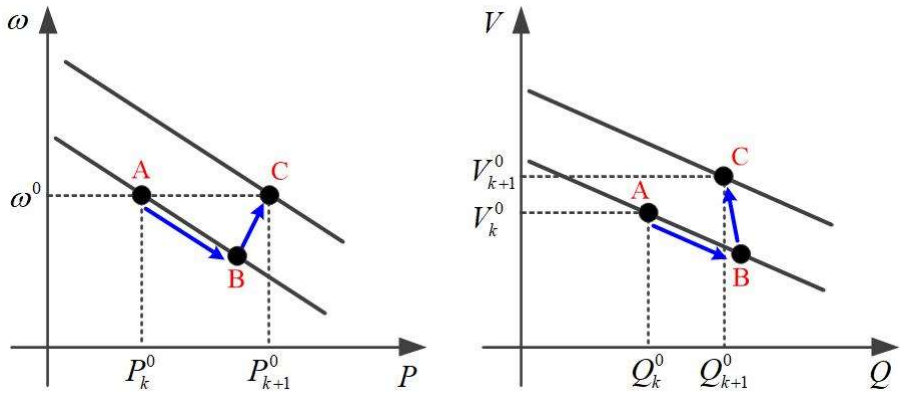

(a) (b)

Fig. 4.7 Droop-based DG operation. (a) P–ω droop, and (b) Q–V droop.

4.3.3. Set-point calculation using sensitivity values

The control variable should be updated in a short time period to obtain our control objective. This can be achieved by formulating the preceding optimization problem with the variation in the control variables. However, the objective function and constraints include the frequency and voltage magnitude. To formulate the problem as a variation in the control variables, the relationship between the control and system variables (frequency and voltage) is needed. To this end, we use the sensitivity, as it can help obtain the next steady-state value in advance for the output variation.

Because of the droop control of the IC, the output variations in the AC and DC grids affect each grid. This increases the complexity of calculating and utilizing the sensitivity. In addition, the AC grid and the DC grid may be disconnected to protect their own operation due to the IC fault or other emergency situation. Therefore, first, the IC is regarded as a constant power mode (the second terms on the right-hand sides of (2.14) and (2.15) are neglected). Then, the sensitivities for the AC and DC grids are easily calculated and are used to update the control variables. By doing so, the proposed control method can even be extended to the situation where the AC and DC grid are disconnected, or more than one DC grid are connected to the AC grid, and to a pure AC or DC microgrid in islanded mode,

AC grid

The voltage sensitivity can be calculated by the inverse of the Jacobian matrix in the NR power flow method. As described in Section 3, the conventional Jacobian matrix using the slack, PV, and PQ bus cannot reflect the characteristic of the droop control, and the modified Jacobian matrix including the droop control bus should be used. In addition, the IC is regarded as constant power mode, which means the coupling of the AC frequency and the DC voltage disappears. Therefore, (3.1) is not directly used, and the following Jacobian matrix only for the AC grid is used

(superscript ac in $\boldsymbol{P}_{mis}$ and $\boldsymbol{Q}_{mis}$ is omitted to avoid complexity). It is assumed that the dependency of the line impedance on the frequency is neglected.

$$J_{ac}=\begin{bmatrix} \dfrac{\partial \boldsymbol{P}_{mis}}{\partial \boldsymbol{V}} & \dfrac{\partial \boldsymbol{P}_{mis}}{\partial \omega} & \dfrac{\partial \boldsymbol{P}_{mis}}{\partial \boldsymbol{\theta}} \\ \dfrac{\partial \boldsymbol{Q}_{mis}}{\partial \boldsymbol{V}} & \dfrac{\partial \boldsymbol{Q}_{mis}}{\partial \omega} & \dfrac{\partial \boldsymbol{Q}_{mis}}{\partial \boldsymbol{\theta}} \end{bmatrix} \tag{4.33}$$

From the (3.2) and (3.3), the active and reactive power mismatches of AC bus i can be expressed as follows:

$$P_{mis,i}=P_{g,i}+P_{b,i}+P_{r,i}+P_{IC,i}-P_{L,i}-P_i \tag{4.34}$$

$$Q_{mis,i}=Q_{g,i}+Q_{b,i}+Q_{IC,i}-Q_{L,i}-Q_i \tag{4.35}$$

It is assumed that the RES is operated with unity power factor. By taking the negative inverse transform of J_{ac} at the current operating point k=0, the frequency, voltage magnitude, and voltage angle sensitivity matrices with respect to $\boldsymbol{P}_{mis}$ and $\boldsymbol{Q}_{mis}$ can be obtained as

$$\begin{bmatrix} \boldsymbol{S}_{\boldsymbol{P}}^{\boldsymbol{V}} & \boldsymbol{S}_{\boldsymbol{Q}}^{\boldsymbol{V}} \\ \boldsymbol{S}_{\boldsymbol{P}}^{\omega} & \boldsymbol{S}_{\boldsymbol{Q}}^{\omega} \\ \boldsymbol{S}_{\boldsymbol{P}}^{\boldsymbol{\theta}} & \boldsymbol{S}_{\boldsymbol{Q}}^{\boldsymbol{\theta}} \end{bmatrix}=\left[-J_{ac}\big|_{k=0}\right]^{-1}=\begin{bmatrix} \dfrac{\partial \boldsymbol{V}}{\partial \boldsymbol{P}_{mis}} & \dfrac{\partial \boldsymbol{V}}{\partial \boldsymbol{Q}_{mis}} \\ \dfrac{\partial \omega}{\partial \boldsymbol{P}_{mis}} & \dfrac{\partial \omega}{\partial \boldsymbol{Q}_{mis}} \\ \dfrac{\partial \boldsymbol{\theta}}{\partial \boldsymbol{P}_{mis}} & \dfrac{\partial \boldsymbol{\theta}}{\partial \boldsymbol{Q}_{mis}} \end{bmatrix} \tag{4.36}$$

For simplicity, the subscript *mis* is omitted from the sensitivity matrices. Note that the sensitivity values strongly depend on the droop slopes. The voltage sensitivity also depends on the bus location, whereas the frequency sensitivity is almost irrelevant to the location because the frequency is the same in all areas in the steady-state. However, the frequency sensitivities are slightly different because they reflect the line loss change.

The deviations in the frequency and AC voltage magnitude j at time k can be calculated using sensitivities, such that

$$\Delta\omega_k=\sum_{i\in B_{ac}} S_{P_i}^{\omega}\Delta P_{tot,i,k} \tag{4.37}$$

$$\Delta V_{j,k} = \sum_{i \in B_{ac}} \left(S_{P_i}^{V_j} \Delta P_{tot,i,k} + S_{Q_i}^{V_j} \Delta Q_{tot,i,k} \right) \tag{4.38}$$

where

$$\Delta P_{tot,i,k} = \Delta P_{g,i,k}^{0} + \Delta P_{b,i,k} - \Delta P_{r,i,k}^{cur} + \Delta P_{IC,i,k}^{0} \tag{4.39}$$

$$\Delta Q_{tot,i,k} = \Delta Q_{g,i,k}^{0} + \Delta Q_{b,i,k} + \Delta Q_{IC,i,k}^{0} \tag{4.40}$$

The droop control terms of $P_{g,i}$ and $Q_{g,i}$, the second terms on the right-hand sides of (2.1) and (2.2), are functions of frequency and voltage. They are differentiated and included in J_{ac}. Hence, they are adjusted to maintain the power balance considering the changes in the other terms not related to the frequency and voltage. In other words, the sensitivity (4.36) is valid for the increment in the set-point, and not for the final output including the droop control. Thus, the variation in the output set-point of the DG, $\Delta P_{g,i}^{0}$ and $\Delta Q_{g,i}^{0}$, should be multiplied to the sensitivity value. In cases of BESS and RES, we can directly use their output variations in (4.39) and (4.40), as they are not related to the frequency and voltage magnitude. For the IC, the droop control was ignored, and the power set-point variations, $\Delta P_{IC,i}^{0}$ and $\Delta Q_{IC,i}^{0}$, are included in (4.39) and (4.40).

As the persistence model is used for the disturbance prediction in short-term operation, the predicted variations in the load and RES output are zero over the optimization time horizon. However, if the predicted load demand differs from the current value (using other forecasting algorithms), disturbance variation term should be added on the right-hand sides of (4.39) and (4.40).

In (4.37), only active power affects the frequency deviation in the AC grid. However, although P–ω and Q–V droop control are chosen to control the DGs in the AC grid, the frequency may also be influenced by the reactive power because the line loss and load demand are dependent on the bus voltage magnitude [76]. The frequency deviation considering both active and reactive power change can be expressed as

$$\Delta\omega_k = \sum_{i \in B_{ac}} S_{P_i}^{\omega} \Delta P_{tot,i,k} + S_{Q_i}^{\omega} \Delta Q_{tot,i,k} \tag{4.41}$$

When only linear relationship between the frequency and reactive power is used, the reactive power is likely to be set minimum or maximum value depending on the sign of $S_{Q_i}^{\omega}$. In order to reflect the reactive power on the system frequency properly, the second-order frequency sensitivity is used. The additional frequency deviation using the second-order frequency sensitivity can be expressed as

$$\Delta\omega_k^{add} = \Delta \boldsymbol{P}_{tot,k}^T \frac{\partial^2 \omega}{\partial \boldsymbol{P}^2} \Delta \boldsymbol{P}_{tot,k} + \Delta \boldsymbol{Q}_{tot,k}^T \frac{\partial^2 \omega}{\partial \boldsymbol{Q}^2} \Delta \boldsymbol{Q}_{tot,k} \tag{4.42}$$

where $\boldsymbol{P}_{tot,k}$ and $\boldsymbol{Q}_{tot,k}$ are vector expression of (4.39) and (4.40), respectively, and $\partial^2\omega/\partial\boldsymbol{P}^2$ and $\partial^2\omega/\partial\boldsymbol{Q}^2$ are the second-order frequency derivative in terms of active and reactive mismatch power of the AC grid, respectively. The calculation method of the second-order frequency derivative is very similar to that of loss derivative (3.21). The difference is that only the AC grid quantities should be used in this case (P_{loss} and J_{new} are replaced with ω and J_{ac}, respectively, and the AC quantities in $\boldsymbol{X}$ and $\boldsymbol{Y}$ ($\boldsymbol{V}^{ac}$, ω, $\boldsymbol{\theta}$, $\boldsymbol{P}^{ac}$, and $\boldsymbol{Q}^{ac}$ are used). The calculation process is very similar to (3.21)–(3.23), so it is not detailed in this section. If the second-order frequency sensitivity is considered, the amount of the total frequency deviation is summation of (4.41) and (4.42). In other words, the proposed method is divided into two types according to the calculation of the frequency deviation:

- Proposed method 1: Using (4.37)
- Proposed method 2: Using the summation of (4.41) and (4.42).

DC grid

A similar process can be applied to the DC grid. In the DC grid, the power mismatch can be expressed as voltage deviation using the modified Jacobian matrix, J_{dc}, as follows:

$$J_{dc} = \frac{\partial \boldsymbol{P}_{mis}}{\partial \boldsymbol{V}} \tag{4.43}$$

The power mismatch expression for the DC grid is equivalent to that for the AC grid. By taking the negative inverse transform of J_{dc} at k=0, we have

$$\boldsymbol{S}_{\boldsymbol{P}}^{\boldsymbol{V}} = \left[-J_{dc}\big|_{k=0} \right]^{-1} = \frac{\partial \boldsymbol{V}}{\partial \boldsymbol{P}_{mis}} \tag{4.44}$$

The deviation in the DC voltage j can be expressed as

$$\Delta V_{j,k} = \sum_{i \in B_{dc}} S_{P_i}^{V_j} \Delta P_{tot,i,k} \tag{4.45}$$

where $\Delta P_{tot,i,k}$ is the same formulation as that used for the AC grid (4.39); however, the active power of the IC for the DC grid has the same value but with an opposite sign compared to that for the AC grid (2.19). Similar to the AC grid, the output set-point of the droop control (2.3) should be applied to the sensitivity (4.44).

Set-point adjustment

The set-points of the DGs are adjusted; however, their final output variation can be different from the set-point variation because of the droop control term as the frequency and voltage change. The set-point is applied to use the sensitivity, but the final output should be used to calculate the generation cost (4.18) and apply the output limits (4.22) and (4.23). Considering the variation of the droop control term, the final active and reactive power variations of the DGs in the AC grid are expressed as

$$\Delta P_{g,i,k} = \Delta P_{g,i,k}^{0} - k_{p,i} \Delta \omega_k, \qquad i \in B_{ac} \tag{4.46}$$

$$\Delta Q_{g,i,k} = \Delta Q_{g,i,k}^{0} - k_{q,i} \Delta V_{i,k}, \qquad i \in B_{ac} \tag{4.47}$$

The final output variation of the DGs in the DC grid is expressed as

$$\Delta P_{g,i,k} = \Delta P_{g,i,k}^{0} - k_{p,i} \Delta V_{i,k}, \qquad i \in B_{dc} \tag{4.48}$$

In (4.46)–(4.48), the final output contains the deviations in the frequency and voltage magnitude. The final output can be expressed as only set-points, which are control variables, by substituting (4.37), (4.38), and (4.45) into (4.46), (4.47), and (4.48), respectively. If the second-order frequency sensitivity is used, the frequency

change is the summation of (4.41) and (4.42), and it should be assigned to (4.46). Note that the frequency is set to exactly its nominal value (4.21). Thus, the active output power of the DG in the AC grid at time k is equal to $P^0_{g,i,0}+\Delta P^0_{g,i,k}$. In this case, the final active power can be expressed without considering the frequency change if the set-point at the current time, i.e., $P^0_{g,i,0}$, is known.

The optimization problem is a form of the multi-objective formulation. In general, it can be solved by evolutionary algorithm [77], but this algorithm may have high computation burden, difficulty of constraints handling, parameter tuning, and limited problem size [78]. On the other hand, using the first-order sensitivity values, the frequency and voltage magnitude can be expressed as a linear function of the control variables. Then, the objective function (4.19) can be formulated as a quadratic function of the control variables using (4.38) and (4.45). In addition, constraints (4.21) and (4.32) can be linearized using (4.37), (4.38), and (4.45). Thus, the problem becomes quadratic programming (QP) formulation which is suitable for MPC controller [79]. When using the second-order sensitivity, the frequency variation is expressed as a quadratic function of the control variables. In this case, the equality constraint (4.21) is converted to be quadratic; thus, the problem is a form of a quadratic constrained QP (QCQP).

Initially, the IC was deemed as a constant power mode to separate the AC and DC grids and to calculate the sensitivity of each grid; however, the droop control is implemented in actual operation. The final reference of the IC should be equivalent to the solution, even though the droop control is added. Thus, the set-point of error in (2.15) and voltage magnitude in (2.14) should be updated such that the droop compensation is zero. Based on the predicted values at time k, the normalized frequency, DC voltage, and hence the error set-point can be calculated. The voltage set-point in (2.14) is updated in a similar manner.

When only the output set-points of the DGs, $P^0_{g,i,k}$ and $Q^0_{g,i,k}$ are updated, the final output reference may not lie in the safe range if the droop control is no longer

employed for some reason. Thus, to prevent this, after the optimization problem is solved, the output set-point of the DGs should be substituted into the final outputs using (4.46)–(4.48). Accordingly, the voltage set-point also should be changed to the predicted value using (4.38) and (4.45). For the set-point of P–ω droop control, the frequency set-point remains the nominal value.

According to the calculation of the frequency deviation, the proposed method is divided into two types. Fig. 4.8 shows the flow chart for the proposed method 1. At the initial operating point, the frequency and AC/DC voltage sensitivities are calculated using (4.36) and (4.44). After the deviation in the frequency and AC/DC voltage magnitude are measured, the optimization problem formulated as QP using the sensitivity is solved. Then, the MGCC sends the set-points to the resources. Measuring the deviations, solving the optimization problem, and updating the set-points are repeated in a short cycle. Note that once the sensitivity matrix is calculated at the initial operating point, it can be continuously used as long as the operating point does not change significantly. If the current operating point is much different from the initial operating point, the sensitivity should be updated by additionally measuring the bus net load demand.

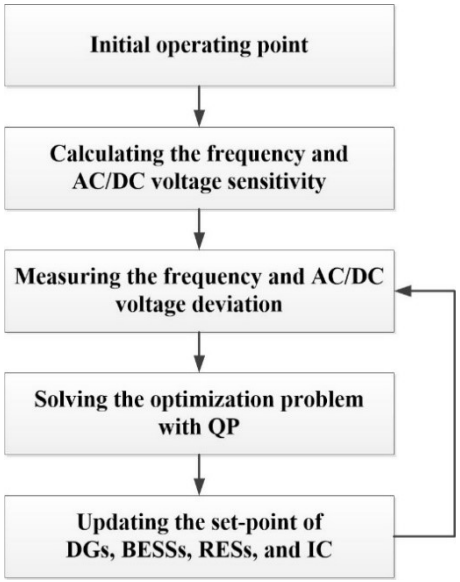

Fig. 4.8 Flow chart for the proposed method 1.

The flow chart for the proposed method 2 is shown in Fig. 4.9. Compared to the proposed method 1, the sensitivity matrix should be updated at the new operating point in the proposed method 2 to fairly reflect the effect of the reactive power on the frequency. To this end, the bus net load demand as well as the deviation in the frequency and AC/DC voltage magnitude should be measured. Then, the sensitivity matrix is updated at the current operating point and the optimization problem which is the form of the QCQP is solved. Finally, the new set-points are sent to the resources. Note that the repeating process contains the sensitivity update.

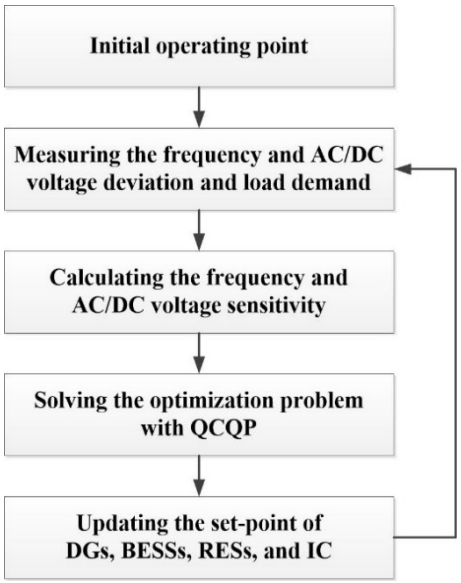

Fig. 4.9 Flow chart for the proposed method 2.

The proposed method is fundamentally based on the power system linearization. The comparison of the conventional linearization method and the proposed methods are shown in Table. 4.1. The conventional linearization method uses (4.6)–(4.8) to linearize the AC and DC grid. The common decision variables are the set-points of the DGs, BESSs, RESs, and IC, but the conventional method has additional decision variables, AC voltage magnitude and angle and DC voltage. The proposed methods can express the state variables such as the frequency and voltage magnitude by using the sensitivity and common decision variables. Regarding the required data, the

conventional method needs all the bus active and reactive load demand to solve the optimization problem. The proposed method 1 needs the current system frequency and bus voltage magnitude. When the sensitivity matrix is updated, the bus net load is also needed. However, the data is not used in the repeating process because the update cycle is long. In the proposed method 2, both data used in the conventional method and the proposed method 1 are required, and the equality constraint is quadratic and the sensitivity should be updated, as shown in Fig. 4.9.

Table 4.1 Comparison of the optimization methods.

	Decision variables	Required data	Remark
Conventional linearization method	· Output of DGs · Dis/charge of BESSs · RES curtailment · Set-point of ICs · AC voltage magnitude · AC angle · DC voltage magnitude	· Bus active & reactive load demand	-
Proposed method 1	· Set-point of DGs · Dis/charge of BESSs · RES curtailment · Set-point of ICs	· Frequency · Bus voltage magnitude	-
Proposed method 2	· Set-point of DGs · Dis/charge of BESSs · RES curtailment · Set-point of ICs	· Frequency · Bus voltage magnitude · Bus active & reactive load demand	· Update sensitivity · Quadratic equality constraint

Chapter 5. Case Study

In this chapter, to analyze the effectiveness of the operation methods developed in the chapters 3 and 4, the test system is constructed and some case studies are conducted. Both operation methods for grid-connected mode and islanded mode deal with steady-state values with short time intervals. The case studies were conducted in MATLAB.

5.1 Test system configuration

To analyze the operation method for HMG properly, the well-designed HMG should be constructed. To the best of author's knowledge, there are no standard multi-bus HMGs. Many researches have used the standard AC test grid and sample DC grid, and they are connected by implementing an IC to certain AC and DC bus. Particularly, IEEE 33-bus system is broadly used as a AC test system, and small-size radial or ring type DC grid is usually connected. In this dissertation, the IEEE 33-bus system was selected as the AC grid, the line and base load data of which were obtained from [80]. The DC grid was selected from [81] and slightly modified, in which all DC line resistances were set to 0.01 p.u. Fig. 5.1 shows the test system configuration used in case studies. The AC grid is radial configuration and the DC grid is ring type configuration. Note that the proposed methods are independent on the system configuration. The AC voltage rating was 12.66 kV, and the DC voltage rating was determined based on the voltage converting equation. The steady-state line to line AC voltage of VSC can be expressed as follows [30], [82]:

$$V_{LL_{rms}}^{ac} = K_{vsc} M V^{dc} \tag{5.1}$$

where M is the modulation index, V^{dc} is the DC side voltage, and K_{vsc} is the converter constant depending on the converter type. According to the range of M (0–1), the DC voltage rating should satisfy the following inequality:

$$V^{dc} \geq \frac{V_{LL_{rms}}^{ac}}{K_{vsc}} \tag{5.2}$$

It is assumed that the type of the VSC is one-stage, so $K_{vsc}=\sqrt{3}/2\sqrt{2}$. Thus, as in the above inequality condition (5.2), the DC grid voltage rating is chosen as 20.67 kV. Further, AC bus 22 and DC bus 1 were interconnected with the IC, as shown in Fig. 5.1. The IC can be composed of small inverters in parallel due to the inverter capacity limits, but it is equivalent to the one inverter from the viewpoint of the operator and can be controlled as one devices. The active and reactive power capacity of the IC are 1.5 MW and 1.5 MVar, respectively.

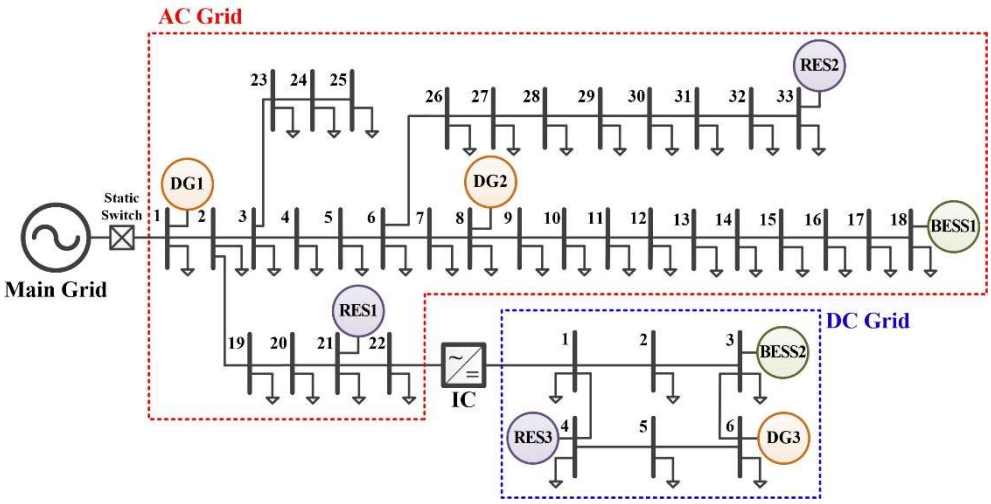

Fig. 5.1 Test system configuration.

Total three DGs, two BESSs, and three RESs were connected in the total system. The DGs were located at AC bus 1 and 8 and DC bus 6. Note that the proposed method can be applied regardless of the type of DGs. Any DG that is capable of controlling output power can participate in the generation adjustment. The information of DGs regarding cost coefficients and output limits are shown in Table 5.1. The active and reactive power limits were selected as a square with 2 MW and 2 MVar, respectively (i.e. the apparent power limit is $\sqrt{2}$ times of active power limit

for DGs in the AC grid).

The BESSs were placed at bus 18 in the AC grid and bus 3 in the DC grid one by one. The information of BESSs are shown in Table 5.2. The efficiency of BESS was assumed to be the same value as 95% in all output range (both charge and discharge). The battery lifetime cost c_b is 300 $ per MWh based on the install price, capacity, and safe SOC range of the daily-cycle lithium-ion battery [83]. The battery energy capacity is 1 MWh, and similar to the output limits of the DGs, the power limits are 0.5 MW and 0.5 MVar.

Table 5.1 Information of DGs.

DG No.	Cost Coefficients			Output Limits	
	c_2 [$/MW^{2}h]	c_1 [$/MWh]	c_0 [$/h]	P_g^{max} [MW]	Q_g^{max} [MVar]
1	150	55	0	2	2
2	90	110	0	2	2
3	120	60	0	1.4	-

Table 5.2 Information of BESSs.

BESS	c_b [$/MWh]	P_b^{max} [MW]	Q_b^{max} [MVar]	E_b [MWh]	η_b [%]
1	300	0.5	0.5	1	95
2	300	0.5	0.5	1	95

The capacities of RES 1–3 were 0.8, 0.8, and 0.6 MW, and they were located at AC bus 21, 33 and DC bus 4, respectively. This implies that the system had a high RES penetration (approximately 50% of the total base load demand). The active power of the RESs was controlled in MPPT, and the reactive power of all RESs was assumed to be zero (unify power factor). Like the DGs, any type of RES whose output has intermittency can be applied in the proposed method.

The AC loads are modeled as ZIP model (2.20) and (2.21). In microgrids, the AC bus type is typically classified as residential, commercial, or industrial, and their ZIP coefficients are experimented in [28]. Based on the experimental results, the ZIP coefficients of active and reactive load for each type is shown in Table 5.3. The

reactive load demand is more influenced by the voltage magnitude. The type of each AC bus was given in [84] and shown in Table 5.4. For the DC grid, the load portion of the constant current and constant power were assumed to be 25% and 75% for all DC buses, respectively.

Table 5.3 ZIP coefficients of AC grid.

Type	Active Power			Reactive Power		
	z_p	i_p	p_p	z_q	i_q	p_q
Residential	1.4	-2.0	1.6	8.4	-13.8	6.4
Commercial	0.5	-0.6	1.1	5.5	-9.7	5.2
Industrial	1.2	-1.6	1.4	4.4	-7.1	3.7

Table 5.4 Bus type of AC grid.

Type	Bus location
Residential	2, 5, 12, 14, 19, 22, 31, 32
Commercial	1, 4, 7, 8, 10, 11, 13, 15, 17, 20, 23, 24, 25, 26, 28, 29, 30, 33
Industrial	3, 6, 9, 16, 18, 21, 27

5.2 Case study for grid-connected mode

The proposed method for grid-connected mode is to adjust the amount of the generation from the base point. The base point should be obtained using OPF without any approximation, but because the power flow equations of the AC and DC grid are nonlinear functions, the optimization problem is a form of the nonlinear programming. Among many solution methods for solving the problem with nonlinear functions, the sequential QP method is used. The Jacobian matrix is composed of the first-order derivatives, which is the linearization of the power flow equations. Using the Jacobian matrix, the nonlinear constraints are converted into the linear constraints, and the problem is QP formulation, which is similar to the proposed method for islanded mode. By repetitively solving QP, updating the Jacobian matrix, and re-formulating new QP, the optimization problem with nonlinear constraints for HMG can be solved and the base point can be obtained. As this dissertation concentrates on the generation adjustment, the detail method to obtain the optimal base point is not provided.

5.2.1. Performance of the proposed method

Accuracy of loss sensitivity

The accuracy of the loss sensitivity, which is applicable to HMG and has different values by load location, was verified. The conventional loss sensitivity was calculated by the method in [63] with AC bus 1 as slack bus, and the proposed method uses (3.17) and repeated as shown in Fig. 3.3. The simulation was carried out with increasing the load demand at each bus by 10% one by one. Fig. 5.2 shows the average loss error with DGs that is the average of the absolute difference between the predicted loss using the sensitivity and the actual loss obtained by the power flow solution. The line loss at the base point was 89.18 kW. Compared with the conventional method using one loss sensitivity per DG, there was almost no error

when the different loss sensitivities were applied for each load location. From the result, the optimal participation factor of DGs is expected to vary in the load location.

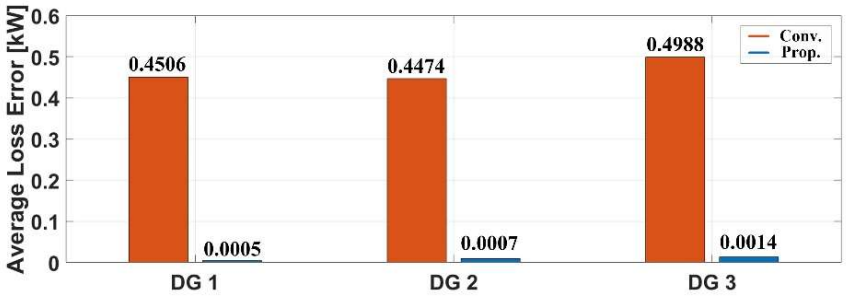

Fig. 5.2 Average loss error with DGs.

Verification of equal GLIC

The calculation method of the BDPF is in essence based on the fact that the GLIC of all DGs has same value at the optimal point, like the equal incremental cost property. Thus, the equal GLIC property should be verified in order to utilize the BDPF for generation adjustment. The GLIC was calculated for total of three load demand, which are 60%, 100%, and 140% of the base load, are investigated. Further, as mentioned in section 3, the reactive power control mode affects the GLICs and corresponding BDPFs. Thus, the cases where the DGs are controlled as a fixed reactive power and as a fixed voltage magnitude are also investigated, respectively. The output powers of RESs and BESSs are zero in order to identify the influence of the load demand, and the interface flow of the main grid is 0.3 MW and 0.3 MVar. To clarify the equal GLIC property, it is assumed that there is no constraints violation.

Tables 5.5–5.7 show the GLIC of all DGs at each bus for 60%, 100%, and 140% of the load demand in fixed reactive power and fixed voltage magnitude, respectively. As load demand increased, the GLICs are larger owing to the high output power. In addition, for each reactive power control mode, all DGs have same GLIC for the same bus (the row elements of each reactive power control mode in Tables 5.5–5.7 are all same), which indicates that the operating point is optimal solution with respect

to the generation cost minimization. For one DG, the GLICs differed for each bus because the influence of the DG on the line loss depends on the bus location. Supplying energy to the bus with high GLIC needs more cost because of the high line loss. In other words, the DGs have to generate more power to supply the same amount of energy to the load. The total cost of fixed V is larger than that of fixed Q, because the reactive power is adjusted so that the voltage magnitude is 1.0 p.u. in fixed V. In fixed Q, the amount of the reactive power is controlled toward the reduction of total cost. In other words, the constraints that keep the voltage constant decrease the objective value of the optimal point. Note that the GLIC of fixed V was not higher than that of fixed Q in all buses. Since AC bus 22 and DC bus 1 are connected via the IC and the IC is assumed to be lossless, the GLICs at their buses have same value.

Table 5.5 GLIC of all DGs at each bus for 60% base load.

Bus		Fixed Q			Fixed V		
		DG1	DG2	DG3	DG 1	DG 2	DG 3
AC	1	263.53	263.53	263.53	260.52	260.52	260.52
	2	263.60	263.60	263.60	260.83	260.83	260.83
	3	264.62	264.62	264.62	263.09	263.09	263.09
	4	264.79	264.79	264.79	264.18	264.18	264.18
	5	264.89	264.89	264.89	265.26	265.26	265.26
	6	265.05	265.05	265.05	267.50	267.50	267.50
	7	264.81	264.81	264.81	267.74	267.74	267.74
	8	263.69	263.69	263.69	268.43	268.43	268.43
	9	264.68	264.68	264.68	269.41	269.41	269.41
	10	265.61	265.61	265.61	270.34	270.34	270.34
	11	265.77	265.77	265.77	270.49	270.49	270.49
	12	266.04	266.04	266.04	270.76	270.76	270.76
	13	266.99	266.99	266.99	271.71	271.71	271.71
	14	267.29	267.29	267.29	272.01	272.01	272.01
	15	267.53	267.53	267.53	272.24	272.24	272.24
	16	267.75	267.75	267.75	272.46	272.46	272.46
	17	268.03	268.03	268.03	272.74	272.74	272.74
	18	268.12	268.12	268.12	272.83	272.83	272.83
	19	263.38	263.38	263.38	260.61	260.61	260.61
	20	261.15	261.15	261.15	258.49	258.49	258.49
	21	260.49	260.49	260.49	257.85	257.85	257.85
	22	259.26	259.26	259.26	256.67	256.67	256.67
	23	265.31	265.31	265.31	263.77	263.77	263.77
	24	266.54	266.54	266.54	264.99	264.99	264.99
	25	267.17	267.17	267.17	265.61	265.61	265.61
	26	265.33	265.33	265.33	267.78	267.78	267.78
	27	265.69	265.69	265.69	268.14	268.14	268.14
	28	266.99	266.99	266.99	269.42	269.42	269.42
	29	267.89	267.89	267.89	270.33	270.33	270.33
	30	268.36	268.36	268.36	270.79	270.79	270.79
	31	268.94	268.94	268.94	271.36	271.36	271.36
	32	269.06	269.06	269.06	271.48	271.48	271.48
	33	269.10	269.10	269.10	271.52	271.52	271.52
DC	1	259.26	259.26	259.26	256.67	256.67	256.67
	2	257.88	257.88	257.88	255.33	255.33	255.33
	3	256.34	256.34	256.34	253.83	253.83	253.83
	4	258.11	258.11	258.11	255.56	255.56	255.56
	5	256.65	256.65	256.65	254.13	254.13	254.13
	6	254.65	254.65	254.65	252.18	252.18	252.18

Table 5.6 GLIC of all DGs at each bus for 100% base load.

Bus		Fixed Q			Fixed V		
		DG1	DG2	DG3	DG 1	DG 2	DG 3
AC	1	406.29	406.29	406.29	400.65	400.65	400.65
	2	406.41	406.41	406.41	401.19	401.19	401.19
	3	408.62	408.62	408.62	405.57	405.57	405.57
	4	408.72	408.72	408.72	407.31	407.31	407.31
	5	408.64	408.64	408.64	408.94	408.94	408.94
	6	408.31	408.31	408.31	412.30	412.30	412.30
	7	407.49	407.49	407.49	412.33	412.33	412.33
	8	403.87	403.87	403.87	411.92	411.92	411.92
	9	406.45	406.45	406.45	414.48	414.48	414.48
	10	408.90	408.90	408.90	416.90	416.90	416.90
	11	409.31	409.31	409.31	417.31	417.31	417.31
	12	410.03	410.03	410.03	418.02	418.02	418.02
	13	412.56	412.56	412.56	420.52	420.52	420.52
	14	413.36	413.36	413.36	421.32	421.32	421.32
	15	413.99	413.99	413.99	421.94	421.94	421.94
	16	414.59	414.59	414.59	422.53	422.53	422.53
	17	415.35	415.35	415.35	423.28	423.28	423.28
	18	415.58	415.58	415.58	423.51	423.51	423.51
	19	405.84	405.84	405.84	400.65	400.65	400.65
	20	400.22	400.22	400.22	395.32	395.32	395.32
	21	398.55	398.55	398.55	393.72	393.72	393.72
	22	395.46	395.46	395.46	390.78	390.78	390.78
	23	410.41	410.41	410.41	407.34	407.34	407.34
	24	413.67	413.67	413.67	410.56	410.56	410.56
	25	415.32	415.32	415.32	412.19	412.19	412.19
	26	409.05	409.05	409.05	413.04	413.04	413.04
	27	410.03	410.03	410.03	414.00	414.00	414.00
	28	413.52	413.52	413.52	417.45	417.45	417.45
	29	415.99	415.99	415.99	419.90	419.90	419.90
	30	417.26	417.26	417.26	421.15	421.15	421.15
	31	418.87	418.87	418.87	422.74	422.74	422.74
	32	419.21	419.21	419.21	423.07	423.07	423.07
	33	419.31	419.31	419.31	423.17	423.17	423.17
DC	1	395.46	395.46	395.46	390.78	390.78	390.78
	2	392.00	392.00	392.00	387.43	387.43	387.43
	3	388.17	388.17	388.17	383.70	383.70	383.70
	4	392.59	392.59	392.59	388.01	388.01	388.01
	5	388.93	388.93	388.93	384.45	384.45	384.45
	6	383.97	383.97	383.97	379.62	379.62	379.62

Table 5.7 GLIC of all DGs at each bus for 140% base load.

Bus		Fixed Q			Fixed V		
		DG1	DG2	DG3	DG 1	DG 2	DG 3
AC	1	552.77	552.77	552.77	544.10	544.10	544.10
	2	552.98	552.98	552.98	544.93	544.93	544.93
	3	556.97	556.97	556.97	552.10	552.10	552.10
	4	556.96	556.96	556.96	554.51	554.51	554.51
	5	556.58	556.58	556.58	556.67	556.67	556.67
	6	555.46	555.46	555.46	561.02	561.02	561.02
	7	553.73	553.73	553.73	560.56	560.56	560.56
	8	546.21	546.21	546.21	557.84	557.84	557.84
	9	551.21	551.21	551.21	562.78	562.78	562.78
	10	555.98	555.98	555.98	567.49	567.49	567.49
	11	556.78	556.78	556.78	568.28	568.28	568.28
	12	558.18	558.18	558.18	569.66	569.66	569.66
	13	563.17	563.17	563.17	574.58	574.58	574.58
	14	564.76	564.76	564.76	576.15	576.15	576.15
	15	566.00	566.00	566.00	577.38	577.38	577.38
	16	567.18	567.18	567.18	578.54	578.54	578.54
	17	568.70	568.70	568.70	580.04	580.04	580.04
	18	569.17	569.17	569.17	580.49	580.49	580.49
	19	551.93	551.93	551.93	543.95	543.95	543.95
	20	541.57	541.57	541.57	534.16	534.16	534.16
	21	538.47	538.47	538.47	531.22	531.22	531.22
	22	532.75	532.75	532.75	525.79	525.79	525.79
	23	560.45	560.45	560.45	555.53	555.53	555.53
	24	566.82	566.82	566.82	561.81	561.81	561.81
	25	570.06	570.06	570.06	565.01	565.01	565.01
	26	556.94	556.94	556.94	562.49	562.49	562.49
	27	558.89	558.89	558.89	564.41	564.41	564.41
	28	565.91	565.91	565.91	571.32	571.32	571.32
	29	570.93	570.93	570.93	576.26	576.26	576.26
	30	573.50	573.50	573.50	578.79	578.79	578.79
	31	576.83	576.83	576.83	582.06	582.06	582.06
	32	577.54	577.54	577.54	582.76	582.76	582.76
	33	577.75	577.75	577.75	582.97	582.97	582.97
DC	1	532.75	532.75	532.75	525.79	525.79	525.79
	2	526.37	526.37	526.37	519.61	519.61	519.61
	3	519.30	519.30	519.30	512.76	512.76	512.76
	4	527.47	527.47	527.47	520.70	520.70	520.70
	5	520.72	520.72	520.72	514.17	514.17	514.17
	6	511.60	511.60	511.60	505.27	505.27	505.27

Calculation of BDPF

At the base point, the BDPF of all buses is calculated using (3.31). Table 5.8 shows the BDPF of all buses at each bus for 100% load demand. The conventional participation factors for DGs 1–3 calculated using the incremental cost (3.9) were 0.2565, 0.4396, and 0.3038, respectively. From Table 5.8, the network loss has significantly influence on the optimal participation factor. The BDPFs differed for each bus, and the maximum differences in BDPF were approximately 3.9%, 10.1%, and 11.6% for DG 1–3, respectively, in fixed Q mode. For fixed V mode, the maximum differences were approximately 4.1%, 16.9%, and 14.7% for DGs 1–3, respectively. The maximum and minimum BDPFs are highlighted in Table 5.8. The difference in fixed V mode is larger than that in fixed Q mode, because the reactive power for keeping the voltage constant makes the difference of the influence of the DG on line loss severe. Like the GLIC, the BDPF at AC bus 22 and DC bus 1 have the same value owing to the lossless IC. Fig. 5.3 shows the stacked bar of the BDPF of the DGs. On the horizontal axis, bus 1 to 33 on the left are the AC buses, and the remaining bus 1 to 6 are the DC buses. The summation of the BDPF at each bus is one, and the difference in participation factor is remarkable for each bus.

The AC grid of the test system is radial configuration. It leads to the fact that the BDPF from the DG connection point to the end bus was almost similar. In this test system, since the DG2 was connected to the AC bus 8, the BDPF between AC bus 8 and 18 are similar. For fixed Q mode, the values are still slightly different due to the line impedance. The loss increases to the end bus, so DG 2 should compensate more power. Thus, DG 2 had slight high BDPF toward each end bus. For fixed V mode, the BDPFs of those buses are relatively similar compared to those of fixed Q mode.

Table 5.8 BDPF of all DGs at each bus for 100% base load.

Bus		Fixed Q			Fixed V		
		DG1	DG2	DG3	DG 1	DG 2	DG 3
AC	1	0.2878	0.4346	0.2776	0.2976	0.4144	0.2880
	2	0.2862	0.4348	0.2790	0.2948	0.4169	0.2883
	3	0.2825	0.4421	0.2754	0.2847	0.4366	0.2787
	4	0.2797	0.4476	0.2727	0.2772	0.4512	0.2716
	5	0.2768	0.4533	0.2699	0.2695	0.4662	0.2643
	6	0.2706	0.4657	0.2637	0.2530	0.4983	0.2487
	7	0.2691	0.4685	0.2624	0.2492	0.5056	0.2452
	8	0.2639	0.4788	0.2573	0.2352	0.5329	0.2319
	9	0.2637	0.4792	0.2571	0.2352	0.5329	0.2319
	10	0.2635	0.4796	0.2569	0.2352	0.5329	0.2319
	11	0.2635	0.4797	0.2568	0.2352	0.5329	0.2319
	12	0.2634	0.4798	0.2568	0.2352	0.5329	0.2319
	13	0.2632	0.4802	0.2566	0.2352	0.5329	0.2319
	14	0.2632	0.4803	0.2565	0.2352	0.5329	0.2319
	15	0.2631	0.4804	0.2565	0.2352	0.5329	0.2319
	16	0.2631	0.4805	0.2564	0.2352	0.5329	0.2319
	17	0.2630	0.4806	0.2564	0.2352	0.5329	0.2319
	18	0.2630	0.4806	0.2564	0.2352	0.5329	0.2319
	19	0.2847	0.4326	0.2827	0.2933	0.4148	0.2919
	20	0.2706	0.4122	0.3172	0.2790	0.3953	0.3257
	21	0.2667	0.4065	0.3268	0.2750	0.3899	0.3351
	22	0.2599	0.3966	0.3435	0.2681	0.3804	0.3515
	23	0.2825	0.4422	0.2753	0.2847	0.4366	0.2787
	24	0.2824	0.4423	0.2753	0.2846	0.4367	0.2787
	25	0.2824	0.4423	0.2753	0.2846	0.4367	0.2787
	26	0.2705	0.4658	0.2637	0.2530	0.4983	0.2487
	27	0.2705	0.4659	0.2636	0.2530	0.4983	0.2487
	28	0.2702	0.4663	0.2635	0.2529	0.4984	0.2487
	29	0.2701	0.4666	0.2633	0.2529	0.4984	0.2487
	30	0.2700	0.4668	0.2632	0.2529	0.4984	0.2487
	31	0.2699	0.4670	0.2631	0.2529	0.4984	0.2487
	32	0.2699	0.4670	0.2631	0.2529	0.4984	0.2487
	33	0.2677	0.4636	0.2687	0.2504	0.4949	0.2547
DC	1	0.2599	0.3966	0.3435	0.2681	0.3804	0.3515
	2	0.2561	0.3909	0.3530	0.2643	0.3750	0.3607
	3	0.2524	0.3852	0.3624	0.2605	0.3695	0.3700
	4	0.2561	0.3909	0.3530	0.2643	0.3749	0.3608
	5	0.2523	0.3852	0.3625	0.2605	0.3695	0.3700
	6	0.2486	0.3795	0.3719	0.2567	0.3641	0.3792

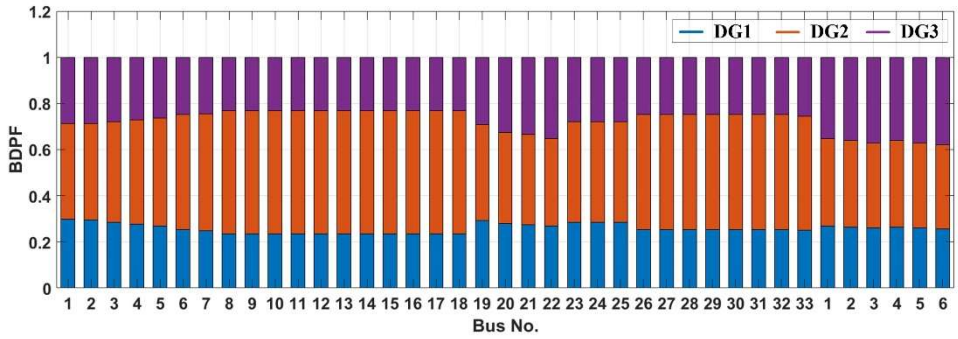

Fig. 5.3 Stacked bar of BDPF of DGs.

The value of GLIC derivative and loss sensitivity are dependent on the base point. In other words, the BDPF depends on the system condition such as generation and loading level. Thus, the BDPFs for different loading level were calculated. Fig. 5.4 shows the boxplot of BDPF of DG 1–3 with loading level 60% to 140% for fixed Q mode, respectively. On each box, the central mark indicates the median, and the bottom and top edges of the box indicate the 25th and 75th percentiles, respectively. The whiskers extend to the most extreme data points not considered outliers.

From Fig. 5.4, the maximum BDPF differences of DG 1, 2, and 3 with loading level were 1.04%, 2.06%, and 2.87% on average, respectively. This may result in the performance degradation of the proposed method if the BDPF first obtained is used in all loading level. However, while the loading level changes significantly like 60% to 140%, the base point will continue to be updated at certain time intervals. The BDPF can also be updated at the same time interval, so the BDPF is enough valid between two consecutive updating time. For fixed V mode, the results were very similar to those for fixed Q mode, so the boxplots are not shown. The average of the maximum difference of BDPFs of DG 1, 2, and 3 were 1.24%, 3.43%, and 3.20%, respectively.

The load variation of each bus may be different from others. Thus, the BDPF variation was calculated by randomly changing the net load of each bus from 60% to 140% of its base demand, respectively. The calculation was repeated 100 times.

The average of the maximum difference of BDPFs of DG 1, 2, and 3 were 0.64%, 1.01%, and 1.33% for fixed Q, respectively, and 1.02%, 1.82%, and 1.45% for fixed V, respectively. The BDPF variation of this case was smaller than that of the case where the load demand of each bus changed at the same rate.

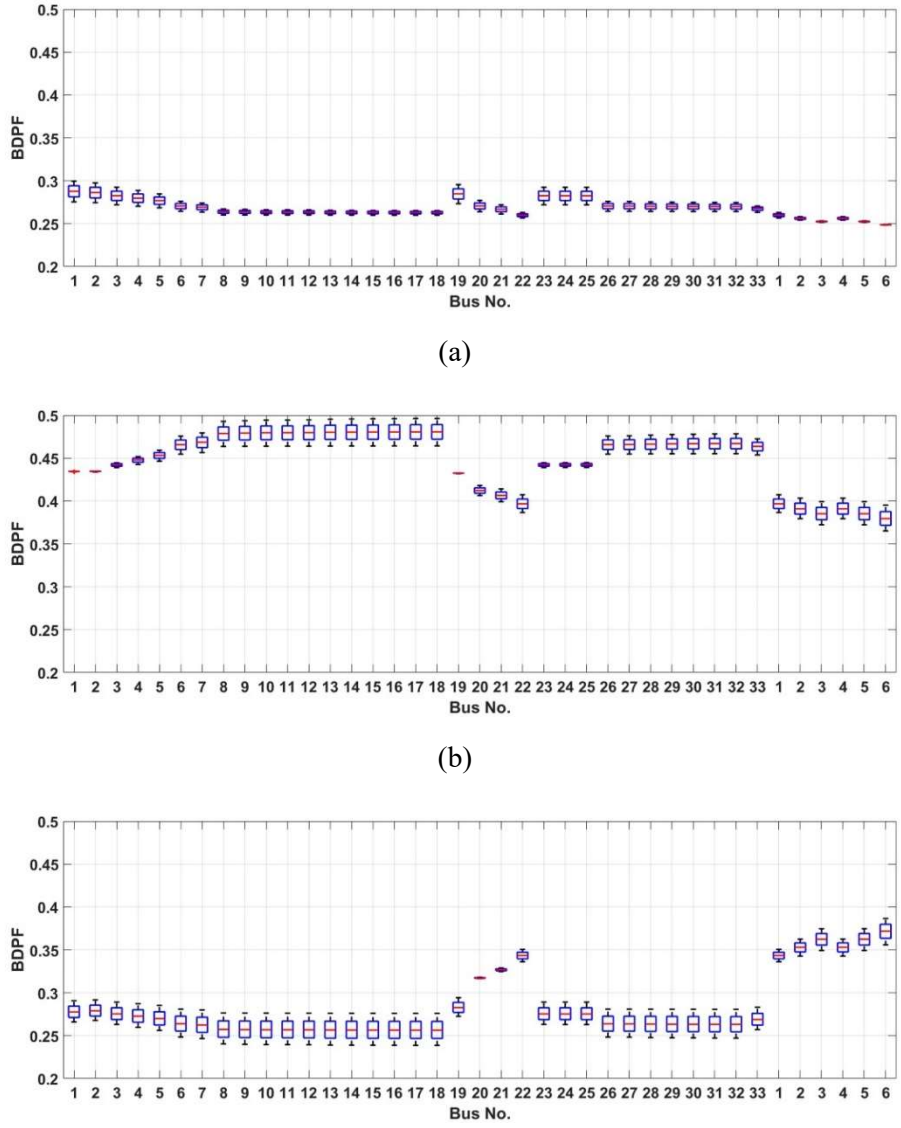

(a)

(b)

(c)

Fig. 5.4 Boxplot of BDPF for different loading level: (a) DG 1, (b) DG 2, (c) DG 3.

5.2.2. Comparative analysis

To figure out the performance of the proposed method, four methods for adjusting the generation were compared. Since the DG 1 is connected to the PCC of the main grid, it is able to perform the FFC locally as shown in Fig. 2.11, which is the first method (M-G 1). The second method (M-G 2) was the conventional method where the generation was adjusted proportionally to the conventional participation factor using (3.9). The third method (M-G 3) was the proposed method, which mainly used the BDPF. The last method (M-G 4) was the OPF method, which found a new optimal point for comparison. Note that using M-G 1, the power imbalance is completely resolved by the DG 1. Using M-G 4, the generation is a feasible solution because it solves the nonlinear power flow equation. However, the M-G 2 and M-G 3 lead to the inevitable minor power imbalance owing to linearization. Thus, in these methods, the results were divided into two cases in which the imbalance is compensated by the main grid and the DG 1, respectively (The DG 1 can compensate it with FFC). Hence, for accurate comparison, the power flow method should be solved for resolving the imbalance after the generation was adjusted.

Accuracy of BDPF

After the base point and the BDPF at that point were calculated, the net load change of some buses was made arbitrary to verify the accuracy of BDPF, and the snapshot results of DGs' output, total cost, and interface power variation were investigated. To clarify that the optimal participation factor is dependent on the bus location, fixed V mode was selected as a reactive power control.

Case 1: Table 5.9 shows the net load variation in Case 1, and the results where the small imbalance was compensated by the main grid (Case 1-1) and by a DG (Case 1-2) after the generations were adjusted are summarized in Tables 5.10 and 5.11, respectively. The M-G 1 makes the interface power variation zero, but it leads to the high total cost. Regarding Case 1-1, in M-G 3, DG 3 decreased its output

power more than it did with the M-G 2 because the BDPFs of DG 3 at AC bus 21, DC buses 4, and 6, where load variation occurred, were larger than the conventional participation factors. In contrast to DG 3, the output power of DG 2 obtained with the M-G 3 was larger than that obtained with the M-G 2. In the case of DG 1, the output was almost same for M-G 2 and M-G 3 owing to the offset of the participation factor difference. In the M-G 3, the output power of DGs was very close to those of the M-G 4, resulting in almost zero interface power variation. For both M-G 2 and M-G 3, because the main grid is rather provided more power, the total cost of them is lower than that of M-G 4. It leads to the unfair total cost comparison. Regarding Case 1-2, the results of M-G 1 and M-G 4 are same as those of Case 1-1. M-G 2 and M-G 3 were the same except that the interface power variation was eliminated by DG 1. The total cost of M-G 3 was very close to the optimal point (M-G 4).

Table 5.9 Net load change of Case 1.

Bus	Net Load Variation [kW]
AC 21	-100
DC 4	-100
DC 6	-100

Table 5.10 Comparison results of Case 1-1.

	M-G 1	M-G 2	M-G 3	M-G 4
DG 1 [MW]	0.8646	1.0752	1.0752	1.0754
DG 2 [MW]	1.6774	1.5455	1.5712	1.5704
DG 3 [MW]	1.3318	1.2406	1.2222	1.2241
Total Cost [$/h]	890.1552	876.6420	880.1630	880.6101
Standard Deviation [MW]	0.1837	0.0208	0.0014	-
Interface Power Variation [MW]	-	0.0108	0.0012	-

Table 5.11 Comparison results of Case 1-2.

	M-G 1	M-G 2	M-G 3	M-G 4
DG 1 [MW]	0.8646	1.0860	1.0764	1.0754
DG 2 [MW]	1.6774	1.5455	1.5712	1.5704
DG 3 [MW]	1.3318	1.2406	1.2222	1.2241
Total Cost [$/h]	890.1552	880.734	880.6110	880.6101
Standard Deviation [MW]	0.1837	0.0224	0.0016	-
Interface Power Variation [MW]	-	-	-	-

Case 2: Table 5.12 shows the load variation in Case 2. The load variation occurred at three buses, but the total net change was zero. Tables 5.13 and 5.14 list the results, like Case 1. As shown in Table 5.13, although the total net change was zero, the interface power of M-G 2 and M-G 3 changed because of the line loss change. In M-G 3, DG 3 decreased their output power, while DG 2 increased its output power; this is because the BDPF of DG 2 at DC bus 3 was smaller than that at AC bus 15 and 33, whereas DG 3 showed the opposite trend. In the case of DG 1, the average BDPF at AC bus 15 and 33 was slightly larger than that at DC bus 3. Due to the loss change, the interface power variation of M-G 2 highly increased. When the DG 1 compensated the interface power variation, M-G 2 had the same result as M-G 1, and M-G 3 was very similar to M-G 4, as shown in Table 5.14.

Table 5.12 Net load change of Case 2.

Bus	Net Load Variation [kW]
AC 15	+70
AC 33	+80
DC 3	-150

Table 5.13 Comparison results of Case 2-1.

	M-G 1	M-G 2	M-G 3	M-G 4
DG 1 [MW]	1.1666	1.1522	1.1533	1.1532
DG 2 [MW]	1.6774	1.6774	1.7046	1.7043
DG 3 [MW]	1.3318	1.3318	1.3164	1.3161
Total Cost [$/h]	998.7532	992.9574	998.8870	998.6109
Standard Deviation [MW]	0.0240	0.0215	0.0001	-
Interface Power Variation [MW]	-	0.0144	-0.0007	-

Table 5.14 Comparison results of Case 2-2.

	M-G 1	M-G 2	M-G 3	M-G 4
DG 1 [MW]	1.1666	1.1666	1.1526	1.1532
DG 2 [MW]	1.6774	1.6774	1.7046	1.7043
DG 3 [MW]	1.3318	1.3318	1.3164	1.3161
Total Cost [$/h]	998.7532	998.7532	998.6109	998.6109
Standard Deviation [MW]	0.0240	0.0240	0.0005	-
Interface Power Variation [MW]	-	-	-	-

Case 3: Table 5.15 shows the load variation in Case 3, in which the net load at the same location of Case 1 increased, which leads to the generation limit violation. Tables 5.16 and 5.17 list the results of Case 3-1 and 3-2, respectively. Once the output power was adjusted using Table 5.8, the output of DG 3 exceeded its output limit (1.2092, 1.7544, and 1.4128 for DG1–3, respectively). The re-distribution process was performed, and the output of DG 3 was set to 1.4 MW, which is its maximum output limit. After the re-distribution, the result of M-G 3 was still almost same as M-G 4. As the re-distribution was carried out, the difference between M-G 1 and M-G 2 in output of DG 1 and DG 2 was relatively reduced, and it results in the total cost of M-G 2 similar to that of M-G 4. Clearly, the proposed method worked well on the constraints of output power limits.

Table 5.15 Net load change of Case 3.

Bus	Net Load Variation [kW]
AC 21	+50
DC 4	+80
DC 6	+90

Table 5.16 Comparison results of Case 3-1.

	M-G 1	M-G 2	M-G 3	M-G 4
DG 1 [MW]	1.3660	1.2086	1.2130	1.2139
DG 2 [MW]	1.6774	1.7741	1.7613	1.7619
DG 3 [MW]	1.3318	1.3986	1.4000	1.4000
Total Cost [$/h]	1085.4746	1082.6411	1079.5997	1080.1760
Standard Deviation [MW]	0.1321	0.0092	0.0005	-
Interface Power Variation [MW]	-	-0.0058	0.0014	-

Table 5.17 Comparison results of Case 3-2.

	M-G 1	M-G 2	M-G 3	M-G 4
DG 1 [MW]	1.3660	1.2028	1.2144	1.2139
DG 2 [MW]	1.6774	1.7741	1.7613	1.7619
DG 3 [MW]	1.3318	1.3986	1.4000	1.4000
Total Cost [$/h]	1085.4746	1080.2190	1080.1761	1080.1760
Standard Deviation [MW]	0.1321	0.0117	0.0006	-
Interface Power Variation [MW]	-	-	-	-

Figs. 5.4 and 5.5 show the comparison results clearly. The absolute value of the interface flow variation was used in Fig. 5.5. The proposed method (M-G 3) significantly reduced the interface flow variation compared to M-G 2 for cases 1–3. M-G 1 can keep the interface flow constant, but it caused high total cost because only DG 1 compensated the net load variation. Fig. 5.6 shows the total cost difference between M-G 1–3 and the optimal cost. The total cost of the proposed method was almost same as the optimal cost for cases 1–3.

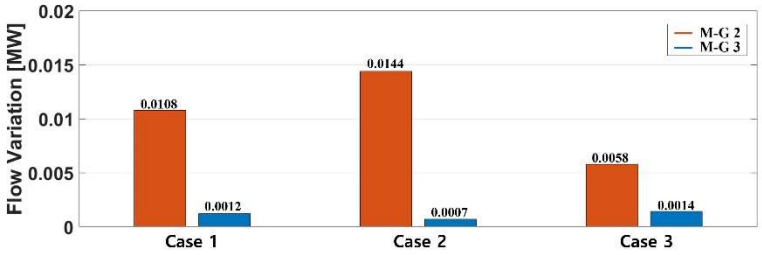

Fig. 5.5 Comparison of the interface power variation.

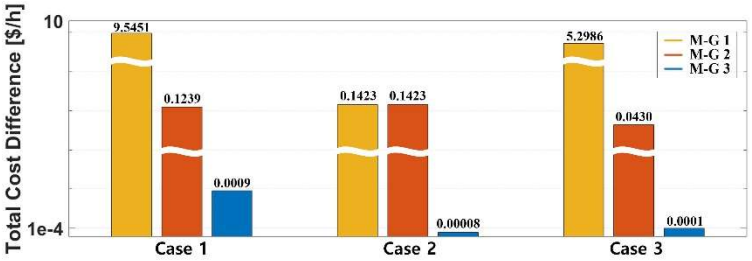

Fig. 5.6 Comparison of the total generation cost.

Continuous operation

So far, the effectiveness of the proposed method was verified for the snapshot. To clarify the performance of the proposed method, the results of continuously applying the proposed method were examined. The high penetration level of the RES mainly causes the net load fluctuation; thus, the output variation occurs at AC bus 21, 33, and DC bus 4. The total net load fluctuation from the base point is shown in Fig. 5.7. It fluctuates from about -100 to +100 kW for 10 min. Note that it is the total

net load variation, and the amount of variation by buses was different (Increase and decrease in the output of RESs were offset by buses).

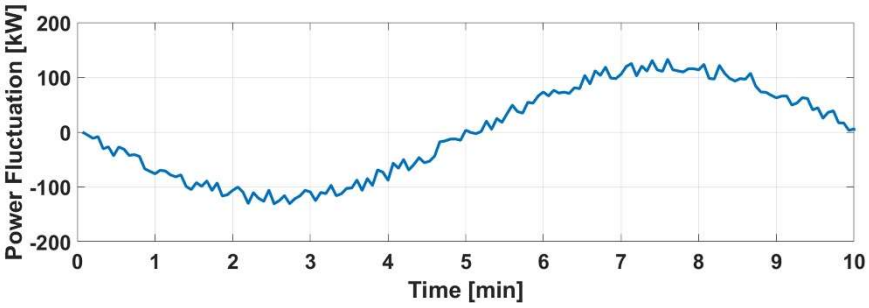

Fig. 5.7 Net load variation over time.

The time-domain result of the interface power variation is shown in Fig. 5.8, where the power unbalance was compensated by the main grid. In M-G 2, the interface power fluctuated from about -10 kW to 20 kW. Negative variation means that DGs generate more powers than internal fluctuation and the main grid receives the remaining power, and positive variation represents the opposite situation. In M-G 3, the interface power fluctuated from about 0 to +5 kW regardless of the sign of net load variation. At the base point, the interface power of the main grid was 300 kW. The conventional method was -3.33 to 6.67 % away from the base point, and the proposed method was 0 to 1.67 % away. The base interface power and the amount of the fluctuation by buses may affect the performance of the methods, but the proposed method maintained the interface flow better than the conventional method.

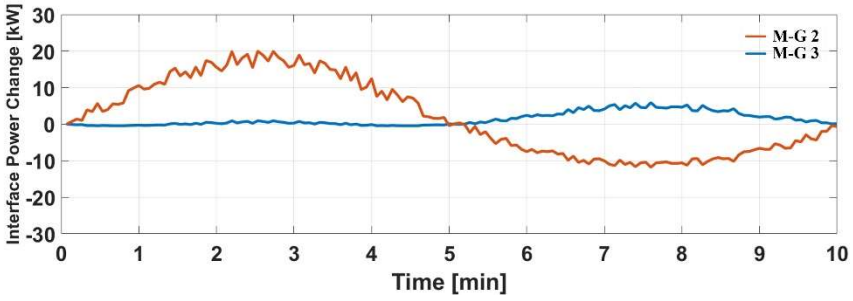

Fig. 5.8 Interface power variation over time.

The total cost comparison was conducted in the case where the power unbalance after generation adjustment using participation factors is compensated by the DG 1. The total cost difference between M-G 4 and the other methods is shown in Fig. 5.9. At all time, the total cost of the proposed method is closest to the optimal value that is obtained by M-G 4. The proposed method did not reduce the total cost significantly because all method adjusts the output power from the base point which is optimal point for cost minimization, but it can helpful if it is applied continuously.

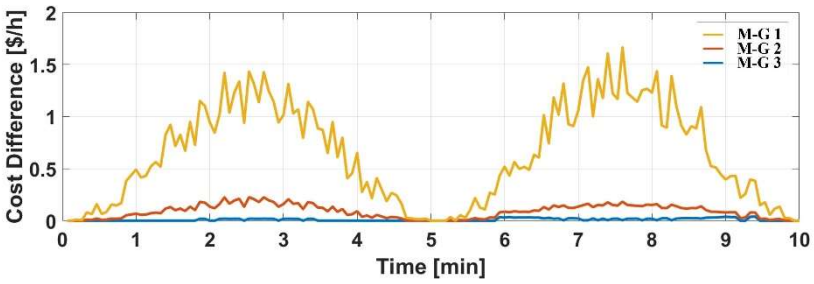

Fig. 5.9 Total cost difference with OPF method over time.

The simulation results indicated that the proposed method performed very well. It effectively alleviates the burden of the main grid while reducing generation cost. Note that if the DG 1 is not connected to the PCC of the main grid, the interface power variation exists (without FFC). It may reduce the total cost in some cases by taking the power from the main grid, but it imposes the burden to main grid and may pay a penalty depending on the contract. Even if the DG 1 performs FFC, the proposed method is more economically effective. The proposed method may be less effective if the amount and location of the load variation result in offsetting the difference between the BDPF and the conventional participation factor. However, in practice, the amount of load change varies with the buses, and the RES is located on certain buses depending on local geographical factors. Moreover, high penetration of RESs intensifies this distinction between buses. Therefore, if the power variation of each bus can be monitored in real time, the proposed method would enable the grid-connected HMG to operate more reliably and economically.

5.3 Case study for islanded mode

The proposed method for islanded mode is divided into two stage (long-term and short-term operation). The long-term operation determines the on/off decision of DGs and controllable loads, and the final output power is calculated in the short-term operation. The main focus of this dissertation is the short-term operation; thus, the case studies of the long-term operation are briefly presented, and those of the short-term operation are investigated in more detail.

5.3.1. Performance of the proposed method

Net load forecasting

To schedule the DGs and controllable loads, the time-series net load should be forecasted. The forecasting is performed using NARX algorithm. To properly learn the forecasting algorithm, sufficient data representing the algorithm are required. In this dissertation, because the real PV output for a year can be used, the PV output forecasting is conducted. Note that the load demand and wind power can also be forecasted in a similar way, but they were assumed to be predicted as a general time-series pattern and real data from a specific region due to the lack of the data.

Among the learning input data, 75% of data was used for training and 25% of data was used for validation. The delay time is 4 (i.e. the input and output data before 1–4 steps are used as feedback). The number of neurons and hidden layer are 20 and 1, respectively. The NARX algorithm in MATLAB neural network toolbox is used. If the actual output is measured in real-time, the NARX openloop algorithm can be used; thus, the NARX openloop and closeloop are investigated, respectively.

Figs. 5.10 and 5.11 show the PV forecasting results of openloop and closeloop NARX for 5 days with 15 min step, respectively. The forecasting error of the openloop NARX was 2.31%, which is much smaller than that of the closeloop NARX (4.42%). From Fig. 5.10, since the last actual output is fed back to the

algorithm input in the openloop NARX, the forecasted value is similar to the time-shifted actual value. From the results, the prediction using the NARX algorithm is valid enough to decide the on/off decision. Still, the error inevitably exists and the output can be fluctuated in short time (e.g. 1 min), which will be handled in short-term operation.

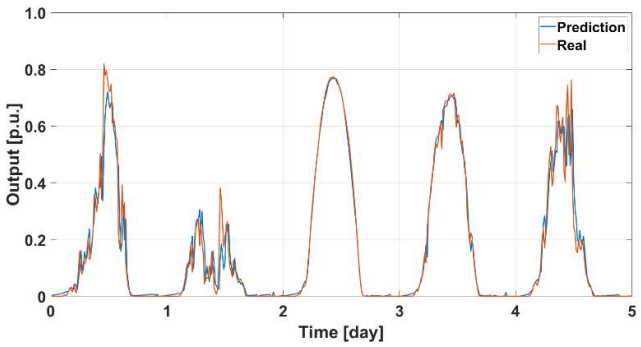

Fig. 5.10 PV forecasting result of openloop NARX.

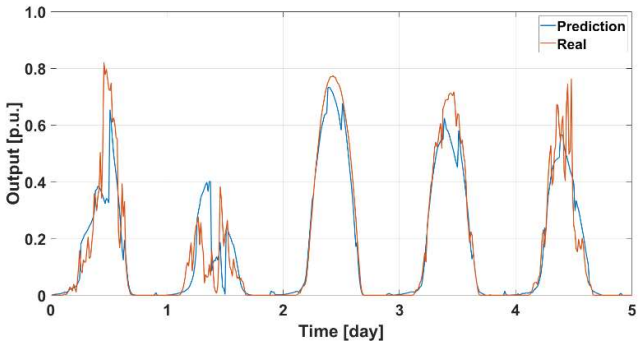

Fig. 5.11 PV forecasting result of closeloop NARX.

Result of long-term operation

Based on the time-series forecasted value and linearization method, the on/off decision can be decided by the long-term operation. To simulate a situation where the generation is insufficient, it is assumed that the RES output was low and the load demand was high. The total net load over time is shown in Fig. 5.12. The x-axis represents the long-term prediction time step and the y-axis is the load gain from the

base load demand. The controllable loads (L1–L5) are 100, 60, 100, 40, and 40 kW and they are connected at AC bus 2, 4, 14, 26 and DC bus 2 with the weight factors w_L 1000, 1000, 2000, 4000, and 4000, respectively.

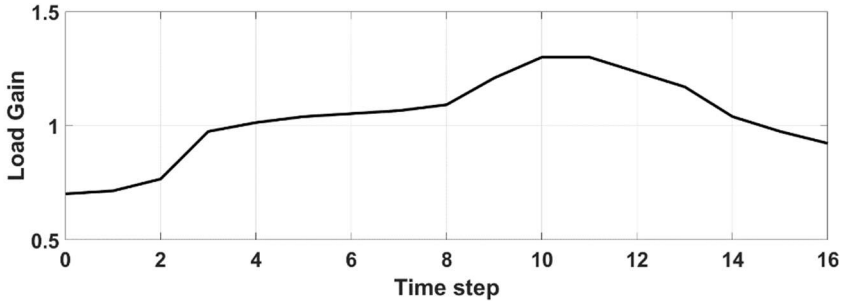

Fig. 5.12 Total net load prediction for long-term operation.

Table 5.18 shows the on/off decision of controllable loads. The L2 was first turned off because its w_L was the smallest and the amount of the load was less than the L1. Since the net load was highest at time steps 10 and 11, the L1–L3 were turned off. From the long-term operation, the output power of DGs can also be obtained; however, the cost function was approximated to piecewise linear function, and it may not provide the optimal output power. Only the on/off decision will be used for short-term operation.

Table 5.18 Controllable loads on/off decision.

	1	2	3	4	5	6	7	8	9	10	11	12	13	14	15	16
L1	O	O	O	O	O	O	O	O	X	X	X	X	X	O	O	O
L2	O	O	O	O	O	O	O	X	X	X	X	X	X	O	O	O
L3	O	O	O	O	O	O	O	O	O	X	X	O	O	O	O	O
L4	O	O	O	O	O	O	O	O	O	O	O	O	O	O	O	O
L5	O	O	O	O	O	O	O	O	O	O	O	O	O	O	O	O

Verification of sensitivity

To investigate the short-term operation, two load sets, namely the heavy load and light load, were considered. They are based on the predicted net load, but the

fluctuation occurred at short time interval due to the high uncertainty. Fig. 5.13 shows two net load profiles for an interval of 1 min, which is the time interval Δt_s. The reactive power demand in the AC grid was set to the same power factor as the base load demand. Since the lowest load demand for one day is 20 to 35 % of maximum demand, which is dependent on the load type [85], the light load may have almost zero net load at some time.

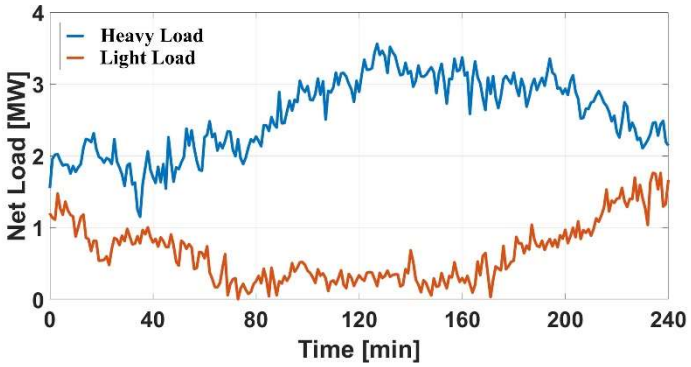

Fig. 5.13 Net load variation.

As the sensitivity values are used to predict the frequency and voltage magnitude, the actual values may be different and the final output of the DGs may also be different because of the LC. To clarify the accuracy of the sensitivity, the average error, which is the absolute value of the difference between the actual value and the predicted value, was calculated for (4.37), (4.38), and (4.45) (The proposed method 1 is used). To find the actual value, the power flow of the islanded HMG was solved after updating the set-points.

Table 5.19 Average sensitivity error.

Average Error	Heavy Load	Light Load
Frequency [Hz]	27e-4	20e-4
AC Voltage Magnitude [p.u.]	0.86e-4	0.59e-4
DC Voltage Magnitude [p.u.]	0.89e-4	0.67e-4
Active Power of DG [MW]	18e-4	13e-4
Reactive Power of DG [MVar]	27e-4	20e-4

Table 5.19 lists the average linearization errors for heavy and light loads related to the frequency, AC and DC voltage magnitude for one bus, and active and reactive powers of one DG. In both the load sets, the average errors of all the quantities were significantly lower than their rated value. Therefore, the sensitivity can be used with high accuracy.

Performance results

Depending on the calculation of frequency variation, the proposed method for short-term operation can be divided into two cases; one uses only (4.37) to calculate frequency variation, and the other uses (4.41) and (4.42). To analyze the characteristics of the proposed method, the results of the proposed method 1 was analyzed for both heavy load and light load. The proposed method 2 shows the similar results. The following case studies were conducted with time interval (Δt_s) of 1 min and prediction time horizon (T_h) of 10 min. The weight factors w_c and w_v were one and 10^4, respectively. As the supervisory control is focused, the results of the primary control that occur between the two successive time steps are not shown in the following simulation results. The results were obtained from 1 min (Δt_s) snapshot with steady-state values.

Heavy Load: Fig. 5.14 shows the performance results for the heavy load. The active power of the DGs increased until their incremental cost was close to the cost coefficient of the BESS. The cost coefficient c_b can be regarded as an incremental cost of the BESS. Hence, an equal incremental cost point is obtained when the output of DG becomes $(c_b–c_1)/2c_2$, which are approximately 0.82, 1.06, and 1.00 MW for DG 1–3. The point was slightly different because of the effect on the line loss and voltage profile. Although BESS 1 and 2 had the same c_b, the output power of BESS 1 increased first. As the BESS cost was modeled as a linear function and there was a difference in the influence of the line loss reflected by the sensitivity, one was more beneficial than the other. For the same reason, the output of DGs was slightly higher when BESS 2 discharges than when BESS 1 discharges. After BESS 1 reached its

maximum discharge output (0.5 MW) or minimum SOC (20%), BESS 2 started to discharge. Note that as the BESS SOC was close enough to the minimum value, the output decreased gradually because the MPC controller considered the prediction time horizon T_h. As shown in Fig. 5.14(c), the frequency was kept close to the nominal value, i.e., 60 Hz.

Fig. 5.14(d) shows the reactive power output, and Fig. 5.14(e) shows the maximum and minimum voltages among the total AC and DC buses. As load demand increased, the DG 1 and 2 reached their reactive power limits. BESS 1 started to decrease the reactive power when it discharged. The voltage magnitude of both the AC and DC grid were well maintained near their rated value.

Light Load: Fig. 5.15 shows the results of the light load case. After the outputs of the DGs reached their minimum set values as the net load decreased, the BESS started to charge. The minimum output of the DGs were set to 5% of their rating power. It is not a physical constraint but rather the value determined by the system operator in order to prevent degradation of inverter efficiency for low output and to cope with excessive RES generation. Unlike the heavy load case, BESS 2 charged first, and BESS 1 started to charge before BESS 2 reached its maximum charge output (–0.5 MW) or maximum SOC (90%) to maintain the voltage magnitude. The amount of charge of BESS 2 decreased as the SOC reached its maximum value. As shown in Fig. 5.15(c), the frequency was well maintained at the rated value.

For the reactive power, DG 1 and 2 changed their reactive power similar to the net load pattern. Contrary to the heavy load, BESS 1 increased the reactive power when it charged. At this time, the reactive power of DGs fluctuated, but all the voltage magnitudes were closer to the rated value compared to the heavy load case because the voltage drop due to the line impedance was low (low line current).

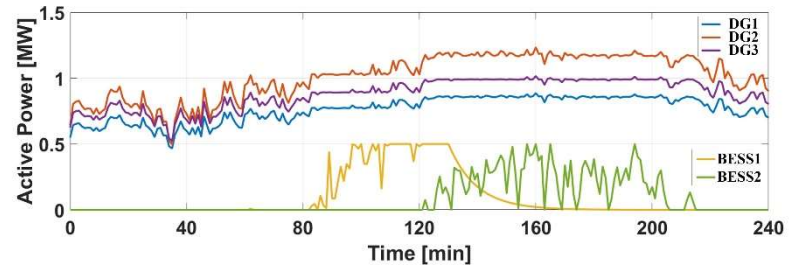

(a)

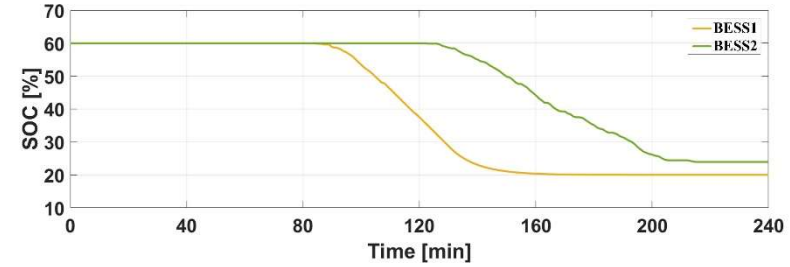

(b)

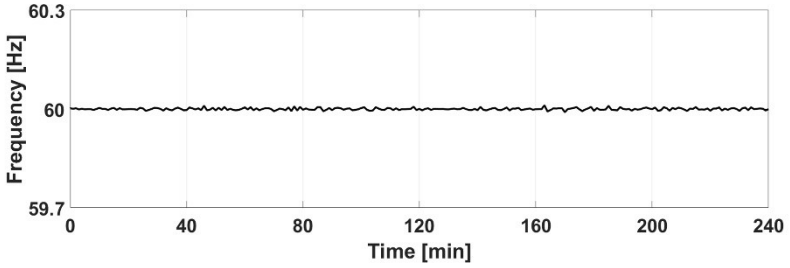

(c)

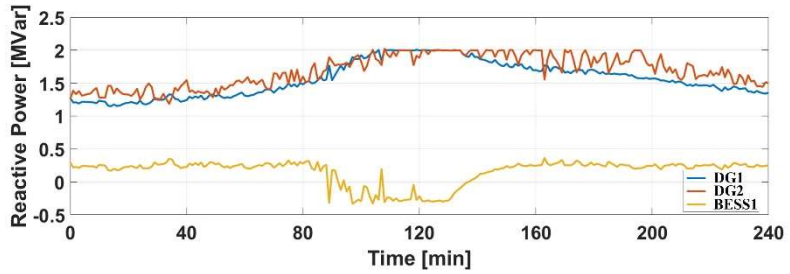

(d)

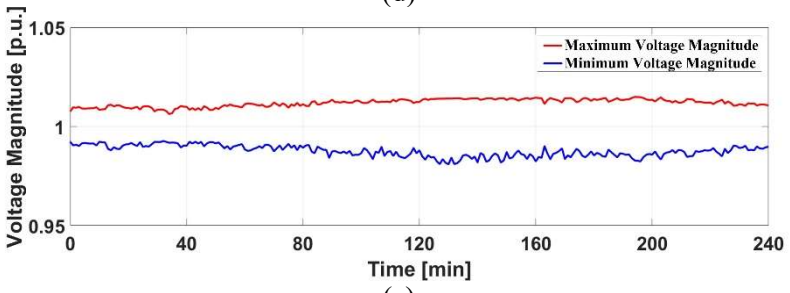

(e)

Fig. 5.14 Results for the heavy load: (a) Active power, (b) SOC, (c) Frequency, (d) Reactive power, (e) Voltage magnitude.

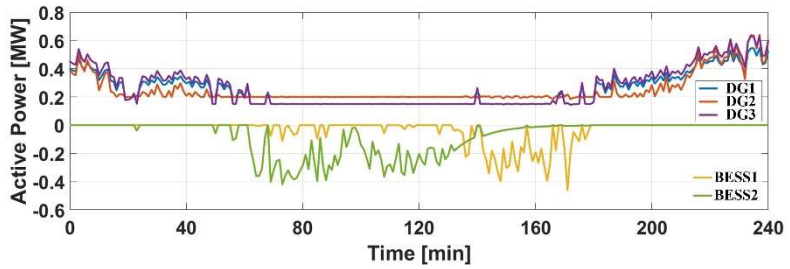

(a)

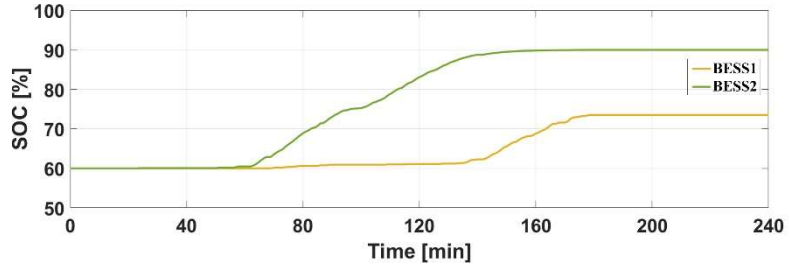

(b)

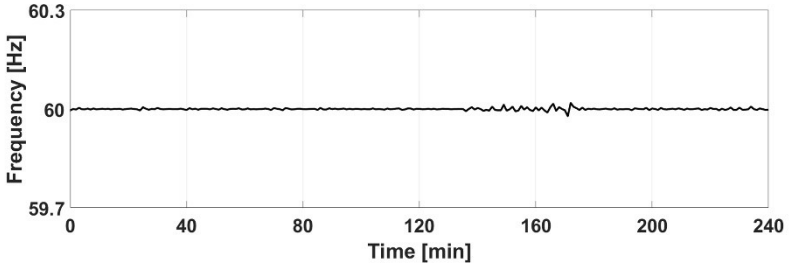

(c)

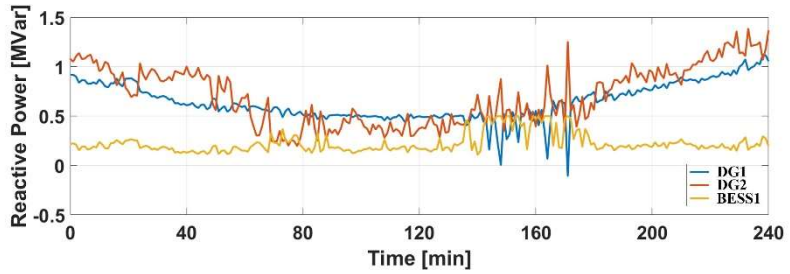

(d)

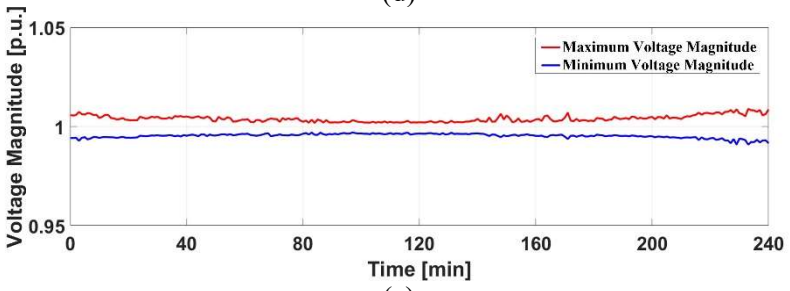

(e)

Fig. 5.15 Results for the light load: (a) Active power, (b) SOC, (c) Frequency, (d) Reactive power, (e) Voltage magnitude.

5.3.2. Comparative analysis

A total of four methods composed the case studies for comparison. M-I 1 is the case where all resources operate with only droop control after setting the initial set-point. This method was used to verify the effectiveness of updating the set-points in a short cycle. M-I 2 is the case where the optimization problem is solved using a standard linearized power flow model [69], [70]. In this method, the AC line flows are linearized with respect to AC voltage angle and magnitude (4.6) and (4.7). The analogous method is applied to the DC grid. The DC line flow is modeled as a linear expression of DC voltage (4.8). The proposed method basically uses the derivatives to consider the system state and solve the optimization problem; thus, M-I 2 was chosen for comparative analysis. M-I 3 and 4 are the proposed methods; M-I 3 uses only (4.37) to calculate frequency variation, the proposed method 1, and M-I 4 considers the frequency variation (4.41) and (4.42), the proposed method 2.

Note that during the simulation, M-I 1 operates locally, and M-I 2 requires all bus load data and RES output per iteration. M-I 3 requires the frequency, voltage magnitude, and RES output per iteration. The frequency can be measured locally, so only voltage magnitude and RES output should be communicated. If the bus load data are collected, the sensitivity matrix can be updated. However, in M-I 3, the sensitivity calculated at the beginning of the simulation time is used during the total simulation time. In contrast, the sensitivity matrix should be updated per iteration in M-I 4 to prevent the sudden change of output reactive powers; thus, M-I 4 requires all the information used in M-I 2 and M-I 3.

Comparison results

To verify the effectiveness of the proposed method comparatively, M-I 1 to 4 were compared for frequency and voltage deviation, generation cost of DG, amount of SOC variation, and average computation time. The total deviation for verifying frequency and voltage restoration is defined as

$$Total\ Deviation = \left\| \boldsymbol{y}_k - \boldsymbol{y}^n \right\|_2 \tag{5.3}$$

where $\boldsymbol{y}$ can be the frequency, AC and DC voltage magnitude vectors.

Table 5.20 Comparison of the methods for heavy load.

	M-I 1	M-I 2	M-I 3	M-I 4
Total Frequency Deviation [Hz]	7.6106	0.8797	0.0524	0.0033
Total AC Voltage Deviation [kV]	16.4533	8.1741	7.4857	8.1511
Total DC Voltage Deviation [kV]	15.4422	3.1069	2.6807	2.4168
Generation Cost of DG [$]	1924.9	1983.1	1943.8	1973.7
Discharge of BESS [MWh]	0.7571	0.6139	0.7225	0.5040
Average Computation Time [s]	-	0.0803	0.0689	0.0890

Table 5.21 Comparison of the methods for light load.

	M-I 1	M-I 2	M-I 3	M-I 4
Total Frequency Deviation [Hz]	4.3883	0.2965	0.0523	0.0201
Total AC Voltage Deviation [kV]	10.5261	2.8410	2.5691	2.7545
Total DC Voltage Deviation [kV]	7.4183	1.1300	1.0049	0.9728
Generation Cost of DG [$]	375.9195	360.7946	353.7904	350.6184
Charge of BESS [MWh]	0.6049	0.5013	0.4576	0.4543
Average Computation Time [s]	-	0.0732	0.0682	0.0879

Tables 5.20 and 5.21 show the comparison results for the heavy load and light load, respectively. Regarding both load cases, M-I 1 had relatively large frequency and voltage deviation owing to the droop control. Compared to M-I 2, the frequency was better kept in M-I 3 and 4, and especially M-I 4 significantly reduced the frequency deviation because it considered reactive power and second-order sensitivity for frequency. In M-I 3 and 4, the voltage magnitude was also slightly better restored than the conventional method M-I 2. The total AC voltage deviation was the smallest in M-I 3, and the total DC voltage deviation was the smallest in M-I 4. The light load case shows similar trends, although it was relatively less effective.

The cost of DGs and the discharge amount of BESSs were slightly different by methods, both of which can be represented by the value of the objective function (4.18). The total costs of M-I 1 to 4 for heavy load, including the cost of the discharge, are 2152.1, 2167.3, 2160.5, and 2124.9 $, respectively. M-I 1 had lower total cost

than M-I 2 and 3, because the voltage magnitude decreased due to the droop control as the net load increased. The conservative voltage reduction effect reduced the amount of the load consumption and consequently reduced the total cost. If the dependency of the load on the voltage is low, M-I 1 has higher total cost than other methods. The total cost of M-I 3 and 4 was less than that of M-I 2. In particular, M-I 4 had better performance, because it can make the frequency deviation almost zero and final output can be closer to the optimal set-point. In the light load case, the direct cost comparison is less meaningful because the BESSs were charged. M-I 3 and 4 can estimate the required active power well, they reduced the output of DGs and the charging of BESSs. M-I 2 had a relatively large amount of BESS charge, and the output of DGs also increased accordingly.

Regarding the computation time, M-I 3 was around 7.3–16.5% times faster than M-I 2, and M-I 4 required slightly more time than M-I 2. All methods decide the set-point of the resources, but compared to M-I 3 and 4, M-I 2 additionally needs AC voltage angle, magnitude, and DC voltage as decision variables per iteration, i.e., in this test system, it needs additional decision variables of 72 (33+33+6) times the number of time steps of the prediction horizon. Using the sensitivity, these system variables can be expressed as the set-point of the resources, so the number of decision variables can be reduced in the proposed method, which resulted in less computation time in M-I 3. The equality constraint was quadratic in M-I 4, so the computation time was slightly higher than in M-I 2 although the number of decision variables is small.

Weight factor of objective function

The objective function (4.20) is composed of two objective functions, and the performance of the proposed method depends on the weight factor combination; thus, the analysis of the combination of the weight factors was conducted. Five weight factor ratios (WFRs) were studied; WFR1–5 referred to weight factor ratios (w_v/w_c) 0, 10^2, 10^3, 10^4, and 10^5, respectively. From WFR 1 to 5, the weight factor for voltage

restoration was larger. M-I 3 and 4 were conducted for heavy load case, and Tables 5.22 and 5.23 show the results for the two objectives, total cost (4.18) and voltage restoration (4.19). In M-I 3, unlike the DC voltage, the AC voltage magnitude was well restored at even low WFR because this method considers reactive power effect on only the AC voltage magnitude. However, it resulted in low difference in total cost between WFR 1 and 5. Meanwhile, M-I 4 is a model that includes the effects of the reactive power on the frequency (indirect effect on the total required active power), so both AC and DC voltage restoration and total cost variation became apparent as WFR changes. Figs. 5.16 and 5.17 clearly show the tendency of M-I 3 and 4 according to the weight factor, respectively. From the results, the system operator can select the combination of weight factors according to the operation priority.

Table 5.22 Result of M-I 3 for different weight factors.

	WFR 1	WFR 2	WFR 3	WFR 4	WFR 5
Total AC Voltage Deviation [kV]	8.9434	7.4987	7.4970	7.4857	7.4116
Total DC Voltage Deviation [kV]	34.9778	21.3093	3.4511	2.6807	2.2640
Total Cost [$]	2116.4	2157.3	2160.9	2160.6	2161.3

Table 5.23 Result of M-I 4 for different weight factors.

	WFR 1	WFR 2	WFR 3	WFR 4	WFR 5
Total AC Voltage Deviation [kV]	42.6072	42.1895	13.7122	8.1511	7.4024
Total DC Voltage Deviation [kV]	35.3059	25.6325	3.6038	2.4168	2.0749
Total Cost [$]	2031.9	2034.0	2093.0	2124.9	2158.8

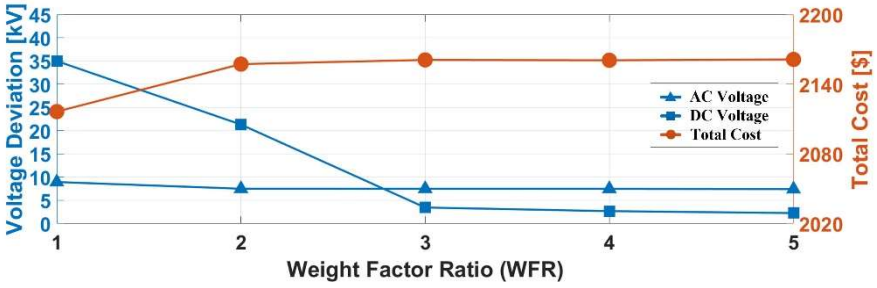

Fig. 5.16 Effect of the weight factor ratio for M-I 3.

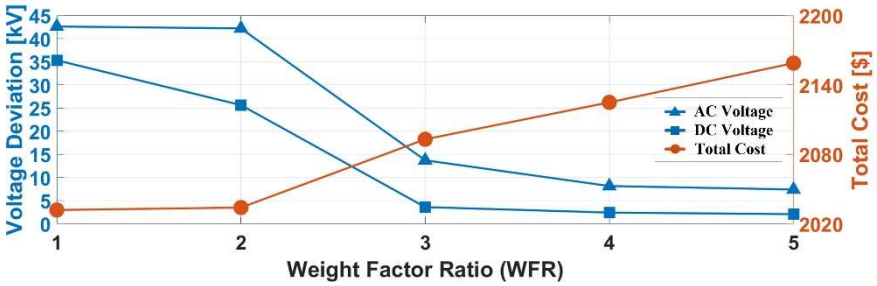

Fig. 5.17 Effect of the weight factor ratio for M-I 4.

Extreme net load case

The excessive generation is handled by the RES curtailment. To investigate the RES curtailment of the proposed method, the extreme net load profile was applied to M-I 2 to 4. The load profile is shown in Fig. 5.18. Compared to the light load, the extreme net load had lower values over a longer period. In this load case, the net load has highly negative value in some time range owing to the high output power of the RES; thus, excessive RES output should be curtailed after reaching the maximum charging power or SOC limits of the BESSs. The results are shown in Table 5.24. The BESSs were almost fully charged in all methods (From (2.8), the required energy to reach the maximum SOC limit with 95% efficiency is around 0.6316 MWh). M-I 3 and 4 had lower generation cost and the amount of RES curtailment while maintaining better frequency and voltage than M-I 2, which does not consider network loss well. The average computation time had almost the same trend as in previous studies, except for being slightly high in M-I 4.

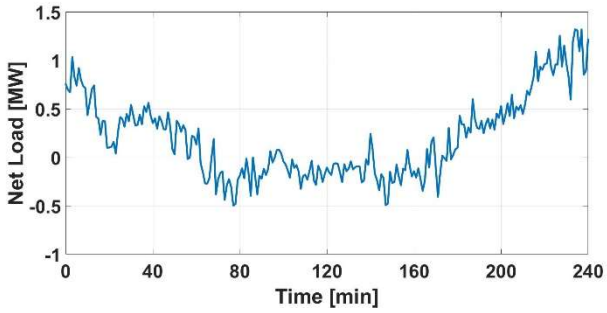

Fig. 5.18 Extreme net load profile.

Table 5.24 Comparison of the methods for extreme load.

	M-I 2	M-I 3	M-I 4
Total Frequency Deviation [Hz]	0.2773	0.0509	0.0193
Total AC Voltage Deviation [kV]	2.4476	2.2481	2.2537
Total DC Voltage Deviation [kV]	0.9533	0.8442	0.8332
Generation Cost of DG [$]	274.8031	265.3383	264.8461
Charge of BESS [MWh]	0.6313	0.6309	0.6283
RES Curtailment [MWh]	0.2089	0.1372	0.1344
Average Computation Time [s]	0.0823	0.0742	0.1419

To clearly show the comparison results, the summary of the conventional method (M-I 2) and the proposed methods (M-I 3 and 4) are shown in the bar plot. The deviations in the frequency and AC/DC voltage magnitude were compared for the all net load profile, as shown in Figs. 5.19–5.21. The average computation time was shown in Fig. 5.22. In M-I 4, the second-order frequency sensitivity is used and the quadratic equality constraint should be solved, which requires more computation time. The computation time for extreme load was particularly high, and the time may become higher as the system size increases. However, the proposed method is applied to microgrids, whose total number of buses is at most about one hundred in general (In general, IEEE 123 bus system is the largest test system used by other studies on the microgrid). Thus, M-I 4 can be used on the microgrid system scale. The total cost was compared for only the heavy load since it can reflect the discharge cost of the BESS (Fig. 5.23), and the amount of the RES curtailment was compared for only extreme load case (Fig. 5.24).

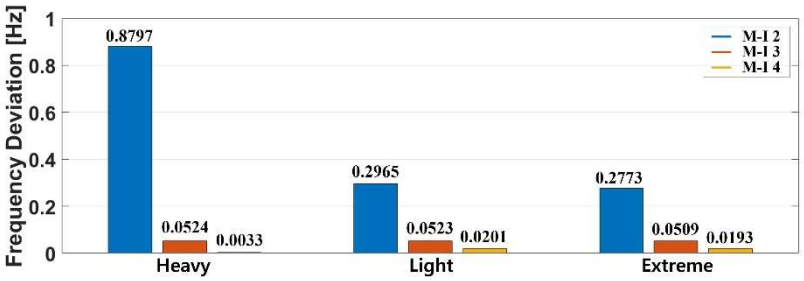

Fig. 5.19 Comparison of the frequency deviation.

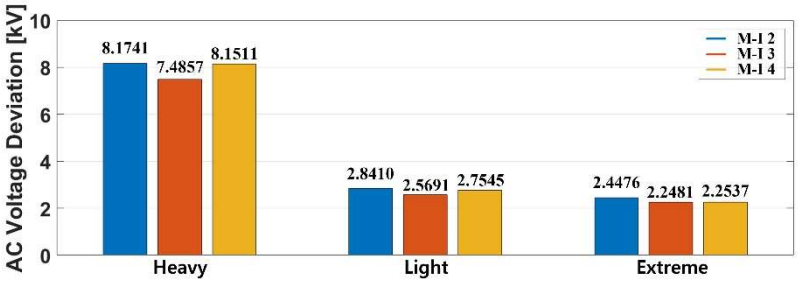

Fig. 5.20 Comparison of the AC voltage deviation.

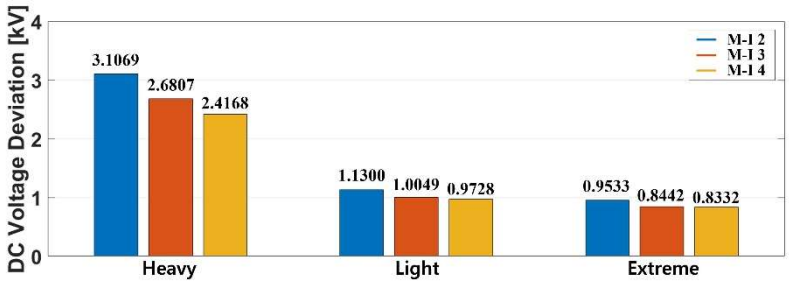

Fig. 5.21 Comparison of the DC voltage deviation.

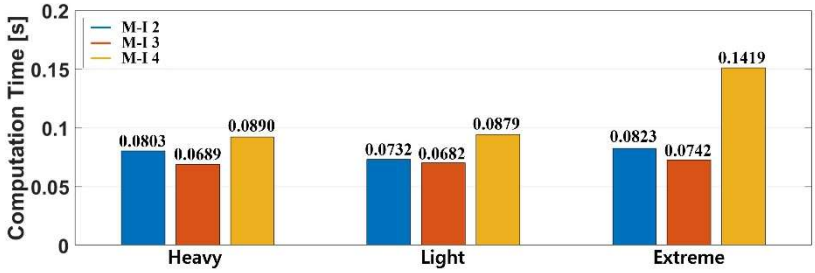

Fig. 5.22 Comparison of the average computation time.

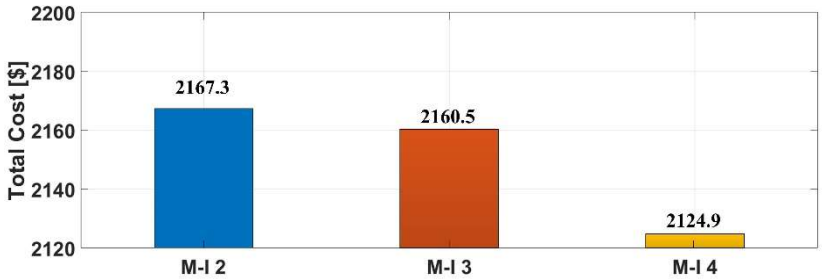

Fig. 5.23 Comparison of the total cost for heavy load.

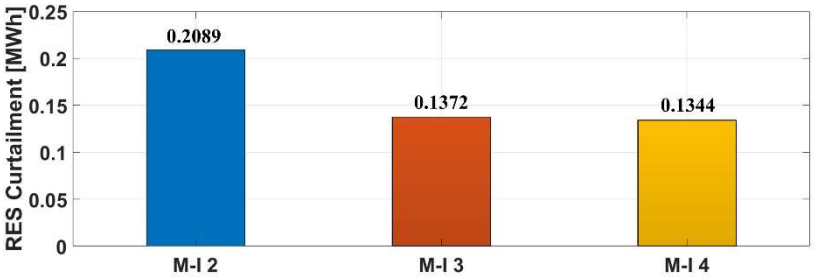

Fig. 5.24 Comparison of the RES curtailment for extreme load.

Effect of line parameter uncertainty

To calculate the frequency and voltage sensitivity, all line resistance and reactance should be known. However, it is difficult for system operator to know all the line parameter exactly. To verify the effect of the parameter uncertainty on the performance of the proposed method, the maximum 10%, 20%, and 30% uncertainty was added to each line parameter randomly when the sensitivity was calculated. The simulation was performed with M-I 3 and M-I 4 for heavy load case and repeated 30 times, and the results are shown in Figs. 5.25–5.28 as box plots.

The frequency deviation of M-I 3 was changed the most compared to others as the uncertainty increased. However, the amount of the deviation is still small enough that the frequency is well restored to its nominal value. The AC voltage deviation of M-I 3 was almost unchanged. The DC voltage deviation and total cost of M-I 3 and all quantities of M-I 4 were maintained within small range. From the results, the proposed methods work well despite of the line parameter uncertainty.

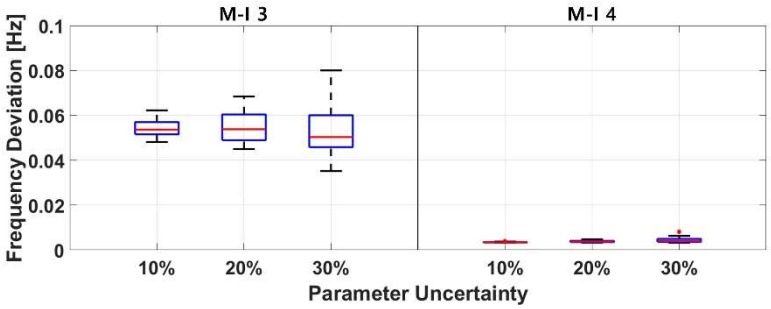

Fig. 5.25 Frequency deviation for parameter uncertainty.

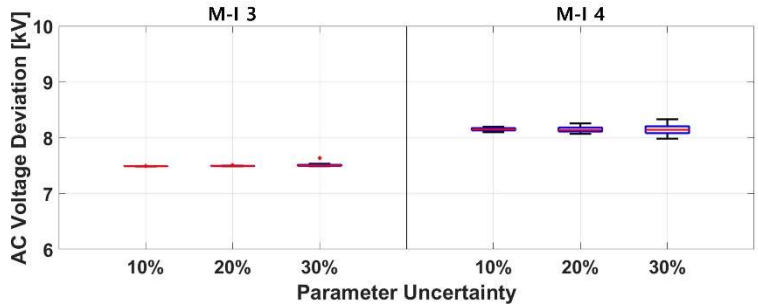

Fig. 5.26 AC voltage deviation for parameter uncertainty.

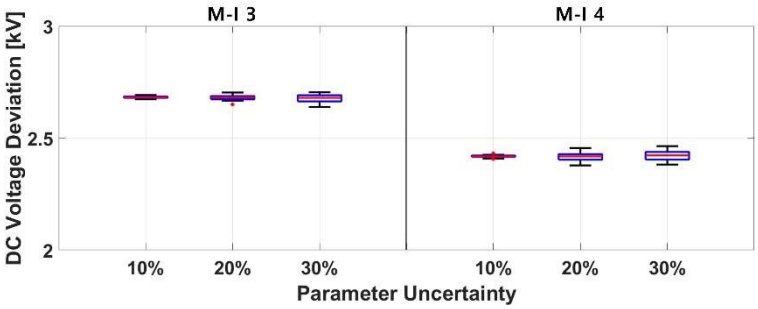

Fig. 5.27 DC voltage deviation for parameter uncertainty.

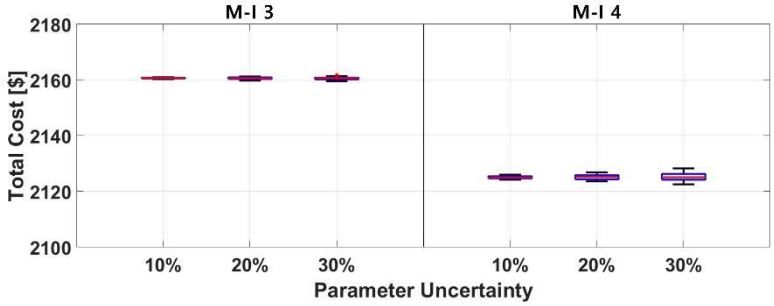

Fig. 5.28 Total cost for parameter uncertainty.

The simulation results show the effectiveness of the proposed methods, in which the frequency and voltage magnitude of both AC and DC grids were effectively restored along with the reduction in the generation cost. M-I 3 needs only frequency, voltage magnitude, and RES output to solve the optimization problem. In addition, the average computation time per iteration was sufficiently small. M-I 4 needs the net load of each bus as well as the frequency and voltage magnitude, and

the quadratic equality constraint should be solved. However, it outperformed M-I 3 in frequency restoration and cost reduction and the computation time was also sufficiently small, even though the second-order derivative was used. Thus, they are suitable for repeating the method periodically at short time intervals. For both methods, it is important to decide the proper weight factors. As stable operation is more essential for islanded mode, it would be better to select high w_v/w_c.

Although the performance can differ depending on the time of net load variation (between the successive 1 min snapshots), the time interval was small enough to verify the effectiveness of the proposed method as supervisory control. In addition, the communication delay can affect the performance in practical scenarios. This may result in degradation of the effectiveness of the proposed method because the net load fluctuates constantly. However, the one-way communication delay for supervisory control is several tens of millisecond [86], and the total required time to fulfill the method once is still small enough to repeat the operation in cycles of tens of seconds or several minutes.

Chapter 6. Conclusions and Future Extensions

6.1 Conclusions

This dissertation presents a supervisory control method of hybrid AC/DC microgrid for grid-connected mode and islanded mode to achieve a reliable and cost-effective system operation under the high penetration of RESs with the uncertainty.

Due to the environmental, social and geographical issues, the penetration level of RES is significantly increasing, but it inevitably leads to the high uncertainty. In addition, the microgrid is small-sized system, in which the uncertainty of the load demand is also increasing. Meanwhile, the growth of DC technology leads to the construction of the HMG for improving energy efficiency, in which the AC grid and DC grid is connected via IC. Therefore, the operation methodology for a HMG to cope with high uncertainty is needed.

The HMG can be operated in either grid-connected or islanded mode. In grid-connected mode, the main grid is regarded as an ideal voltage source, but high uncertainty and multi-microgrid have an impact on the steady-state and dynamic performance of the main grid. The HMG should act as one controllable entity from the viewpoint of the main grid in order to relieve the burden of the main grid by controlling the amount of the interface power flow. In islanded mode, the P–ω and Q–V droop control in the AC grid and the P–V droop control in the DC grid is typically used for power sharing, but it leads to the frequency and voltage deviation. In addition to the deviation, the output power also may be far from the optimal point, which can be obtained to reduce the generation cost. For reliable and cost-effective operation, the deviations should be restored to nominal values while reducing the generation cost at short time intervals.

For grid-connected mode, to compensate the net load fluctuation within a HMG and keep the interface power constant (i.e. controllable single entity), a new

participation factor-based generation adjustment method is proposed. The participation factor, which can be calculated based on the incremental cost considering the line loss for economic operation, can be used to cope with the unexpected net load variation. However, the conventional incremental cost considers only the generators position, which may have less accuracy of the cost change owing to the line loss. To accurately reflect the cost change of output variation, the proposed method introduces the GLIC which is the total cost variation that considers both the generator and load position. Using the GLIC and its derivative, the optimal participation factor can be calculated for each bus (i.e. BDPF). The GLIC can fairly reflect line loss changes; in addition, the second-order loss sensitivity is used to improve the accuracy of the BDPF. To calculate the first and second-order loss sensitivity, the Jacobian matrix containing both the AC and DC grid is used by manipulating the droop slope. The output power can be easily adjusted from the base point, using each load variation and the corresponding BDPF. In addition, the effective power variation gain, which converts the load variation from the point of the generator position, is used to improve the accuracy. Subsequently, re-adjustment is performed if constraint violations exist. Since the BDPF that was previously obtained at the base point is used, the amount of generation adjustment can be calculated instantly. The method can be extended to a pure AC or DC microgrid.

For islanded mode, the operation method is divided into two stage, long-term and short-term, in order to maintain the power balance using only internal resources. Regarding the long-term operation, the on/off decisions of DGs and controllable loads are decided. In this process, the machine learning-based forecasting algorithm is used for net load prediction and the HMG is simply linearized to solve the MILP. In the short-term operation where the final set-point is determined, an MPC-based operation method is proposed, whose objective is to restore the frequency, AC and DC voltage and to reduce the generation cost. In order to be suitable for MPC that updates the set-point in a short cycle, the optimization problem is formulated as a QP using the sensitivities of the AC and DC grids considering the droop control. In

addition, second-order frequency sensitivity, which can accurately account for the influence of the reactive power on the frequency, is selectively utilized. In this case, the performance for frequency restoration and cost reduction can be enhanced with slight modification of only the frequency constraint. Since the problem is repetitively solved in a short period, a persistence model is applied to the prediction algorithm with easy implementation. Like the grid-connected mode, the operation method for islanded mode can also be extended to a pure AC or DC microgrid.

To prove the effectiveness of the proposed operation methods, the HMG test system was constructed and various case studies were conducted for grid-connected and islanded mode, respectively. The proposed methods and comparison methods were implemented in MATLAB. Using the proposed method for grid-connected mode, the disturbance within the HMG due to the high uncertainty can be effectively resolved, which means that the interface flow can be kept as the scheduled value with low generation cost. Moreover, regarding the proposed method for islanded mode, the sensitivity was accurate enough to predict the frequency and voltage. The frequency and voltage deviations caused by the droop control are restored to the nominal values while reducing the generation cost with the cooperative control of the resources.

By using the proposed operation methods, it is anticipated that the penetration level of intermittent RESs and the utilization of the DC technology into the power system will increase, and further the system operation can be more reliable and economical, particularly in situations, where frequent and rapid variations in the load demand and RES output power occur.

6.2 Future extensions

The proposed methods can be improved considering following contents:

- In grid-connected mode, only DGs participate in the generation adjustment, and BESSs are assumed to follow the scheduled output power. If DGs have no enough reserve power and the BESS cost is well-modeled, BESSs can participate in the generation adjustment. In addition, the output efficiency as well as the line loss can be incorporated in the proposed method. Therefore, the generation adjustment considering both DGs and BESSs with high accuracy of the loss model can be one of the future research.

- The proposed method considers the AC grid as a three-phase balanced system. If the AC grid is a three-phase unbalanced system especially in islanded mode, the three-phase sensitivity matrix should be used. Through the inverse of the Jacobian matrix, the sensitivity of the voltage for each phase (A, B, and C) can be known with respect to the power injection of each phase [87]. Using the relationship between the power injection of each phase and our control variable, the proposed method can be extended to an unbalanced system, and it will be handled in future work.

- Dynamic analysis can be another further study. The proposed method focuses on the steady-state performance using the static models. However, since the operation is repeated in a short cycle, it may influence the local controller. To identify the entire system operation, the dynamic simulation containing local controller is required, which gives the time-domain result of the shorter time interval. In this process, the effect of the communication delay can also be investigated.

Bibliographies

[1] B. T. Patterson, "DC, come home: DC microgrids and the birth of the 'Enernet,'" *IEEE Power Energy Mag*., vol. 10, no. 6, pp. 60–69, Nov./Dec. 2012.

[2] L. Zhang *et al*., "Converting AC distribution lines to DC to increase transfer capacities and DG penetration," *IEEE Trans. Smart Grid*, to be published.

[3] T.-F. Wu, C.-H. Chang, L.-C. Lin, G.-R. Yu, and Y.-R. Chang, "DC-bus voltage control with a three-phase bidirectional inverter for DC distribution systems," *IEEE Trans. Power Electron*., vol. 28, no. 4, pp. 1890–1899, Apr. 2013.

[4] T.-T. Nguyen, H.-J. Yoo, and H.-M. Kim, "A comparison study of MVDC and MVAC for deployment of distributed wind generations," in *Proc. IEEE Int. Conf. Sustain. Energy Technol*. (ICSET), Nov. 2016, pp. 138–141.

[5] P. Wang, L. Goel, X. Liu, and F. H. Choo, "Harmonizing AC and DC: A hybrid AC/DC future grid solution," *IEEE Power Energy Mag*., vol. 11, no. 3, pp. 76–83, May/Jun. 2013.

[6] D. E. Olivares *et al*., "Trends in microgrid control," *IEEE Trans. Smart Grid*, vol. 5, no. 4, pp. 1905–1919, Jul. 2014.

[7] A. J. Wood and B. F. Wollenberg, *Power Generation, Operation and Control*. New York, NY: Wiley, 1994.

[8] J. Carpentier, "Contribution to the economic dispatch problem," *Bull. Soc. Francaise Electriciens*, vol. 3, pp. 431–447, Aug. 1962.

[9] R. H. Lasseter, "Microgrids," in *Proc. IEEE Power Eng. Soc. Winter Meeting*, Jan. 2002, vol. 1, pp. 305–308.

[10] A. Gupta, S. Doolla, and K. Chatterjee, "Hybrid AC-DC microgrid: systematic evaluation of control strategies," *IEEE Trans. Smart Grid*, vol. 9, no. 4, pp. 3830–3843, Jul. 2018.

[11] J. M. Guerrero, J. C. Vasquez, J. Matas, L. G. de Vicuña, and M. Castilla, "Hierarchical control of droop-controlled AC and DC microgrids-a general approach toward standardization," *IEEE Trans. Ind. Electron*., vol. 58, no. 1, pp. 158–172, Jan. 2011.

[12] L. Meng *et al*., "Flexible system integration and advanced hierarchical control architectures in the microgrid research laboratory of Aalborg university," *IEEE Trans. Ind. Appl*. Vol. 52, no. 2, pp. 1736–1749, Mar./Apr. 2016.

[13] F. Katiraei and M. R. Iravani, “Power management strategies for a microgrid with multiple distributed generation units,” *IEEE Trans. Power Syst*., vol. 21, no. 4, pp. 1821-1831. Nov. 2006.

[14] F. Kanellos, A. Tsouchnikas, and N. Hatziargyriou, “Micro-grid simulation during grid-connected and islanded modes of operation,” in *Proc. Int. Conf. Power Syst*. Transient, Paper No. IPST05 113, 2005.

[15] Y.-S. Kim, E.-S. Kim, and S.-I. Moon, “Frequency and voltage control strategy of standalone microgrids with high penetration of intermittent renewable generation systems,” *IEEE Trans. Power Syst*., vol. 31, no. 1, pp. 718–728, Jan. 2016.

[16] W. Kramer, S. Chakraborty, B. Kroposki, and H. Thomas, “Advanced power electronic interfaces for distributed energy systems–I: System and topologies,” National Renewable Energy Laboratory, Golden, CO, Tech. Rep. NREL/TP-581–42672, Mar. 2008.

[17] A. D. Paquette, M. J. Reno, R. G. Harley, and D. M. Divan, “Sharing transient loads: Causes of unequal transient load sharing in islanded microgrid operation,” *IEEE Ind. Appl. Mag*., vol. 20, no. 2, pp. 23–34, Mar./Apr. 2014.

[18] K. Ogata, *Modern Control Engineering*. Englewood Cliffs, NJ, USA: Prentice Hall, 2001.

[19] I. U. Nutkani, P. C. Loh, P. Wang, and F. Blaabjerg, “Cost-prioritized droop schemes for autonomous AC microgrids,” *IEEE Trans. Power. Electron*., vol. 30, no. 2, pp. 1109–1119, Feb. 2015.

[20] M. Braun, “Reactive power supply by distributed generators,” in *Proc. IEEE Power Energy Soc. Gen. Meet*., Pittsburgh, PA, USA, Jul. 2008, pp. 1–8.

[21] X. Zhang, C. Huang, S. Hao, F. Chen, and J. Zhai, “An improved adaptive-torque-gain MPPT control for direct-driven PMSG wind turbines considering wind farm turbulences,” *Energies*, vol. 9, no. 11, pp. 977–992, Nov. 2016.

[22] S.-K. Kim, J.-H. Jeon, C.-H. Cho, E.-S. Kim, and J.-B Ahn, “Modeling and simulation of a grid-connected PV generation system for electromagnetic transient analysis,” *Sol. Energy*, vol. 83, no. 5, pp. 664–678, May 2009.

[23] D. S. Morales, “Maximum power point tracking algorithms for photovoltaic applications,” M.S. thesis, Faculty Electron., Commun. Autom., Aalto Univ., Espoo, Finland, Dec. 2010.

[24] F. Nejabatkhah and Y. W. Li, "Overview of power management strategies of hybrid AC/DC microgrid," *IEEE Trans. Power Electron*., vol. 30, no. 12, pp. 7072–7089, Dec. 2015.

[25] N. Eghtedarpour and E. Farjah, "Power control and management in a hybrid AC/DC microgrid," *IEEE Trans. Smart Grid*, vol. 5, no. 3, pp. 1494–1505, May 2014.

[26] P. C. Loh, D. Li, Y. K. Chai, and F. Blaabjerg, "Autonomous operation of hybrid microgrid with ac and dc subgrids," *IEEE Trans. Power Electron*., vol. 28, no. 5, pp. 2214–2223, May 2013.

[27] P. Kunder, *Power System Stability and Control*. New York, NY, USA: McGraw-Hill, 1994.

[28] A. Bokhari *et al*., "Experimental determination of the ZIP coefficients for modern residential, commercial, and industrial loads," *IEEE Trans. Power Del*., vol. 29, no. 3, pp. 1372–1381, Jun. 2014.

[29] A. A. Eajal, M. A. Abdelwahed, E. F. El-Saadany, and K. Ponnambalam, "A unified approach to the power flow analysis of ac/dc hybrid microgrids," *IEEE Trans. Sustain. Energy*, vol. 7, no. 3, pp. 1145–1158, Jul. 2016.

[30] E. Aprilia, K. Meng, M. A. Hosani, H. H. Zeineldin, and Z. Y. Dong, "Unified power flow algorithm for standalone AC/DC hybrid microgrids," *IEEE Trans. Smart Grid*, to be published.

[31] H. M. A. Ahmed, A. B. Eltantawy, and M. M. A. Salama "A generalized approach to the load flow analysis of AC-DC hybrid distribution systems," *IEEE Trans. Power Syst*., vol. 33, no. 2, pp. 2117–2127, Mar. 2018.

[32] M. Manbachi and M. Ordonez, "AMI-based energy management for islanded AC/DC microgrids utilizing energy conservation and optimization," *IEEE Trans. Smart Grid*, to be published.

[33] Q. Zhou, M. Shahidehpour, Z. Li, and X. Xu, "Two-layer control scheme for maintaining the frequency/voltage and the optimal economic operation of hybrid AC/DC microgrids," *IEEE Trans. Power Syst*., to be published.

[34] N. Hatziargyriou *et al*., "Contribution to bulk system control and stability by distributed energy resources connected at distribution network," *IEEE Power Energy Soc*., Piscataway, NJ, USA, Tech. Rep. TR-22, 2017.

[35] S. W. Kim, "A devolved scheme of active distribution system operator for

utilizing flexibility options under market environment," Ph.D. dissertation, Dept. Elect. Eng., Seoul National Univ., Seoul, Korea, 2018.

[36] S.-J. Ahn, "A new power sharing method for distributed generations in the next-generation grid," Ph. D. dissertation, Dept. Elect. Eng., Seoul National Univ., Seoul, Korea, 2009.

[37] L. N. Khanh, J.-J. Seo, Y.-S. Kim, and D.-J. Won, "Coordinate control and energy management strategies for a grid-connected hybrid system," *IEEE Trans. Power Del*., vol. 25, no. 3, pp. 1874–1882, Jul. 2015.

[38] D. Pattabiraman, R. H. Lasseter, and T. M. Jahns, "Feeder flow control method with improved power sharing performance in microgrids," in *Proc. IEEE PES Gen. Meeting*, 2017.

[39] V. R. Pandi, A. Al-Hinai, and A. Feliachi, "Adaptive coordinated feeder flow control in distribution system with the support of distributed energy resources," *Int. J. Elect. Power Energy Syst*., vol. 85, pp. 190–199, Feb. 2017.

[40] Z. Yang *et al*., "LMP revisited: A linear model for the loss-embedded LMP," *IEEE Trans. Power Syst*., vol. 32, no. 5, pp. 4080–4090, Sep. 2017.

[41] Y. Tang, J. Zhong, and J. Liu, "A generation adjustment methodology considering fluctuations of loads and renewable energy sources," *IEEE Trans. Power Syst*., vol. 31, no. 1, pp. 125–132, Jan. 2016.

[42] P. Xing *et al*, "Control strategy of seamless operation mode switch for AC/DC hybrid microgrid," in *Proc. IEEE Int. Conf. Aircraft Utility Systems (AUS)*, Beijing, China, Oct. 2016, pp. 1030–1034.

[43] Q. Xu, J. Xiao, P. Wang, and C. Wen, "A decentralized control strategy for economic operation of autonomous AC, DC, and hybrid AC/DC microgrids," *IEEE Trans. Energy Convers.*, vol. 32, no. 4, pp. 1345–1355, Dec. 2017.

[44] H. Xiao, A. Luo, Z. Shuai, G. Jin, and Y. Huang, "An improved control method for multiple bidirectional power converters in hybrid AC/DC microgrid," *IEEE Trans. Smart Grid*, vol. 7, no. 1, pp. 340–347, Jan. 2016.

[45] J. M. Guerrero, M. Chandorkar, T.-L. Lee, and P. C. Loh, "Advanced control architectures for intelligent microgrids–Part I: Decentralized and hierarchical control," *IEEE Trans. Ind. Electron*., vol. 60, no. 4, pp. 1254–1262, Apr. 2013.

[46] J. M. Guerrero, L. G. de Vicuna, M. Castilla, and J. Miret, "Wireless-control strategy for parallel operation of distributed-generation inverter," *IEEE Trans.*

Ind. Electron., vol. 53, no. 5, pp. 1461–1470, Oct. 2006.

[47] IEEE guide for design, operation, and integration of distributed resource island systems with electric power systems, IEEE Standards Association, IEEE Standard 1547.4-2011.

[48] P. Yang and A. Nehorai, "Joint optimization of hybrid energy storage and generation capacity with renewable energy," *IEEE Trans. Smart Grid*, vol. 5, no. 4, pp. 1566–1574, Jul. 2014.

[49] Y.-S. Kim, E.-S. Kim, and S.-I. Moon, "Distributed generation control method for active power sharing and self-frequency recovery in an islanded microgrid," *IEEE Trans. Power Syst*., vol. 32, no. 1, pp. 544–551, Jan. 2017.

[50] E. Mayhorn, L. Xie, and K. Butler-Purry, "Multi-time scale coordination of distributed energy resources in isolated power systems," *IEEE Trans. Smart Grid*, vol. 8, no. 2, pp. 998–1005, Mar. 2017.

[51] Y. Li *et al*., "Optimal operation of multimicrogrids via cooperative energy and reserve scheduling," *IEEE Trans. Ind. Informat*., vol. 14, no. 8, pp. 3459–3468, Aug. 2018.

[52] Z. Zhao, K. Wang, G. Li, X. Jiang, and Y. Zhang, "Affinely adjustable robust optimal dispatch for island microgrids with wind power, energy storage and diesel generators," in *Proc. IEEE conf. Energy Internet Energy Syst. Integr. (E12)*, Beijing, China, Nov. 2017.

[53] L. G. Weber, A. Nasiri, and H. Akbari, "Dynamic modeling and control of a synchronous generator in an AC microgrid environment," *IEEE Trans. Ind. Appl*., vol. 54, no. 5, pp. 4833–4841, Sep./Oct. 2018.

[54] A. R. Bergen and V. Vittal, *Power Systems Analysis*, 2nd ed. Upper Saddle River, NJ, USA: Prentice Hall, 2006.

[55] Y. Levron, J. M. Guerrero, and Y. Beck, "Optimal power flow in microgrids with energy storage," *IEEE Trans. Power Syst*., vol. 28, no. 3, pp. 3226–3234, Aug. 2013.

[56] P. Malysz, S. Sirouspour, and A. Emadi, "An optimal energy storage control strategy for grid-connected microgrids," *IEEE Trans. Smart Grid*, vol. 5, no. 4, pp. 1785–1796, Jul. 2014.

[57] M. Ross, C. Abbey, F. Bouffard, and G. Joós, "Microgrid economic dispatch with energy storage systems," *IEEE Trans. Smart Grid*, vol. 9, no. 4, pp. 3039–3047,

Jul. 2018.

[58] F. Bouffard and F. Galiana, “Stochastic security for operations planning with significant wind power generation,” *IEEE Trans. Power Syst*., vol. 23, no. 2, pp. 306–316, May 2008.

[59] J. J. Grainger and W. D. Stevenson, *Power System Analysis*. New York, NY, USA: McGraw-Hill, 1994.

[60] D. P. Kothari and J. S. Dhillon, *Power System Optimization*. New Delhi, India: Prentice-Hall, 2006.

[61] A. M. Kettner and M. Paolone, “On the properties of the power systems nodal admittance matrix,” *IEEE Trans. Power Syst*., vol. 33, no. 1, pp. 1130–1131, Jan. 2018.

[62] J.-O. Lee, Y.-S. Kim, E.-S. Kim, and S.-I. Moon, “Generation adjustment method based on the bus-dependent participation factor,” *IEEE Trans. Power Syst*., vol. 33, no. 2, pp. 1959–1969, Mar. 2018.

[63] H. H. Happ, “Optimal power dispatch,” *IEEE Trans. Power App. Syst*., vol. PAS-93, no. 3, pp. 820–830, May 1974.

[64] A. D. D. Craik, “Prehistory of Faá di Bruno’s Formula,” *Amer. Math. Monthly*, vol. 112, no. 2, pp. 119–130, Feb. 2005.

[65] M. Majidi-Qadikolai, and R. Baldick, “Integration of N–1 contingency analysis with systematic transmission capacity expansion planning: ERCOT case study,” *IEEE Trans. Power Syst*., vol. 31, no. 3, pp. 2234–2245, May 2016.

[66] P. Chiradeja and R. Ramakumar, “An approach to quantify the technical benefits of distributed generation,” *IEEE Trans. Energy Convers*., vol. 19, no. 4, pp. 764–773, Dec. 2004.

[67] H. Demuth, M. Beale, and M. Hagan, *Neural Network Toolbox 5 User’s Guide*. Natick, MA: The MathWorks, 2007.

[68] L. Wu, “A tighter piecewise linear approximation of quadratic cost curves for unit commitment problems,” *IEEE Trans. Power Syst*., vol. 26, no. 4, pp. 2581–2583, Nov. 2011.

[69] P. A. Trodden, W. A. Bukhsh, A. grothey, and K. I. M. McKinnon, “Optimization-based islanding of power networks using piecewise linear AC power flow,” *IEEE Trans. Power Syst*., vol. 29, no. 3, pp. 1212–1220, May 2014.

[70] H. Yuan, F. Li, Y. Wei, and J. Zhu, “Novel linearized power flow and linearized

OPF models for active distribution networks with application in distribution LMP," *IEEE Trans. Smart Grid*., vol. 9, no. 1, pp. 438–448, Jan. 2018.

[71] Z. Yang, H. Zhong, A. Bose, Q. Xia, and C. Kang, "Optimal power flow in AC-DC grids with discrete control devices," *IEEE Trans. Power Syst*., vol. 33, no. 2, pp. 1461–1472, Mar. 2018.

[72] P. P. Vergara, J. C. López, M. J. Rider, and L. C. P. da Silva, "Optimal operation of unbalanced three-phase islanded droop-based microgrids," *IEEE Trans. Smart Grid*, to be published.

[73] B. Seal, "Common functions for smart inverters," EPRI Rep., 2014.

[74] W. Chang, "A literature review of wind forecasting methods," *J. Power Energy Eng*., vol. 2, no. 4, pp. 161–168, 2014.

[75] J. Sachs and O. Sawodny, "A two-stage model predictive control strategy for economic diesel-PV-battery island microgrid operation in rural areas," *IEEE Trans. Sustain. Energy*, vol. 7, no. 3, pp. 903–913, Jul. 2016.

[76] J.-O. Lee, E.-S. Kim, and S.-I. Moon, "Analysis of the optimal reactive power of distributed generators for improving energy efficiency in distribution networks," in *Proc. 52th Int. Univ. Power Eng. Conf. (UPEC)*, 2017.

[77] C. A. C. Coello, "Evolutionary multi-objective optimization: A historical view of the field," *IEEE Comput. Intell. Mag*., vol. 1, no. 1, pp. 28–36, Feb. 2006.

[78] G. Venter, "Review of optimization techniques," in *Encyclopedia of Aerospace Engineering*. Hoboken, NJ, USA: Wiley, 2010, pp. 1–12.

[79] E. F. Camacho and C. Bordons, *Model Predictive Control*. New York: Springer-Verlag, 2007.

[80] M. E. Baran and F. F. Wu, "Network reconfiguration in distribution systems for loss reduction and load balancing," *IEEE Trans. Power Del*., vol. 4, no. 2, pp. 1401–1407, Apr. 1989.

[81] P. Kankanala, S. C. Srivastava, A. K. Srivastava, and N. N. Schulz, "Optimal control of voltage and power in a multi-zonal MVDC shipboard power system," *IEEE Trans. Power Syst*., vol. 27, no. 2, pp. 642–650, May 2012.

[82] D. G. Holmes and T. A. Lipo, *Pulse Width Modulation for Power Converters: Principles and Practice*, vol. 18, New York, NY, USA: Wiley, 2003.

[83] N. DiOrio, A. Dobos, and S. Janzou, "Economic analysis case studies of battery energy storage with SAM," Nat. Renewable Energy Lab., Golden, CO. USA,

2015.

[84] D. Singh, R. K. Misra, and D. Singh, “Effect of load models in distributed generation planning,” *IEEE Trans. Power Syst*., vol. 22, no. 4, pp. 2204–2212, Nov. 2007.

[85] S. Papathanassiou, N. Hatziargyriou, and K. Strunz, “A benchmark low voltage microgrid network,” presented at the CIGRE Symp. Power Syst., Dispersed Gener., Athens, Greece, Apr. 2005.

[86] X. Xie, Y. Xin, J. Xiao, J. Wu, and Y. Han, “WAMS applications in Chinese power system,” *IEEE Power Energy Mag*., vol. 4, no. 1, pp. 54–63, Jan./Feb. 2006.

[87] P.-I. Hwang, “A new reactive power control method of intermittent distributed generators for conservation voltage reduction,” Ph. D. dissertation, Dept. Elect. Eng., Seoul National Univ., Seoul, Korea, 2014.

Appendix A. Second-order Derivative of Power Flow Equations

The power flow equation in the AC grid is a function of voltage magnitude and angle (It is assumed that the frequency has no influence on the equation, because the main grid keeps the frequency nominal value in grid-connected mode and the frequency restoration is performed at short cycle in islanded mode). The active power flow equation in the AC grid is (3.4), and the second-order derivatives of the equation are as follows:

$$\frac{\partial^2 P_i}{\partial V_j \partial V_k} = \begin{cases} 2G_{ii} & \text{for } i = j = k \\ 0 & \text{for } i \neq j = k \\ G_{ik}\cos\theta_{ik} + B_{ik}\sin\theta_{ik} & \text{for } i = j \neq k \\ G_{ij}\cos\theta_{ij} + B_{ij}\sin\theta_{ij} & \text{for } i = k \neq j \\ 0 & \text{for } i \neq j \neq k \end{cases} \tag{A.1}$$

$$\frac{\partial^2 P_i}{\partial \theta_j \partial V_k} = \begin{cases} -Q_i / V_i - B_{ii} V_i & \text{for } i = j = k \\ V_i\left[G_{ij}\sin\theta_{ij} - B_{ij}\cos\theta_{ij}\right] & \text{for } i \neq j = k \\ -V_i\left[G_{ik}\sin\theta_{ik} - B_{ik}\cos\theta_{ik}\right] & \text{for } i = j \neq k \\ V_i\left[G_{ij}\sin\theta_{ij} - B_{ij}\cos\theta_{ij}\right] & \text{for } i = k \neq j \\ 0 & \text{for } i \neq j \neq k \end{cases} \tag{A.2}$$

$$\frac{\partial^2 P_i}{\partial V_j \partial \theta_k} = \frac{\partial^2 P_i}{\partial \theta_k \partial V_j} \tag{A.3}$$

$$\frac{\partial^2 P_i}{\partial \theta_j \partial \theta_k} = \begin{cases} -P_i + 2G_{ii}V_i^2 & \text{for } i = j = k \\ V_i V_j\left[-G_{ij}\cos\theta_{ij} - B_{ij}\sin\theta_{ij}\right] & \text{for } i \neq j = k \\ V_i V_k\left[G_{ik}\cos\theta_{ik} + B_{ik}\sin\theta_{ik}\right] & \text{for } i = j \neq k \\ V_i V_j\left[G_{ij}\cos\theta_{ij} + B_{ij}\sin\theta_{ij}\right] & \text{for } i = k \neq j \\ 0 & \text{for } i \neq j \neq k \end{cases} \tag{A.4}$$

Here, the relation between buses i, j, and k are divided into five according to their equality condition.

The reactive power flow equation in the AC grid is (3.5), and the second-order derivatives of the equation are as follows:

$$\frac{\partial^2 Q_i}{\partial V_j \partial V_k} = \begin{cases} -2B_{ii} & \text{for } i=j=k \\ 0 & \text{for } i\neq j=k \\ G_{ik}\sin\theta_{ik} - B_{ik}\sin\theta_{ik} & \text{for } i=j\neq k \\ G_{ij}\sin\theta_{ij} - B_{ij}\sin\theta_{ij} & \text{for } i=k\neq j \\ 0 & \text{for } i\neq j\neq k \end{cases} \tag{A.5}$$

$$\frac{\partial^2 Q_i}{\partial \theta_j \partial V_k} = \begin{cases} P_i/V_i - G_{ii}V_i & \text{for } i=j=k \\ -V_i\left[G_{ij}\cos\theta_{ij} + B_{ij}\sin\theta_{ij}\right] & \text{for } i\neq j=k \\ V_i\left[G_{ik}\cos\theta_{ik} + B_{ik}\sin\theta_{ik}\right] & \text{for } i=j\neq k \\ -V_i\left[G_{ij}\cos\theta_{ij} + B_{ij}\sin\theta_{ij}\right] & \text{for } i=k\neq j \\ 0 & \text{for } i\neq j\neq k \end{cases} \tag{A.6}$$

$$\frac{\partial^2 Q_i}{\partial V_j \partial \theta_k} = \frac{\partial^2 Q_i}{\partial \theta_k \partial V_j} \tag{A.7}$$

$$\frac{\partial^2 Q_i}{\partial \theta_j \partial \theta_k} = \begin{cases} -Q_i - 2B_{ii}V_i^2 & \text{for } i=j=k \\ -V_iV_j\left[G_{ij}\sin\theta_{ij} - B_{ij}\sin\theta_{ij}\right] & \text{for } i\neq j=k \\ V_iV_k\left[G_{ik}\sin\theta_{ik} - B_{ik}\sin\theta_{ik}\right] & \text{for } i=j\neq k \\ V_iV_j\left[G_{ij}\sin\theta_{ij} - B_{ij}\sin\theta_{ij}\right] & \text{for } i=k\neq j \\ 0 & \text{for } i\neq j\neq k \end{cases} \tag{A.8}$$

The power flow equation in the DC grid is (3.6), and the second-order derivatives of the equation are as follows:

$$\frac{\partial^2 P_i}{\partial V_j \partial V_k} = \begin{cases} 2G_{ii} & \text{for } i=j=k \\ 0 & \text{for } i\neq j=k \\ G_{ik} & \text{for } i=j\neq k \\ G_{ij} & \text{for } i=k\neq j \\ 0 & \text{for } i\neq j\neq k \end{cases} \tag{A.9}$$

For the DC grid, the equation is simple since there is no voltage angle and reactive power. Note that when the Jacobian matrix is differentiated in (3.23), the second-order derivatives of (2.20) and (2.21) should be included. The droop control is a linear function of the frequency and voltage, so the second-order derivatives are zero.

Appendix B. Singularity of Square Matrix in (3.31)

Let M_r denote the square matrix in (3.31). Except for the last row, the main component of M_r is the derivative of GLIC for load r with respect to generation, $\partial\lambda_r{}^i/\partial P_{g,k}$. In (3.13), $\psi^i{}_k$ is close to one, and $\partial^2 P_{loss}{}^i/\partial P_j \partial P_k$ is relatively small compared to the other cost coefficient terms. Therefore, $\partial\lambda_r{}^i/\partial P_{G,k}$ is less dependent on k (not for $k=i$) and can be rewritten as

$$\frac{\partial \lambda_r^i}{\partial P_{g,k}} = s_{i,r} + \Delta s_{i,r}^k \tag{B.1}$$

where $s_{i,r}$ is a term independent of k, and $\Delta s_{i,r}^k$ is the small deviation according to k. Although (B.1) should be multiplied by $\psi^k{}_r$ in (3.31), its value is also close to one, and $s_{i,r}$ is still dominant. Therefore, using (B.1), M_r can be decomposed as follows (index r is omitted for convenience):

$$M = M^0 + E \tag{B.2}$$

where

$$M^0 = \begin{pmatrix} A_{(m-1)\times 1} & B_{(m-1)\times(m-1)} \\ 1 & \mathbf{1}_{1\times(m-1)} \end{pmatrix} \tag{B.3}$$

$$E = \begin{pmatrix} C_{(m-1)\times m} \\ \mathbf{0}_{1\times m} \end{pmatrix} \tag{B.4}$$

$$A = \begin{pmatrix} s_2 & \cdots & s_m \end{pmatrix}^T \tag{B.5}$$

$$B(i,j) = \begin{cases} -s_1\ , & i = j \\ s_i - s_1, & i \neq j \end{cases} \tag{B.6}$$

$$C(i,j) = \delta_{i,j} \tag{B.7}$$

and $\delta_{i,j}$ is the (i, j) entry of E, which represents the difference between exact value and dominant value of M.

To investigate the singularity of M, let $a_1,\ldots,a_m$ be scalars such that

$$\sum_{i=1}^{m} a_i M_i = \mathbf{0}_{m\times 1} \tag{B.8}$$

where M_i is the ith column vector of M. Using the elements of M^0 and E, (B.8) can be re-arranged as

$$s_1 a_1 = s_i a_i + \sum_{j=1}^{m} \delta_{i,j} a_j, \quad i = 2,...,m \tag{B.9}$$

$$\sum_{i=1}^{m} a_i = 0 \tag{B.10}$$

To satisfy (B.9), a_i is either all zero or approximately inversely proportional to s_i because the magnitude of $\delta_{i,j}$ is relatively small compared to s_i. From (3.20) and the preceding decomposition description, all s_i values are generally negative. Therefore, if a_i is inversely proportional to s_i, all a_i have the same sign and (B.10) cannot be satisfied. By contradiction, all a_i should be zero, and M is nonsingular.

Unlike the aforementioned singularity verification, the exact form of M is necessary for calculating BDPF because the small correction makes a large difference in the value of BDPF. In addition, if the generator cost function is modeled as linear or piecewise linear, the decomposition is invalid and BDPF may not be calculated. However, the quadratic cost function is most commonly used, and the quadratic model in (3.8) is adopted.

초 록

최근들어 전력계통이 소규모화 되고 분산화됨과 동시에 직류 기술의 발전으로 혼합형 마이크로그리드가 구축되고 있다. 또한, 환경 문제에 대한 지속적인 관심과 지속 가능한 에너지원을 얻고자 하는 노력으로 신·재생에너지원 보급률이 점차 증가하고 있다. 하지만, 이러한 상황은 계통에 불확실성을 증가시킨다. 마이크로그리드가 계통연계형으로 동작하는 경우, 불확실성으로 인한 수급 불균형은 주 계통에 부담을 줄 수 있다. 이러한 현상은 불확실성이 커지고 마이크로그리드 수가 늘어날수록 더욱 심화된다. 또한, 독립운전시에는 droop 제어 수행의 결과로 주파수와 전압의 편차가 발생할 수밖에 없으며 출력 또한 비용 효율적인 지점에서 멀어질 수 있다.

본 논문에서는 높은 불확실성 하에서 혼합형 마이크로그리드의 계통연계운전과 독립운전시 신뢰성과 경제성을 동시에 얻을 수 있는 운영방안을 제안한다. 계통연계운전시 하나의 제어 가능한 시스템으로 동작하기 위해서는 내부에서 발생하는 실시간 불확실성을 스스로 처리해야 한다. 참여율 기반 발전량 분배방법은 시스템 구성에 관계없이 상위 운영시스템이 있으면 적용 가능한 방법이다. 기존의 참여율 계산은 발전기의 입장만 고려한 증분비용을 활용했기 때문에 그 정확도가 떨어진다. 이를 개선하고 분산전원의 출력 변동에 대한 비용 변화를 더욱 정확하게 표현하기 위해 본 논문에서는 발전원과 부하 쌍에 대한 증분비용을 새롭게 도입한다. 이 증분비용은 부하 위치에 대한 영향을 반영하기 때문에 손실이 더 정확하게 반영되며, 발전비용 최소화를 위한 최적의 발전기 참여율이 각 모선별로 계산이 된다. 최적 참여율 계산 과정에서 일차 손실민감도뿐만 아니라 이차 손실민감도까지

활용하여 그 정확도를 더욱 향상시켰다. 이 과정에서 AC와 DC 계통을 모두 고려하는 자코비안 행렬이 활용되었다. 참여율을 통한 발전량 조절은 지속적이고 빠르게 발생하는 순부하 변동에 대해 즉각적으로 대응할 수 있기 때문에 높은 불확실성 하에서 적용하기 적합한 방법이다. 또한, 손실을 더욱 정확히 반영하였기 때문에 주계통과의 연계선로 조류를 더욱 정확히 제어할 수 있다. 분산전원이 출력제한에 도달한 상황에서는 재분배를 통해 위배를 해소하는 방안이 제안되었다.

독립운전시에는 내부 자원만을 활용해서 수급균형이 유지되어야 하기 때문에 운영방안이 장주기와 단주기로 나눠진다. 장주기 운영에서는 분산전원과 제어가능한 부하의 동작 여부가 결정되며, 이 과정에서 순부하 예측을 위해 기계학습 기반의 알고리즘이 활용되고 시스템을 선형화하여 혼합정수선형계획법으로 문제를 해결하였다. 최종 출력이 결정되는 단주기 운영에서는 모델예측제어 기반의 운영방안이 제안되었다. Droop 제어에 의해 발생한 주파수와 전압 편차를 회복시키는 것과 동시에 발전비용까지 줄이기 위한 문제가 정식화 되었으며, 짧은 주기로 set-point를 갱신하는 모델예측제어에 적합하도록 주파수와 AC, DC 전압 민감도가 활용되었다. Droop 제어를 포함한 자코비안 행렬을 통해 주파수와 AC, DC 전압 민감도를 계산할 수 있다. 또한, AC 계통에서 주파수에 대한 무효전력의 영향을 반영하기 위해 주파수에 대한 이차 민감도를 선택적으로 활용할 수 있도록 하였다. 이 때, 주파수 제약조건이 2차식으로 표현되나, 더 좋은 효과를 얻을 수 있다. 짧은 주기로 문제가 반복 해결되기 때문에 모델예측제어 내 예측 알고리즘으로 지속 모델 (persistence model)이 적용되어 그 상황에서의 문제와 해결 방안이 제안되었다.

마지막으로 제안한 방법은 MATLAB상에서 알고리즘이 구현되었고 사례연구가 수행되었다. 기존 방법들과 비교하여 혼합형 마이크로그리드

운영시 계통연계운전과 독립운전 각각에 대해 경제성과 신뢰성 두 가지 측면에서 그 효과를 검증할 수 있었다. 제안한 방법을 활용함으로써 전력계통 내에 간헐적인 출력 특성을 가지는 신·재생에너지원의 수용률과 DC 기술의 활용도를 증가시킬 수 있을 것으로 기대한다. 특히 부하와 신·재생에너지 출력이 빈번하고 빠르게 변화하는 상황에서, 마이크로그리드를 더욱 신뢰성있고 비용 효율적으로 운영할 수 있을 것이다.

주요어 : 분산전원, 혼합형 마이크로그리드, 증분비용, 모델예측제어, 신·재생에너지, 참여율
학 번 : 2013-20862